University of Alberta

Multirate Predictive Control and Performance Assessment

by

Xiaorui Wang

A thesis submitted to the Faculty of Graduate Studies and Research in partial fulfillment of the requirements for the degree of **Doctor of Philosophy**.

Department of Electrical and Computer Engineering

Edmonton, Alberta
Spring 2007

Your file Votre référence
ISBN: 978-0-494-29765-0
Our file Notre référence
ISBN: 978-0-494-29765-0

If there are two ways, choose the harder.
— from movie Himalaya

Abstract

The objectives of this thesis are to develop data-driven approaches for control performance assessment and predictive control design for multirate systems. Some related outstanding problems for univariate systems are also addressed. The benchmark is chosen as minimum variance control (MVC) to assess multirate control loop performance because MVC provides us a theoretical lower bound of the output variance under linear feedback control, and it provides useful information such as how well the current controller is performing and how much "potential" there is to improve the control performance.

Generally speaking, a multirate controller performs better than a slow-single rate (SSR) controller but worse than a fast single-rate (FSR) controller in the sense of minimum variance control. This conjecture is theoretically proved in Chapter 2 for a continuous linear time-invariant (LTI) single-input and single-output (SISO) system. The optimal FSR multirate and SSR controllers are designed under the same performance criterion: variance of the fast sampled output. Basic statistical properties of the discretization of continuous stochastic disturbance models are investigated. A linear matrix inequality (LMI) approach is developed to derive the optimal controllers for dual-rate (DR) and SSR loops.

Chapter 3 discusses data-driven MVC design and control performance assessment based on the MVC-benchmark for multirate systems. A lifted model is used to analyze the multirate system in a state-space framework and the lifting technique is applied to derive a subspace equation for multirate systems. From the subspace equation the multirate MVC law and the algorithm to estimate the multirate MVC-benchmark variance or performance index are developed. The multirate optimal controller is derived from a set of input-output open-loop experimental data and thus this approach is data-driven since it does not involve an explicit model.

The presented MVC-benchmark algorithm requires a set of open-loop experimental data and closed-loop routine operating data. In contrast to traditional control performance assessment algorithms, no explicit models or model parameters, namely, transfer function matrices, Markov parameters or interactor matrices, are needed in the data driven approach.

Besides the data-driven MVC control, predictive control laws are also designed in Chapter 3 and 4 for both single-rate and multirate systems via system open-loop input-output data. Comparing with the previous data-driven predictive control approach, the developed predictive controllers can handle systems where only partial on-line outputs measurements are available and multirate systems. This is to circumvent the problems that in reality, some outputs may not be measured in real-time, or are too costly to measure at fast sampling rate.

To my parents

Acknowledgements

A journey is more joyful when you travel together. This thesis is the result of four and half years of work whereby I have been accompanied and supported by many people. It is a pleasant moment that I have now the opportunity to express my gratitude for all of them.

I would like first thank my co-supervisors Dr. Tongwen Chen and Dr. Biao Huang for their patient training, valuable advices, continual encouragement, and insightful comments. Besides the wise supervision in academia, their virtues such as diligence, devotion, integrity, modesty and amiability have deeply impressed me.

Also, I want to express my gratitude to my colleagues in both Electrical Engineering and Chemical Engineering departments at the University of Alberta. Particularly, I would like to thank Dr. Liqian Zhang, Jiandong Wang and Monjur Murshed for the discussions we have had. Many thanks are dedicated to Dr. Yang Shi, Dr. Guofeng Zhang, Dr. Danlei Chu, Dr. Jie Sheng, Jingbo Jiang, Jing Wu, Jing Zhou, and Yutong Qi for the help you have given me.

I gratefully acknowledge the Natural Sciences and Engineering Research Council of Canada, the F.S. Chia Scholarship at the University of Alberta, and Western Canada Fuel Cell Initiative for their financial support.

Finally, I would like to thank my parents and sister in China for their tremendous support and understanding. A special gratitude to my husband: thank you for being my closest teammate, my first audience of all my presentations, and who is always there when I need.

Contents

[1]The materials in this chapter has been published in "X. Wang, L. Zhang, T. Chen, and B. Huang. Minimum variance in fast, slow and dual-rate control loops. Int. J. of Adaptive Contr. and Signal Processing, 19(8):575-600, 2005".

[2]The materials in this chapter will be published in "X. Wang, B. Huang, and T. Chen. Multirate minimum variance control design and control performance assessment: A data-driven subspace approach. IEEE Trans. Contr. Syst. Technol., 15(1): 65-74, 2007".

[3]The materials in this chapter will be published in "X. Wang, B. Huang, and T. Chen. Data-driven predictive control for solid oxide fuel cells. J. of Process Contr., to be published, 2007".

List of Figures

List of Tables

Nomenclature

$\underline{u}$	lifted control signal
$\underline{y}$	lifted output signal
a, a_t, a_k	white noise sequences, driving force of disturbances
d	time delay
e_k	white noise with zero mean and identity covariance matrix
I	identity matrix
J_c	control horizon
L	prediction horizon
L_M	lifting operator with factor M
M	the sampling rate ratio (a positive integer)
T	sampling period
u_f	fast sampled control signal
u_s	slow sampled control signal
u_t	control signal
y_f	fast sampled output signal
y_s	slow sampled output signal
y_t	system output

List of Acronyms

AFC	Alkaline fuel cell
CVA	canonical variate analysis
DMFC	Direct methanol fuel cell
DR	dual-rate
DSR	deterministic and stochastic subspace system identification and realization
FSR	fast single-rate
LMI	linear matrix inequality
LPTV	linear periodically time-varying
LQG	linear quadratic Gaussian
LTI	linear time-invariant
MCFC	Molten carbonate fuel cell
MIMO	multi-input and multi-output
MOESP	multivariable output error state space identification procedure
MPC	model predictive control
MRSD	multirate sampled-data
MVC	minimum variance control
PAFC	Phosphoric acid fuel cell
PEM	prediction error method
PEMFC	Polymer electrolyte/ Proton exchange membrane fuel cell
SISO	single-input and single-output
SOFC	solid oxide fuel cell
SSR	slow-single rate
SVD	singular-value decomposition

Chapter 1

Introduction

With an objective towards data-driven subspace approach for performance assessment and predictive control, the work of this thesis is related to several fundamental subjects in control and identification, such as multirate systems, control performance assessment, subspace identification and subspace-based predictive control. This chapter starts by reviewing existing work in these areas, then discusses the objectives, motivation, and contribution of the thesis research, and finally presents the outline of the thesis.

1.1 Multirate systems

Multirate systems, also known as multirate sampled-data (MRSD) systems, consist of two or more sampling and hold elements that operate with different frequencies. Multirate systems have been widely applied in many industrial fields such as electrical, mechanical and chemical engineering. This is because in large scale multivariable digital systems it is often unrealistic or sometimes impossible to sample all physical signals at one single rate. For example, in chemical processes, different variables such as flows, temperatures and compositions may be sampled at different rates depending on their signal bandwidths. Another reason is that multirate systems can often achieve objectives that cannot be achieved by single-rate systems, for instance, usually the optimal linear quadratic Gaussian (LQG) cost function of a multirate system is larger than that of a fast single-rate (FSR) system and less than that of a slow-single rate (SSR) system; thus a better performance-implementation tradeoff can be obtained by using multirate systems.

The research on multirate systems can be traced back to 1957 [40], when the concept of lifting was developed by Kranc from the switch decomposition technique. From then on, the lifting technique, which converts a linear periodically time-varying (LPTV) multirate system to a linear time-invariant (LTI) one, has been a most powerful tool used for multirate systems design and analysis. Much of the recent work on multirate systems has been in the control design and model identification fields. Multirate LQG design was studied in [47], in which it was noted that the causality constraint was a convex one and hence a numerical technique based on convex optimization was proposed. In [76], explicit optimal solutions for the multirate $\mathcal{H}_2$ optimal problem were obtained by using a projection method. In [11], a direct method was given based on the frequency-domain technique and the nest algebra. A state-space approach was shown in [67], which treated a multirate pure discrete-time system by a state space model and solved the $\mathcal{H}_2$ control problem with the causality constraint in terms of two Riccati equations. A direct state-space solution of the multirate system $\mathcal{H}_2$ optimal control was given in [57], which avoided converting the sampled-data problem to an equivalent discrete-time problem. A generalized predictive control scheme for multirate systems was proposed in [66].

In the multirate model identification area, an algorithm was proposed that uses slowly sampled outputs and fast control inputs to estimate the intersample outputs in [45]. A technique was presented in [74] to estimate the models of periodically time-varying systems. The problem of identifying a fast single-rate model with slow sampling period was studied in [42] based on multirate input-output data, which differs from [74] in that not only a lifted model for the multirate process but also a fast single-rate model was identified. The related issues were further discussed in [78] such as the uniqueness of the fast-rate system, controllability and observability of the lifted system. The paper [65] provided a method estimating the time delay of a SISO continuous-time system by analyzing the interactor matrix of the lifted system. The identifiability of closed-loop identification via fast-sampling direct approach was studied in [77], which gave a new point of view based on cyclostationary signal processing and bispectral analysis showing that a traditional identifiability condition (an external persistently exciting test signal) may be removed.

The study of multirate systems has been very active for decades, but little work has been done in multirate control performance assessment. Like all controllers, multirate controllers need to be maintained, monitored and tuned routinely. Because some problems can not be avoided such as sensor or actuator failure, equipment fouling, feedstock variability, product changes, and seasonal influences, even if a controller initially performs well, the aforementioned factors may lead to its abrupt or gradual performance deterioration. Thus, for those control loops where multirate controllers have been implemented, multirate control performance assessment is necessary to ensure that they are working as designed. This is our initial motivation to choose multirate performance assessment as one of the proposed research topics. Multirate control performance assessment is an intersection between multirate control systems and control performance assessment fields.

1.2 Control performance assessment

Control performance assessment is an important technique to assist process operations with high efficiency. There are many ways to assess the performance of process controllers, but in general they explicitly or implicitly involve comparing the current control quality against some standard. To the best of our knowledge, little work

has been done in multirate control performance assessment, even though multirate sampling or operations are not uncommon in industry. Due to the lack of published work on multirate control performance assessment, we will only review the important research which has been done for single-rate control loops.

For linear systems, it is known that minimum variance control (MVC) is the best possible control in the sense that no other controllers can provide a lower closed-loop variance [5]. Many papers [22, 12, 68, 46, 28] have shown that MVC is a useful benchmark to assess control-loop performance. Several excellent reviews of control performance assessment theoretical issues have been published, such as [55, 21, 70]. The current status in control performance assessment technology and industrial applications was reviewed in [31]. A significant work is [22] by Harris, who presented a new direction and framework for the control performance-assessment area. It applies time-series analysis to find a suitable expression for the feedback controller-invariant terms from closed-loop routine operating data, and subsequently uses it as a benchmark to assess single-input and single-output (SISO) control-loop performance. The filtering and correlation analysis in [28] extends the method in [22] to multi-input and multi-output (MIMO) processes. Other MIMO performance assessment work can also be found in [23]. To estimate the MVC-benchmark variance from routine operating data, the time delay (SISO case) or the interactor matrix (MIMO case) must be known a priori. This is a common point in these aforementioned traditional methods. The factorization of the interactor matrix by singular value decomposition is one of the main contributions in [29]. A similar result is given in [38], which presents a one-shot solution to estimate the MVC-benchmark variance, but it requires the first few Markov parameters in multivariable feedback control loops. A framework based on subspace matrices is studied for the estimation of the MVC-benchmark variance for multivariate feedback control systems [27]. This algorithm consolidates the traditional three-step procedure, model identification, closed-loop time series analysis, and extraction of the MVC benchmark, into a single shot. No prior knowledge, such as Markov parameters or interactor matrices are needed in the algorithm.

There are approaches other than the MVC-based techniques, such as frequency analysis [35], and likelihood ratio methods [71]. The method to estimate the PID-

achievable performance is studied in [37, 18]. A benchmark in terms of user-specified closed-loop dynamics is discussed in [29] by defining in advance what performance is acceptable. To take control action limitation into account, the paper [25] presents a pragmatic approach to evaluate control performance based on the LQG control benchmark via LQG trade-off curves from the estimated plant and disturbance models. In [32], a method to assess the performance with LQG benchmark for univariate model predictive controllers is proposed. A monitoring technique is proposed to detect and flag poor control performance for an individual controlled variable based on analyzing run length distribution [44].

1.3 Subspace identification methods

System identification can be defined as building mathematical models of systems using input-output measurements. Subspace identification methods were developed in the late 80's and early 90's. They allow the identification of a system state space model directly from data, which is very convenient for estimation, filtering, prediction and control. The name "subspace" comes from the fact that the basic objects which are constructed in the algorithms are subspaces generated by the data. A typical subspace identification algorithm contains two steps: the first step is making data projections to obtain subspace matrices; the second step is to extract a state space model from the subspace matrices [52]. Subspace methods are appealing because neither canonical parametrization nor iterative nonlinear optimization is involved; instead, the main computational tools are simple and numerically robust such as orthogonal projections and singular-value decompositions. Moreover, subspace methods have better numerical reliability and modest computational complexity compared with the prediction error method (PEM) particularly when the numbers of outputs and states are large.

Among the subspace identification methods, the canonical variate analysis (CVA) by Larimore [41], the numerical algorithms for subspace state space identification (N4SID) by Van Overschee and De Moor [51], the multivariable output error state space identification procedure (MOESP) by Verhaegen [73] and the deterministic and stochastic subspace system identification and realization (DSR) by Di Ruscio [58] are the algorithms which not only resolve the problem of system identification

but also deal with the additional problem of structure identification. A unifying theorem is given in [52] providing a framework in which several subspace identification methods can be interpreted as a singular-value decomposition (SVD) task with difference choices of weighing. An overview of theoretical and numerical issues about subspace identification methods can be found in [75] and [50]. An instrumental variable subspace identification approach, which gives consistent model estimates under the errors-in-variables situation, is developed using principal component analysis in [79]. A closed-loop subspace identification approach adopted the error in variable structure through a QR projection and SVD decomposition is proposed in [26].

1.4 Subspace-based predictive control

The predictive control has usually been studied under the heading of model predictive control (MPC). This is because MPC has considerable advantages relative to other conventional control strategies: the ability to handle input and state constraints for large scale multivariable plants, the capability of dealing with variables interaction, and the ease of adaptation to new operating conditions [17, 32]. MPC refers to a class of computer control algorithms that utilize an explicit process model to predict the future response of a plant, and then using the predicted response in a cost function minimization to obtain a sequence of future optimal control signals. Only the first optimal control input will be sent into the plant, this is also known as receding horizon control.

Like any other model-based control, conventional MPC relies heavily on process models. An accurate process model is required if the process is to be regulated tightly. Usually there are two ways to obtain process models: the analytic approach where certain process knowledge (such as fundamental physical laws) is required to derive the model and the experimental approach by fitting a model to the input-output data through system identification. Unlike the model-based control design approach, where the system model is required, we follow a new approach based on results from the area of subspace system identification [58, 59] to design optimal control laws when only the input-output data of a given system are available. Figure 1.1 illustrates the difference between the model-based predictive control and the data-driven predictive control, where one can see that the process modelling is

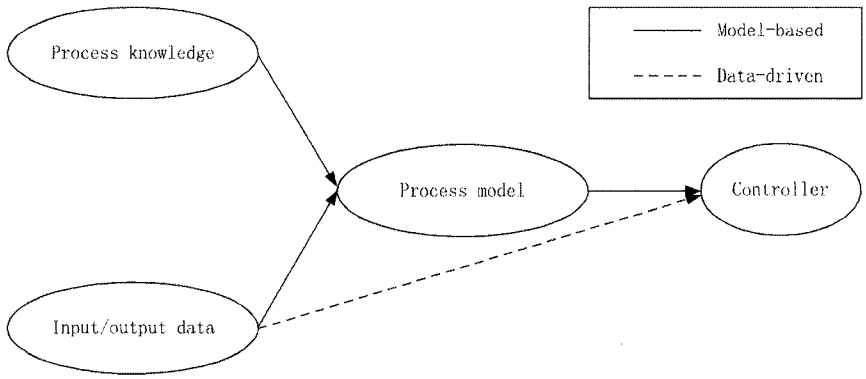

Figure 1.1: Model-based approach vs. data-driven approach.

bypassed. The idea of designing predictive controllers using subspace system identification techniques has been investigated in recent years. For instance, subspace matrices are used in the model-free LQG design [14] and subspace predictive control design [15]. In addition, the extended state space model is used to obtain predictive controllers [60]. The subspace approach to designing a predictive controller with all the important predictive control features is investigated in [34]. A model-free predictive controller based on subspace identification technique with Laguerre polynomials is proposed in [7]. A data-based LQG control design including a data-based observer and an optimal feedback based on the system Markov parameters is developed in [2].

1.5 Motivation and objectives

Our work is motivated by the following reasons:

- Compared with single-rate systems, multirate systems are more complex and challenging. Though much research has been done in single-rate performance assessment areas, the work for multirate performance assessment is rare.
- The data-driven design approaches presented in the literature so far has been limited to single-rate systems. Particularly, they are developed under conditions that all output measurements are obtained on-line in closed-loop systems.

Due to these reasons, the main objectives of this thesis are to develop a data-driven control performance assessment method for multirate systems, and to design optimal control for single-rate systems (when not all outputs are measurable) and

for multirate systems. We choose MVC as the benchmark to assess multirate control loop performance because it provides us a theoretical lower bound of the output variance under linear feedback control, and it gives useful information such as how well the current controller is performing and how much "potential" there is to improve the control quality. Besides the data-driven MVC control, we design a data-driven predictive control which can handle input and state constraints, deal with variables interaction, and adapt to new operating conditions easily. Our detailed objectives are given below:

- Exploring and then analyzing the performance limits caused by time delays of multirate systems and single-rate systems. Theoretically justifying that a multirate controller performs better than an SSR controller but worse than an FSR controller in the sense of minimum variance control. This topic is of importance to control specialists and process engineers who have implemented multirate control systems to their control loops.

- Developing data-driven MVC design and control performance assessment based on MVC-benchmark for multirate systems.

- Designing the single-rate data-driven predictive control based on partially available system outputs. This is to circumvent the problem that in reality, some outputs may not be measured in real time, or are too costly to measure on-line.

- Developing multirate data-driven predictive control based on system input-output data.

1.6 Contributions of this thesis

Oriented by the objectives, we have mainly contributed in:

- Investigation of the minimum variance control problem for single-input single-output linear systems sampled with different rates: fast, dual and slow rates. A discretization method preserving the mean and auto-correlation of a continuous stochastic disturbance model is developed. A linear matrix inequality

(LMI) approach is proposed to derive the minimum variance controllers for the lifted dual-rate and slow-rate control loops. It is theoretically proved that the performance of an optimal dual-rate controller is superior to that of a slow single rate controller but inferior to that of an optimal fast single rate controller in the sense of minimum variance control.

- Development of the data-driven MVC and the MVC-benchmark variance estimation for a multirate system. A multirate subspace input-output equation is derived via the lifting approach, from which the multirate MVC law and the algorithm to estimate the multirate MVC-benchmark variance are developed. The proposed algorithms are data-driven: the multirate MVC controller design only requires a set of input-output experimental data; the presented MVC-benchmark estimation algorithm requires a set of open-loop experimental data and closed-loop routine operating data.

- Proposal of a predictive control strategy that can handle constraints and optimize control performance using the subspace approach. Comparing with the previous data-driven predictive control approach, the developed predictive controller can handle systems where only partial on-line outputs measurements are available. The proposed algorithm is demonstrated through a SOFC model which has been commonly investigated in the dynamic SOFC modeling/control literature lately.

- Development of a multirate data-driven predictive control including feedforward control. The proposed multirate predictive control is data-driven. Particularly, the developed algorithm is applied to a multirate SOFC system, where the explicit dynamic model of SOFC is generally difficult to develop, and the fuel utilization is difficult to sample in the fast rate.

1.7 Organization of the thesis

Chapter 2 investigates the MVC problem for single-input single-output linear systems sampled with different rates: fast, dual and slow rates. The conjecture is theoretically justified that a dual-rate (DR) controller performs better than an

SSR controller but worse than an FSR controller in the sense of minimum variance control. The optimal FSR, DR and SSR controllers are designed under the same performance criterion: variance of the fast sampled output. The discretization of continuous stochastic disturbance models is investigated preserving certain basic statistical properties. An LMI approach is developed to calculate the optimal controllers for DR and SSR loops.

Chapter 3 discusses MVC design and control performance assessment based on the MVC-benchmark for multirate systems. A lifted model is used to analyze the multirate system in a state-space framework and the lifting technique is applied to derive a subspace equation for multirate systems. From the subspace equation the multirate MVC law and the algorithm to estimate the multirate MVC-benchmark variance or performance index are developed. The multirate optimal controller is calculated from a set of input-output open-loop experimental data and thus this approach is data-driven since it does not involve an explicit model. In parallel, the presented MVC-benchmark estimation algorithm requires a set of open-loop experimental data and closed-loop routine operating data. No explicit models, namely, transfer function matrices, Markov parameters or interactor matrices, are needed. This is in contrast to traditional control performance assessment algorithms.

Chapter 4 is concerned with single-rate predictive control design. The predictive control applied is completely data based. In addition, unlike other data-driven predictive control designs, the proposed approach can deal with systems without complete on-line measurement of all output variables. It has been shown in previous studies that control of SOFC is challenging owing to the slow response and tight operating constraints [36]. In Chapter 4, the developed data-driven predictive control approach is applied to solving the control problem of the SOFC system [53, 85], and the simulation results have demonstrated the feasibility and robustness of the control application.

In Chapter 5 we mainly explore a data-driven predictive control law for multirate systems, when only the open-loop input-output data are available. This control design includes both feedback and feedforward control. Particularly, the developed dual-rate predictive control is verified by a multirate SOFC system, where the fuel utilization is sampled in slow rate while other variables are sampled in fast rate.

The last chapter summarizes the work in this thesis, and outlines some possible future research directions.

Chapter 2

Minimum Variance in Fast, Slow and Dual-rate Control Loops[1]

In certain industrial applications, the control updating rate is faster than the output sampling rate by a certain factor, which leads to dual-rate (DR) control problems. Generally speaking, a DR controller performs better than a SSR controller but worse than a FSR controller in the sense of minimum variance control. This conjecture is theoretically justified in this chapter for a continuous LTI single-input and single-output (SISO) system. The optimal FSR, DR and SSR controllers are designed under the same performance criterion: variance of the fast sampled output. The discretization of continuous stochastic disturbance models is investigated preserving certain basic statistical properties. A linear matrix inequality (LMI) approach is developed to calculate the optimal controllers for DR and SSR loops. The theoretical results are illustrated by two simulation examples.

[1]The materials in this chapter has been published in "X. Wang, L. Zhang, T. Chen, and B. Huang. Minimum variance in fast, slow and dual-rate control loops. Int. J. of Adaptive Contr. and Signal Processing, 19(8):575-600, 2005".

2.1 Introduction

In industry, processes almost always operate in continuous time while controllers execute their commands in the discrete-time domain, which constitutes sampled-data systems. Thus a sampled-data system is a hybrid system involving both continuous-time and discrete-time signals. In many applications of electrical, mechanical and chemical engineering, control signals and output measurements need to be sampled at different rates, leading to multirate sampled-data systems. The research on multirate systems began in the late 1950s. Much recent work on multirate systems has been done on the LQG/LQR design [47], the $\mathcal{H}_2$ design [10, 56, 67, 57], the $\mathcal{H}_\infty$ design [10, 11], and model identification and validation [42, 78]. Far less work has been done on multirate control-loop performance-monitoring.

There are many possible limitations or constraints on the achievable performance such as time delays and non-minimum phase dynamics. The most fundamental performance limitation is the time-delay. Time delays are fairly common in chemical processes and pose the main limitation toward minimum variance control [28]. This chapter is concerned with exploring and then analyzing the performance limits caused by time delays of multirate systems and single-rate systems. This topic is of importance to control specialists and process engineers who have implemented multirate control systems to their control loops. It is also meaningful to estimate the benefits of changing control loops from single-rate to multirate. Instead of treating general multirate systems, we consider the DR system where the sampling frequency of the controller output is M times that of the controller input (M is a positive integer). This setup holds most of the fundamental features of multirate systems while maintains some clarity in exposition. Loosely speaking, compared with SSR controllers, DR controllers can yield additional performance because of the fast-rate D/A converters (holds). But they obtain less measurement information than FSR controllers due to the slow-rate A/D converters (samplers). Hence, an intuitive thought is that a DR controller performs superior to an SSR controller but inferior to an FSR controller. This conjecture is proved in this chapter in the sense of minimum variance control by a theoretical analysis and two simulation examples.

To make a fair comparison, a uniform benchmark should be set up for the afore-

mentioned three kinds of control loops. Here we choose the variance of the fast sampled closed-loop output as the control cost function. It is known that the MVC is the best possible control in the sense that no controllers can provide a lower variance for linear systems with time delays. Many papers [22, 12, 68, 46, 28] have shown that minimum variance is a useful benchmark to assess control-loop performance. A significant one is [22] which presented a new direction and framework for the control-loop performance-monitoring area. It applied time-series analysis to find a suitable expression for the feedback controller-invariant term from routine operating data and subsequently used it as a benchmark to assess SISO control-loop performance. The filtering and correlation analysis in [28] extended this method to MIMO processes. An overview of the status of control performance monitoring using minimum variance principles is presented in [55]. In contrast to some results [10, 57] with criteria in continuous time for DR control, this chapter uses a criterion in the discrete-time domain. The rationales are: the existing benchmarks in the performance-monitoring field are all in discrete time; if the fast sampling interval is chosen small enough, we can almost guarantee the control performance even though the plant operates in continuous time; the problem may be simplified by choosing a criterion; considering the fast rate criterion, we may eliminate or reduce the possibility of inter-sample ripples for the slow sampled output in DR and SSR control loops. The advantage will be shown by comparing the control effects under the optimal controllers designed by fast-rate and slow-rate criteria in Section 2.6.

The systems studied are LTI systems driven by white noises (zero mean and unit variance). A fact is that the $\mathcal{H}_2$ norm square of this kind of systems equals the variance of the output signal. Hence, the MVC problem can be treated as a $\mathcal{H}_2$ optimal control problem. Many pieces of work for the $\mathcal{H}_2$ optimal control design of multirate systems have been completed. It is known that in general using the lifting technique [40], a LPTV multirate system can be transferred to an LTI one. In solving the multirate sampled-data $\mathcal{H}_2$ control problem using the lifting approach, one needs to solve a discrete-time $\mathcal{H}_2$ optimal control problem for a generalized plant with the consideration of the so-called causality constraint. This constraint restricts the direct feedthrough terms in lifted controllers to be (block) lower-triangular. This condition is induced by the fact that the control signal can only be a function of

present and past measurements during the period. There exist two techniques to solve this constrained $\mathcal{H}_2$ optimal control problem: a frequency-domain solution is shown in [56]; a more implementable one via state-space approach is presented in [67]. In this chapter the systems of concern are SISO ones, where the lifted controllers have the structures satisfying the causality constraint automatically. As shown in [10], using the state-space method to solve the $\mathcal{H}_2$ optimal control problem, the controllers can be obtained as explicit formulas in terms of the solutions of two Riccati equations. But the generalized plants need to satisfy several regularity assumptions. For the generalized plants of lifted DR and SSR control loops, it turns out that not all the regularity assumptions can be satisfied. Thus an LMI approach is exploited to find the optimal $\mathcal{H}_2$ controllers for DR and SSR control loops using output feedback. With this algorithm, the optimal performance can be obtained together with the optimal control law simultaneously. For the FSR control loops, the MVC law developed in [5, 6, 29] is applied.

This chapter is organized as follows. The problem is described in detail in Section 2.2. Section 2.3 presents a way to discretize a continuous-time noise model preserving the mean and auto-correlation. In Section 2.4, different methods are investigated to design the optimal controllers: the MVC law is applied to FSR control loops; then the solution to the discrete-time $\mathcal{H}_2$ optimal control problem is given via LMIs for plants not satisfying the regularity assumptions, which can handle the lifted DR and SSR control loops. Section 2.5 analyzes the reason why optimal DR controllers have performance between optimal FSR controllers and SSR controllers. Two illustrative examples are provided in Section 2.6, followed by conclusions in Section 2.7.

2.2 Problem statement

Considering a continuous SISO plant, P_c, and a continuous SISO noise, N_c, as shown in Fig. 2.1, where a is a continuous-time standard white noise, and y_t and u_t are the continuous output and control signals, we have three objectives. The first objective is to design discrete output feedback controllers K_f, K_d and K_s, which are shown in Fig. 2.2 where H_f and S_f are the fast hold and sampler, H_s and S_s are the slow hold and sampler, u_f and y_f are the fast sampled control and output signals, and u_s and y_s are the slow sampled signals. Controllers K_f, K_d and K_s are of three

different rates: fast-rate, dual-rate and slow-rate respectively and their targets are the same: minimizing the variance of the fast sampled closed-loop output y_f, which is also defined as:

$$J = \min\left[Var(y_f)\right].$$

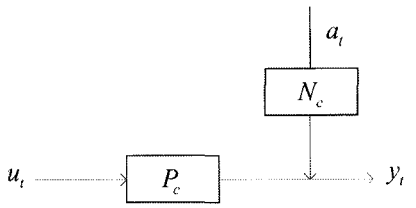

Figure 2.1: The open-loop diagram

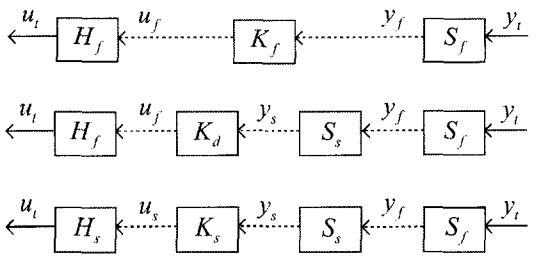

Figure 2.2: The fast-rate, dual-rate and slow-rate controllers

The second objective is to find J_{fast}, J_{dual} and J_{slow} for FSR, DR and SSR control loops respectively after the derivation of the optimal controllers. In general, the DR controllers outperform SSR controllers but are outperformed by FSR controllers, which can be presented as:

$$J_{fast} \leqslant J_{dual} \leqslant J_{slow}.$$

The third objective is to prove this conjecture through a theoretical analysis.

2.3 Noise model discretization

Although our problem begins in the continuous-time domain, to design a discrete controller, the discretization of the noise model is necessary. There are many meth-

ods to discretize LTI continuous systems to discrete-time systems with deterministic inputs, such as zero-order hold, bilinear (Tustin) approximation and impulse-invariant discretization. But now we are concerned with the problem of finding suitable ways to characterize a stochastic continuous disturbance model with a stochastic discrete one. It is desirable to preserve some basic statistical properties. The method to be developed below preserves the properties of the mean and auto-correlation of the continuous system output at the sampling instances.

Theorem 2.1 *Given a stable, strictly proper stochastic continuous disturbance model N_c (the system starts at $t = -\infty$), which has the state space model*

$$N_c = \left[\begin{array}{c|c} A & B \\ \hline C & 0 \end{array}\right]$$

where the input is a standard white noise a, if the discretized model N_d is given by

$$N_d = \left[\begin{array}{c|c} A_d & B_d \\ \hline C & 0 \end{array}\right],$$

where $A_d = e^{hA}$, $B_d B_d^T = \int_0^h e^{tA} B B^T e^{tA^T} dt$, and h is the sampling period, then N_d, subject to a discrete white noise input, preserves the mean and the auto-correlation of the output of N_c at the sampling instances.

Proof. Considering the continuous model N_c, which can be expressed as

$$\begin{aligned} \dot{x} &= Ax + Ba, \\ y &= Cx, \end{aligned}$$

at sampling time t_k, it can be seen that

$$\begin{aligned} x_{t_k} &= e^{hA} x_{t_{k-1}} + \int_{t_{k-1}}^{t_k} e^{(t_k - t)A} B a(t) dt \\ &= \left(e^{hA}\right)^k x_0 + \left(e^{hA}\right)^{k-1} \int_0^h e^{(h-t)A} B a(t) dt + \cdots + \int_{t_{k-1}}^{t_k} e^{(t_k - t)A} B a(t) dt, \end{aligned} \tag{2.1}$$

and

$$\begin{aligned} x_{t_{k+l}} &= e^{hA} x_{tk+l-1} + \int_{t_{k+l-1}}^{t_{k+l}} e^{(t_{k+l}-t)A} Ba(t)dt \\ &= \left(e^{hA}\right)^{k+l} x_0 + \left(e^{hA}\right)^{k+l-1} \int_0^h e^{(t_k-t)A} Ba(t)dt + \cdots \\ &+ \left(e^{hA}\right)^{l} \int_{t_{k-1}}^{t_k} e^{(t_k-t)A} Ba(t)dt + \cdots + \int_{t_{k+l-1}}^{t_{k+l}} e^{(t_{k+l}-t)A} Ba(t)dt. \end{aligned} \tag{2.2}$$

Noticing that $x_0 = 0$ and $y_{t_k} = Cx_{t_k}$, the expectation of y_{t_k} should be zero, i.e.

$$E(y_{t_k}) = 0. \tag{2.3}$$

From (2.1), (2.2) and $A_d = e^{hA}$, the auto-correlation of y_{t_k} can be calculated as

$$\begin{aligned} R\left[y_{t_k}(l)\right] &= E\left\{y_{t_k} y_{t_{k+l}}^T\right\} = CE\left\{x_{t_k} x_{t_{k+l}}^T\right\} C^T \\ &= C\{A_d^{k-1} \int_0^h e^{tA} BB^T e^{tA^T} dt A_d^{Tk+l-1} + \cdots \\ &+ \int_{t_{k-1}}^{t_k} e^{(t_k-t)A} BB^T e^{(t_k-t)A^T} dt A_d^{Tl}\} C^T \\ &= C\{A_d^{k-1} \int_0^h e^{tA} BB^T e^{tA^T} dt A_d^{Tk-1} + \cdots + \int_0^h e^{tA} BB^T e^{tA^T} dt A_d^{Tl}\} C^T. \end{aligned}$$

Substituting $\int_0^h e^{tA} BB^T e^{tA^T} dt = B_d B_d^T$ into the above equation, it gives

$$\begin{aligned} R\left[y_{t_k}(l)\right] &= C\left\{A_d^{k-1} B_d B_d^T A_d^{Tk-1} + A_d^{k-2} B_d B_d^T A_d^{Tk-2} + \cdots + B_d B_d^T\right\} A_d^{Tl} C^T \\ &= C L_d A_d^{Tl} C^T, \end{aligned} \tag{2.4}$$

where L_d is the unique symmetric solution of the discrete Lyapunov equation $L_d = A_d L_d A_d^T + B_d B_d^T$.

Considering the discrete stochastic system N_d, we have

$$\begin{aligned} x_k &= A_d^k x_0 + A_d^{k-1} B_d a_0 + \cdots + A_d B_d a_{k-2} + B_d a_{k-1}, \\ x_{k+l} &= A_d^{k+l} x_0 + A_d^{k+l-1} B_d a_0 + \cdots + A_d^l B_d a_{k-1} + \cdots + B_d a_{k+l-1}. \end{aligned}$$

It can be seen that

$$E(y_k) = 0 \tag{2.5}$$

and

$$\begin{aligned} R\left[y_k\left(l\right)\right] &= E\left\{y_k y_{k+l}^T\right\} = CE\left\{x_k x_{k+l}^T\right\} C^T \\ &= C\left\{A_d^{k-1} B_d B_d^T A_d^{Tk-1} + A_d^{k-2} B_d B_d^T A_d^{Tk-2} + \cdots + B_d B_d^T\right\} A_d^{Tl} C^T \\ &= C L_d A_d^{Tl} C^T. \end{aligned} \tag{2.6}$$

From (2.3)-(2.6), it is clear that

$$E(y_{t_k}) = E(y_k),\ R\left[y_{t_k}\left(l\right)\right] = R\left[y_k\left(l\right)\right].$$

Thus the theorem is proved. ■

It is noticed that the solution of equation $B_d B_d^T = \int_0^h e^{tA} B B^T e^{tA^T} dt$ is not unique. A simple way to solve B_d from this equation is through the Cholesky factorization. But using this method the dimension of B_d may be different from that of B, e.g, in the later numerical simulation example for the given SISO continuous noise model N_c we obtain a 1×2 multi-input single-output (MISO) discrete model $N_d = \left[\begin{array}{cc} N_{d1} & N_{d2} \end{array}\right]$. We need to combine N_{d1} and N_{d2} to a SISO discrete model to keep the same input dimension. To this end the co-inner-outer factorization method is applied. Suppose N_d is stable and has no zeros on the unit circle, the inner-outer factorization of N_d^T is as

$$N_{d(2\times1)}^T = N_{i(2\times1)} N_{o(1\times1)}$$

or

$$N_{d(1\times2)} = N_{o(1\times1)}^T N_{i(1\times2)}^T = N_{co(1\times1)} N_{ci(1\times2)},$$

where N_{co} is the co-outer factor and N_{ci} is the co-inner factor [16]. Because we have $N_{ci}\tilde{N_{ci}} = I$, where $\tilde{N_{ci}}$ is the shorthand for $N_{ci}^T(z^{-1})$. It can be seen that N_{co} and N_d have the same $\mathcal{H}_2$ norm. Thus we can use N_{co} instead of N_d to present the discrete noise model. The algorithm in [30] is applied to calculate the inner-outer factorization, which is numerically effective. Thus till now we have presented a method which discretizes a continuous stochastic disturbance model to a discrete one preserving the mean and the auto-correlation.

2.4 The minimum variance controller design

The objective of this section is to design the optimal controllers for FSR, DR and SSR control loops. As we have discussed before, the MVC problem is similar to the

$\mathcal{H}_2$ optimal control problem for linear systems which are driven by white noises. The MVC law is directly applied to FSR control loops to obtain the optimal controllers. The generalized models of DR and SSR control loops are obtained via the lifting technique. Since it can be found that the derived models do not satisfy all the regularity assumptions of the general discrete-time $\mathcal{H}_2$ optimal control problem [10], an LMI method is developed to handle the lifted DR and SSR control loops.

2.4.1 The FSR control loop

The principle of MVC was pioneered by [5]. A more explicit solution can be found in [29]. Here we design an output feedback controller for the fast-rate loop. The output of the fast-rate loop can be written as

$$\begin{aligned} y_f &= \frac{N_f}{1-P_fK_f}a = \frac{F_f + z^{-d_f}R_f}{1-P_fK_f}a = F_fa + \frac{z^{-d_f}(R_f + \widetilde{P}_fK_fF_f)}{1-P_fK_f}a \\ &= \left(D_n + z^{-1}C_nB_n + z^{-2}C_nA_nB_n + \cdots . + z^{-d_f+1}C_nA_n^{d_f-2}B_n\right)a \\ &+ \frac{z^{-d_f}(R_f + \widetilde{P}_fK_fF_f)}{1-P_fK_f}a, \end{aligned}$$

where N_f, P_f, d_f and K_f are the fast-rate noise, plant, time delay and controller respectively; $\widetilde{P}_f$ is the delay-free plant transfer function; a_k is a discrete-time standard white noise at the fast rate. Using Diophantine equation or long division [6], we have $N_f = F_f + z^{-d_f}R_f$ and F_f is the first d_f controller-invariant term of y_f. The state space model of N_f is given as

$$N_f = \left[\begin{array}{c|c} A_n & B_n \\ \hline C_n & D_n \end{array}\right]. \tag{2.7}$$

It can be observed that when

$$K_f = -\widetilde{P}_f^{-1}R_fF_f^{-1},$$

the variance of y_f is minimal, that is, the minimum variance of the FSR loop is

$$J_{fast} = Var(F_fa) = D_n^2 + (C_nB_n)^2 + (C_nA_nB_n)^2 + \cdots + \left(C_nA_n^{d_f-2}B_n\right)^2. \tag{2.8}$$

2.4.2 The DR control loop

The DR controller K_d in Fig. 2.2 is time-varying due to the presence of H_f and S_s. To avoid dealing with the time-varying DR controller directly, here we introduce the lifting technique, which can be attributed to Kranc in 1957 [40]. Let y be a discrete-time signal:

$$y = \{y(0),\ y(1),\ y(2),\ \cdots\},$$

and $\underline{y}$ be the vectored-valued sequence as follows:

$$\underline{y} = \left\{ \begin{bmatrix} y(0) \\ \vdots \\ y(M-1) \end{bmatrix}, \begin{bmatrix} y(M) \\ \vdots \\ y(2M-1) \end{bmatrix}, \cdots \right\}.$$

The map from y to $\underline{y}$ is then defined as the lifting operator L_M. After lifting, both the signal dimension and the underlying period are increased by a factor of M. The inverse lifting operator L_M^{-1} is defined in the obvious way. It can be seen that $L_M^{-1} L_M = I$.

Introducing the lifting operator and inverse lifting operator, the DR closed-loop can be transferred to an LTI system in Fig. 2.3, where $\underline{P}$ is the lifted version of the fast plant model P_f; $\underline{N}$ is the lifted version of the fast disturbance model N_f; $\underline{y_f}$ is the lifting of the fast sampled output y_f; $\underline{u}$ is the lifting of the fast control signal u_f; a is the nth dimensional lifted version of the discrete standard white noise. Fig. 2.3 can be further simplified to Fig. 2.4, where $\underline{N}$, $\underline{P}$, $\underline{u}$ and a have been defined before; $S = S_s L_M^{-1} = \begin{bmatrix} I & 0 & \cdots & 0 \end{bmatrix}$ (M blocks). Combining the lifting operator L_M and the DR time-varying controller K_d, the lifted DR controller is as: $\underline{K_d} = L_M K_d = \begin{bmatrix} K_1 & K_2 & \cdots & K_M \end{bmatrix}^T$, which is time-invariant and satisfying the causality constraint by its special structure. The generalized model of Fig. 2.4 can be expressed as:

$$\begin{bmatrix} \underline{y_f} \\ y_s \end{bmatrix} = \begin{bmatrix} \underline{N} & \underline{P} \\ S\underline{N} & S\underline{P} \end{bmatrix} \begin{bmatrix} a \\ \underline{u} \end{bmatrix}, \tag{2.9}$$

where $\underline{y_f}$ is the signal to be controlled, a is the disturbance, and y_s, $\underline{u}$ are the controller input and output signals respectively. It is known that stationary random processes, when passed through multirate systems, become cyclo-stationary [4]. Thus the fast-sampled output of the DR system, y_f, is a cyclo-stationary signal. Its

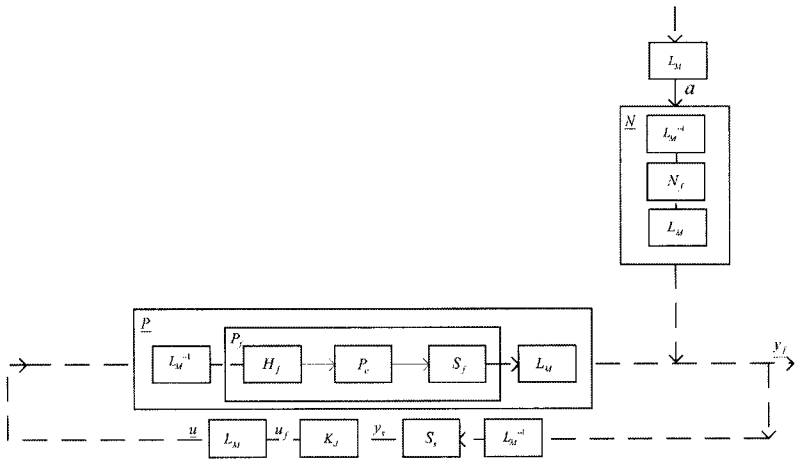

Figure 2.3: The lifted DR closed-loop diagram

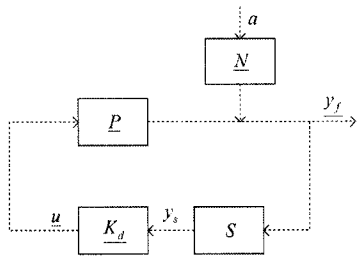

Figure 2.4: The lifted dual-rate closed-loop sketch

variance is periodic with period M. The control objective is to design the optimal controller to minimize the average of the variance of y_f. The minimum cost function of the DR control-loops is defined as:

$$J_{dual} = \min_{K_d} \left[\frac{\sum_{i=1}^{M} Var(y_{fi})}{M} \right] = \min_{K_d} trace \left[\frac{Var(\underline{y_f})}{M} \right], \tag{2.10}$$

where y_{fi} is ith row of the lifted output $\underline{y_f}$.

2.4.3 The SSR control loop

By the lifting technique, the lifted SSR closed-loop diagram can be drawn in Fig. 2.5. Here we change the slow holder $H_s = H_f S_f H_s$. Then Fig. 2.5 can be simplified to Fig. 2.6, where $H = L_M S_f H_s = \left[\begin{array}{ccc} I & \cdots & I \end{array} \right]^T$ (M blocks). The generalized model of Fig. 2.6 can be written as:

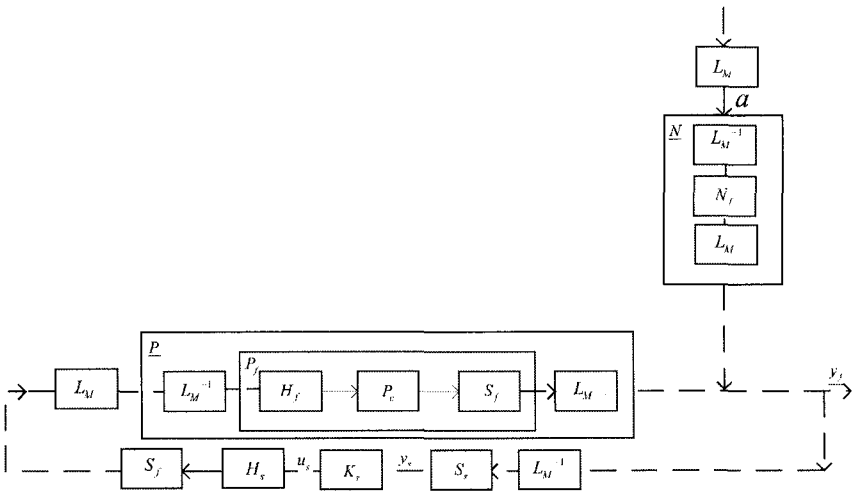

Figure 2.5: The lifted slow-rate closed-loop diagram

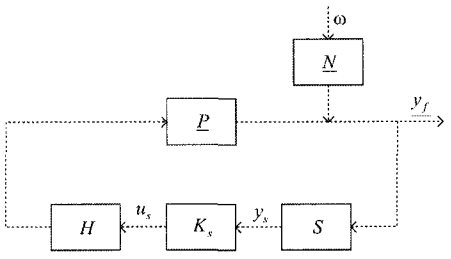

Figure 2.6: The lifted slow rate closed-loop sketch

$$\begin{bmatrix} \underline{y_f} \\ y_s \end{bmatrix} = \begin{bmatrix} \underline{N} & \underline{P}H \\ S\underline{N} & S\underline{P}H \end{bmatrix} \begin{bmatrix} a \\ u_s \end{bmatrix}, \tag{2.11}$$

where $\underline{y_f}$, a and y_s are of the same meanings as defined in the previous subsection. The only difference is that here u_s is the controller output signal. Because y_f is cyclo-stationary, similarly to the DR minimum control cost function, the slow-rate one is defined as:

$$J_{slow} = \min_{K_s} \left[\frac{\sum_{i=1}^{M} Var(y_{fi})}{M} \right] = \min_{K_s} trace \left[\frac{Var(\underline{y_f})}{M} \right]. \tag{2.12}$$

Now we show that the generalized plants do not satisfy all the regularity assumptions for the general discrete-time $\mathcal{H}_2$ optimal control problem by the state-space

approach. The generalized lifted dual-rate and slow-rate models (2.9), (2.11) can be put into the same structure as

$$G = \left[\begin{array}{c|cc} A & B_a & B \\ \hline C_z & D_{za} & D_z \\ C & D_a & D_u \end{array}\right]. \tag{2.13}$$

If the fast-rate plant model is given as

$$P_f = \left[\begin{array}{c|c} A_f & B_f \\ \hline C_f & D_f \end{array}\right], \tag{2.14}$$

then its lifted version is ([10])

$$\underline{P} = \left[\begin{array}{c|ccc} A_f^M & A_f^{M-1}B_f & A_f^{M-2}B_f & \cdots & B_f \\ \hline C_f & D_f & 0 & \cdots & 0 \\ C_fA_f & C_fB_f & D_f & \cdots & 0 \\ \vdots & \vdots & \vdots & \ddots & \vdots \\ C_fA_f^{M-1} & C_fA_f^{M-2}B_f & C_fA_f^{M-3}B_f & \cdots & D_f \end{array}\right] = \left[\begin{array}{c|c} A_l & B_l \\ \hline C_l & D_l \end{array}\right]. \tag{2.15}$$

Considering the generalized model of the lifted DR loop, it can be seen from (2.9) and (2.13) that $D_z = D_l$ and $D_u = SD_l = [\ D_f \ \ 0 \ \cdots \ 0\ ]$ (M blocks). Considering the lifted SSR case, from (2.11) and (2.13) we have $D_z = D_lH$ and $D_u = D_f$. Because the fast plant model has time delays, which means $D_f = 0$, thus in the common model G, D_z does not always have full column rank which violates one of the regularity assumptions in [10]. This is the motivation that we use the LMI approach to find the optimal control solution.

2.4.4 LMI $\mathcal{H}_2$ optimal controller design

In this subsection, we will design the optimal output feedback controller for a generalized model G, which has the state space model as follows

$$G = \left[\begin{array}{c|cc} A & B_a & B \\ \hline C_z & D_{za} & D_z \\ C & D_a & 0 \end{array}\right]. \tag{2.16}$$

The input and output signals of G are $\begin{bmatrix} a(k) \\ u(k) \end{bmatrix}$ and $\begin{bmatrix} z(k) \\ y(k) \end{bmatrix}$ respectively, and the state of G is $x(k)$. The output feedback controller K_d is as

$$\xi(k+1) = A_K\xi(k) + B_K y(k), \tag{2.17}$$

$$u(k) = C_K\xi(k) + D_K y(k), \tag{2.18}$$

where $\xi(k)$ is the state vector of the controller of the same dimension as $x(k)$.

The optimal control problem can be stated as: for the discrete-time system (2.16), find a controller given by (2.17) and (2.18) such that the resulting closed-loop system is stable and its $\mathcal{H}_2$ norm square from a to z, denoted as $\|T_{za}\|_2^2$, is as small as possible, that is

$$\min_{s.t.\|T_{za}\|_2^2<\gamma} \gamma. \tag{2.19}$$

The resulted closed-loop system from G and the controller in (2.17) and (2.18) has the state space model as

$$x_{cl}(k+1) = \tilde{A}x_{cl}(k) + \tilde{B}_a a(k),$$
$$z(k) = \tilde{C}x(k) + \tilde{D}_a a(k),$$

where

$$x_{cl}(k) = \begin{bmatrix} x(k) \\ \xi(k) \end{bmatrix},\ \tilde{A} = \begin{bmatrix} A + BD_KC & BC_K \\ B_KC & A_K \end{bmatrix},\ \tilde{B}_a = \begin{bmatrix} B_a + BD_KD_a \\ B_KD_a \end{bmatrix},$$
$$\tilde{C} = \begin{bmatrix} C_z + D_zD_KC & D_zC_K \end{bmatrix},\ \tilde{D}_a = D_{za} + D_zD_KD_a.$$

The $\mathcal{H}_2$ norm of the closed-loop system is:

$$\|T_{za}\|_2 = \sqrt{trace(\tilde{C}\tilde{Y}\tilde{C}^T + \tilde{D}_a\tilde{D}_a^T)} = \sqrt{trace(\tilde{B}_a^T\tilde{X}\tilde{B}_a + \tilde{D}_a^T\tilde{D}_a)},$$

where $\tilde{X}$ and $\tilde{Y}$ are the symmetric solutions of the following discrete Lyapunov equations:

$$\tilde{A}\tilde{Y}\tilde{A}^T - \tilde{Y} + \tilde{B}_a\tilde{B}_a^T = 0,$$
$$\tilde{A}^T\tilde{X}\tilde{A} - \tilde{X} + \tilde{C}^T\tilde{C} = 0.$$

Based on the above analysis, we have the following theorems:

Theorem 2.2 *[63] For the closed-loop system, $\|T_{za}\|_2^2 < \gamma$ if and only if the following matrix inequalities*

$$\begin{aligned} &trace(\tilde{C}\tilde{Y}\tilde{C}^T + \tilde{D}_a\tilde{D}_a^T) < \gamma, \\ &-\tilde{Y} + \tilde{A}\tilde{Y}\tilde{A}^T + \tilde{B}_a\tilde{B}_a^T < 0 \end{aligned} \tag{2.20}$$

hold for $\tilde{Y} > 0$, or dually

$$trace(\tilde{B}_a^T\tilde{X}\tilde{B}_a + \tilde{D}_a^T\tilde{D}_a) < \gamma, \tag{2.21}$$

$$\tilde{A}^T\tilde{X}\tilde{A} - \tilde{X} + \tilde{C}^T\tilde{C} < 0 \tag{2.22}$$

for $\tilde{X} > 0$.

Theorem 2.3 *For a discrete-time plant G in (2.16), there exists an output feedback controller in (2.17) and (2.18) such that $\|T_{za}\|_2^2 < \gamma$ if and only if the following LMIs are feasible:*

$$\begin{bmatrix} -X & -I & \left(AX + B\hat{C}\right)^T & \hat{A}^T & \left(C_zX + D_z\hat{C}\right)^T \\ -I & -Y & \left(A + B\hat{D}C\right)^T & \left(YA + \hat{B}C\right)^T & \left(C_z + D_z\hat{D}C\right)^T \\ AX + B\hat{C} & A + B\hat{D}C & -X & -I & 0 \\ \hat{A} & YA + \hat{B}C & -I & -Y & 0 \\ C_zX + D_z\hat{C} & C_z + D_z\hat{D}C & 0 & 0 & -I \end{bmatrix} < 0, \tag{2.23}$$

$$\begin{bmatrix} -P & \left(B\hat{D}D_a + B_a\right)^T & \left(\hat{B}D_a + YB_a\right)^T & \left(D_z\hat{D}D_a + D_{za}\right)^T \\ B\hat{D}D_a + B_a & -X & -I & 0 \\ \hat{B}D_a + YB_a & -I & -Y & 0 \\ D_z\hat{D}D_a + D_{za} & 0 & 0 & -I \end{bmatrix} < 0, \tag{2.24}$$

$$trace(P) < \gamma \tag{2.25}$$

If (2.23)-(2.25) are feasible, the controller is given as

$$A_K = N^{-1}\left[\hat{A} - NB_KCX - YBC_KW^T - Y(A + B\hat{D}C)X\right](W^T)^{-1}, \tag{2.26}$$

$$B_K = N^{-1}(\hat{B} - YB\hat{D}), \tag{2.27}$$

$$C_K = (\hat{C} - \hat{D}CX)(W^T)^{-1}, \tag{2.28}$$

$$D_K = \hat{D}. \tag{2.29}$$

Here P, X, Y, $\hat{A}$, $\hat{B}$, $\hat{C}$, $\hat{D}$ are LMI variables where $P > 0$, and X and Y are symmetric. W and N are invertible matrices such that

$$WN^T = I - XY. \tag{2.30}$$

Proof. The similar method to design continuous-time controllers can be found in [64]. Let n be the number of states of the plant. $\tilde{X}$ and $\tilde{X}^{-1}$ can be partitioned as

$$\tilde{X} = \begin{bmatrix} Y & N \\ N^T & * \end{bmatrix}, \ \tilde{X}^{-1} = \begin{bmatrix} X & W \\ W^T & * \end{bmatrix}$$

where X and Y are $n \times n$ and symmetric. Let us now define

$$\Pi_1 = \begin{bmatrix} X & I \\ W^T & 0 \end{bmatrix}, \ \Pi_2 = \begin{bmatrix} I & Y \\ 0 & N^T \end{bmatrix}, \tag{2.31}$$

and the change of controller variables as follows:

$$\hat{A} = NA_KW^T + NB_KCX + YBC_KW^T + Y(A + BD_KC)X, \tag{2.32}$$

$$\hat{B} = NB_K + YBD_K, \tag{2.33}$$

$$\hat{C} = C_KW^T + D_KCX, \tag{2.34}$$

$$\hat{D} = D_K. \tag{2.35}$$

The motivation for this transformation lies in the following identities derived from (2.31)-(2.35):

$$\Pi_1^T\tilde{X}\tilde{A}\Pi_1 = \begin{bmatrix} AX + B\hat{C} & A + B\hat{D}C \\ \hat{A} & YA + \hat{B}C \end{bmatrix},$$

$$\Pi_1^T\tilde{X}\tilde{B}_a = \begin{bmatrix} BD_KD_a + B_a \\ \hat{B}D_a + YB_a \end{bmatrix},$$

$$\tilde{C}\Pi_1 = \begin{bmatrix} C_zX + D_z\hat{C} & C_z + D_z\hat{D}C \end{bmatrix},$$

$$\Pi_1^T\tilde{X}\Pi_1 = \begin{bmatrix} X & I \\ I & Y \end{bmatrix}.$$

From Theorem 2.2, we need (2.21) and (2.22) to hold. By Schur complements, (2.22)

is equivalent to

$$\begin{bmatrix} -\tilde{X} & \tilde{A}^T\tilde{X} & \tilde{C}^T \\ \tilde{X}\tilde{A} & -\tilde{X} & 0 \\ \tilde{C} & 0 & -I \end{bmatrix} < 0 \Leftrightarrow$$

$$\begin{bmatrix} \Pi_1^T & 0 & 0 \\ 0 & \Pi_1^T & 0 \\ 0 & 0 & I \end{bmatrix} \begin{bmatrix} -\tilde{X} & \tilde{A}^T\tilde{X} & \tilde{C}^T \\ \tilde{X}\tilde{A} & -\tilde{X} & 0 \\ \tilde{C} & 0 & -I \end{bmatrix} \begin{bmatrix} \Pi_1 & 0 & 0 \\ 0 & \Pi_1 & 0 \\ 0 & 0 & I \end{bmatrix} < 0 \Leftrightarrow$$

$$\begin{bmatrix} -\Pi_1^T\tilde{X}\Pi_1 & \Pi_1^T\tilde{A}^T\tilde{X}\Pi_1 & \Pi_1^T\tilde{C}^T \\ \Pi_1^T\tilde{X}\tilde{A}\Pi_1 & -\Pi_1^T\tilde{X}\Pi_1 & 0 \\ \tilde{C}\Pi_1 & 0 & -I \end{bmatrix} < 0. \tag{2.36}$$

On the other hand, (2.21) is equivalent to:

$$\tilde{B}_a^T\tilde{X}\tilde{B}_a + \tilde{D}_a^T\tilde{D}_a < P, \tag{2.37}$$

$$trace(P) < \gamma, \tag{2.38}$$

for $P > 0$. By Schur complements again, (2.37) can be written as:

$$\begin{bmatrix} -P & \tilde{B}_a^T\tilde{X} & \tilde{D}_a^T \\ \tilde{X}\tilde{B}_a & -\tilde{X} & 0 \\ \tilde{D}_a & 0 & -I \end{bmatrix} < 0 \Leftrightarrow$$

$$\begin{bmatrix} I & 0 & 0 \\ 0 & \Pi_1^T & 0 \\ 0 & 0 & I \end{bmatrix} \begin{bmatrix} -P & \tilde{B}_a^T\tilde{X} & \tilde{D}_a^T \\ \tilde{X}\tilde{B}_a & -\tilde{X} & 0 \\ \tilde{D}_a & 0 & -I \end{bmatrix} \begin{bmatrix} I & 0 & 0 \\ 0 & \Pi_1 & 0 \\ 0 & 0 & I \end{bmatrix} < 0 \Leftrightarrow$$

$$\begin{bmatrix} -P & \tilde{B}_a^T\tilde{X}\Pi_1 & \tilde{D}_a^T \\ \Pi_1^T\tilde{X}\tilde{B}_a & -\Pi_1^T\tilde{X}\Pi_1 & 0 \\ \tilde{D}_a & 0 & -I \end{bmatrix} < 0. \tag{2.39}$$

After simple calculations, (2.36) and (2.39) can be transferred to (2.23) and (2.24) respectively. Inequality (2.38) is the same as (2.25). Thus the problem is already changed to three LMIs (2.23)-(2.25). If these LMIs are feasible, P, X, Y, $\hat{A}$, $\hat{B}$, $\hat{C}$, $\hat{D}$ can be solved. If W and N are invertible, (2.26)-(2.29) can be obtained from (2.32)-(2.35). It has been proved in [64] that one can always find invertible matrices W and N satisfying (2.30). ■

Noticing that the control objective function shown in (2.19) is to minimize the variance of the lifted fast sampled output of the lifted DR and SSR systems, thus from (2.10) and (2.12) we have

$$J_{dual} = \min \left[\frac{\|T_{za}\|_{2dual}^2}{M} \right], \; J_{slow} = \min \left[\frac{\|T_{za}\|_{2slow}^2}{M} \right], \tag{2.40}$$

where $\|T_{za}\|^2_{2dual}$, $\|T_{za}\|^2_{2slow}$ denote the square of the $\mathcal{H}_2$ norms of the lifted closed-loop DR and SSR systems, respectively.

2.5 Comparison of the minimum variance of FSR, DR and SSR control loops

In this section, the objective is to calculate and then compare the minimum cost functions of FSR, DR and SSR loops, which are denoted as J_{fast}, J_{dual}, and J_{slow}. The conjecture that $J_{fast} \leqslant J_{dual} \leqslant J_{slow}$ is proved theoretically by two parts: the first subsection shows that $J_{dual} \leqslant J_{slow}$; the second subsection shows that $J_{dual} \geqslant J_{fast}$.

2.5.1 Comparison of DR and SSR control loops

In this subsection, J_{dual} and J_{slow} will be compared. The lifted dual-rate closed-loop system (Fig. 2.4) and the lifted slow-rate closed-loop system (Fig. 2.6) can be generalized to the same system (Fig. 2.7), except that the lifted DR controller is $\begin{bmatrix} K_1 & K_2 & \cdots & K_M \end{bmatrix}^T$ while the lifted SSR controller is $\begin{bmatrix} K_s & K_s & \cdots & K_s \end{bmatrix}^T$, where K_s is the SSR optimal controller. From the controller structures we can see that the lifted SSR optimal control problem is a constrained lifted DR optimal problem, i.e., the optimum solution must satisfy $K_1 = K_2 = \cdots = K_M$. Hence, the solution, $\min\left[\|T_{za}\|^2_{2slow}\right]$, obtained from (2.19) in the lifted SSR control-loop is a constrained minimum whereas the solution of the lifted DR control-loop, $\min\left[\|T_{za}\|^2_{2dual}\right]$, is the unconstraint minimum. So according to (2.40), the minimum cost function of DR control-loop must be less than or equal to that of the SSR control-loop, which gives:

$$J_{dual} \leqslant J_{slow}.$$

2.5.2 Comparison of DR and FSR control loops

In this subsection, we will calculate the minimum cost functions of DR and FSR control-loops: J_{dual} and J_{fast} and then prove that $J_{dual} \geqslant J_{fast}$. Recalling (2.8), the fast-rate minimum variance is as

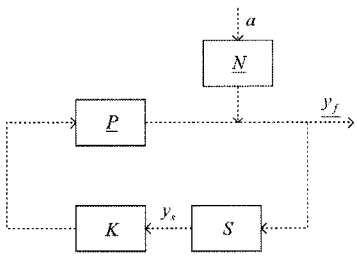

Figure 2.7: The slow/dual-rate closed-loop sketch

$$J_{fast} = D_n^2 + (C_n B_n)^2 + (C_n A_n B_n)^2 + \cdots + \left(C_n A_n^{d_f - 2} B_n\right)^2. \tag{2.41}$$

To calculate J_{dual}, we must know the time delay of the lifted DR loop, which is defined as d_{dual}. The following parts will first investigate the time delay of the lifted plant model, then calculate the minimum cost function of the lifted DR loop.

Pure time delay of the lifted plant model

In this part the pure time delay of the lifted plant model will be discussed. Given the FSR plant transfer function as $P_f(z) = z^{-d_f}\widetilde{P_f}(z)$ where d_f is the fast-rate time delay and $\widetilde{P_f}(z)$ is the delay-free plant transfer function. If the pure time delay of the lifted plant, d_{dual}, is defined as the number of initial zero matrices in the impulse, then it satisfies: when $\frac{d_f}{M} = k$, $d_{dual} = k$; when $\frac{d_f}{M} = k + \frac{i}{M}$, $d_{dual} = k$, where k, i are integers and $i \in \{1, \cdots, M-1\}$. This property can be proved by the following analysis.

The state-space model of the fast rate plant is (2.14), which gives the impulse response of the fast rate plant as follows:

$$H_{P_f} : \{h_0,\ h_1,\ \cdots,\ h_{d_f-1},\ h_{d_f},\ \cdots\}$$

where

$$\begin{aligned} h_0 &= D_f = 0, \\ h_1 &= C_f B_f = 0, \\ &\vdots \\ h_{d_f-1} &= C_f A_f^{d_f-2} B_f = 0, \\ h_{d_f} &= C_f A_f^{d_f-1} B_f \neq 0, \\ &\vdots \end{aligned}$$

When $\frac{d_f}{M} = k$, the impulse response sequence of $\underline{P}$ is as:

$$H_{\underline{P}} = \{h_{\underline{P}0}, \cdots, \ h_{\underline{P}k}, \ \cdots\}$$

where

$$h_{\underline{P}0} = \begin{bmatrix} D_f & 0 & \cdots & 0 \\ C_f B_f & D_f & \cdots & 0 \\ \vdots & \vdots & \ddots & \vdots \\ C_f A_f^{M-2} B_f & C_f A_f^{M-3} B_f & \cdots & D_f \end{bmatrix},$$

$$\vdots$$

$$h_{\underline{P}k} = \begin{bmatrix} C_f A_f^{d_f-1} B_f & 0 & \cdots & 0 \\ C_f A_f^{d_f} B_f & C_f A_f^{d_f-1} B_f & \cdots & 0 \\ \vdots & \vdots & \ddots & \vdots \\ C_f A_f^{d_f+M-2} B_f & C_f A_f^{d_f+M-3} B_f & \cdots & C_f A_f^{d_f-1} B_f \end{bmatrix},$$

$$\vdots$$

Since $C_f A_f^{d_f-1} B_f \neq 0$, it can be seen that: the first k blocks are zero matrices; the $(k+1)\,th$ block $h_{\underline{P}k}$ is the first non-singular one. Hence,

$$d_{dual} = k, \ \underline{P}(z) = z^{-d_{dual}} \widetilde{\underline{P}}(z) \tag{2.42}$$

where $\underline{P}(z)$ is the lifted plant transfer function matrix and $\widetilde{\underline{P}}(z)$ is the pure delay-free transfer function matrix of the lifted plant. When $\frac{d_f}{M} = k + i$, the impulse response of the lifted plant $\underline{P}$ is

$$H_{\underline{P}} = \{h_{\underline{P}0}, \ \cdots, \ h_{\underline{P}k}, \ h_{\underline{P}(k+1)}, \ \cdots\}$$

where

$$h_{\underline{P}0} = \begin{bmatrix} D_f & 0 & \cdots & 0 \\ C_f B_f & D_f & \cdots & 0 \\ \vdots & \vdots & \ddots & \vdots \\ C_f A_f^{M-2} B_f & C_f A_f^{M-3} B_f & \cdots & D_f \end{bmatrix},$$

$$\vdots$$

$$h_{\underline{P}k} = \begin{bmatrix} 0 & 0 & 0 & 0 & 0 & \cdots & 0 \\ 0 & 0 & 0 & 0 & 0 & \cdots & 0 \\ \vdots & \vdots & \vdots & \vdots & \vdots & \cdots & \vdots \\ C_f A_f^{d_f-1} B_f & 0 & 0 & 0 & 0 & \cdots & 0 \\ C_f A_f^{d_f} B_f & C_f A_f^{d_f-1} B_f & 0 & 0 & 0 & \cdots & 0 \\ \vdots & \vdots & \ddots & \vdots & \vdots & \cdots & \vdots \\ C_f A_f^{M(k+1)-2} B_f & C_f A_f^{M(k+1)-3} B_f & \cdots & C_f A_f^{d_f-1} B_f & 0 & \cdots & 0 \end{bmatrix},$$

$$h_{\underline{P}(k+1)} = \begin{bmatrix} C_f A_f^{M(k+1)-1} B_f & 0 & \cdots & 0 \\ C_f A_f^{M(k+1)} B_f & C_f A_f^{M(k+1)-1} B_f & \cdots & 0 \\ \vdots & \vdots & \ddots & \vdots \\ C_f A_f^{M(k+2)-2} B_f & C_f A_f^{M(k+2)-3} B_f & \cdots & C_f A_f^{M(k+1)-1} B_f \end{bmatrix},$$

$$\vdots$$

In the impulse response sequence: the first k blocks are zero matrices; the $(k+1)\,th$ block $h_{\underline{P}k}$ is a singular matrix; and the $(k+2)\,th$ block $h_{\underline{P}(k+1)}$ is the first non-singular one. The trick here is that each block of $H_{\underline{P}}$ is a lower triangular Toeplitz matrix with constant values along all the diagonals, thus if the $(1,1)$ element of a block is non-zero, that block is non-singular. So the pure time delay is as

$$d_{dual} = k.$$

Here we can also write $\underline{P}(z) = z^{-k}\tilde{\underline{P}}(z)$. Hence it has been proved that the pure time delay of the lifted plant is k.

The DR minimum cost function

In this part we will give explicit expression of the DR minimum cost function J_{dual} and show that $J_{dual} \geqslant J_{fast}$. First the lifted models in the DR control loop will be derived, by which the minimum cost function of the lifted output can be calculated.

It is shown in Fig. 2.4 that

$$\underline{y_f} = \underline{N}a + \underline{P}\,\underline{u} \tag{2.43}$$

where $a = \begin{bmatrix} a_1 & \cdots & a_M \end{bmatrix}^T$ denotes the lifted standard white noise and $\underline{u} = \begin{bmatrix} u_1 & \cdots & u_M \end{bmatrix}^T$ denotes the lifted control signal. As the fast disturbance model is shown in (2.7), from [10] we can obtain the lifted noise state space model as

$$\underline{N} = \left[\begin{array}{c|ccc} A_n^M & A_n^{M-1}B_n & A_n^{M-2}B_n & \cdots & B_n \\ \hline C_n & D_n & 0 & \cdots & 0 \\ C_nA_n & C_nB_n & D_n & \cdots & 0 \\ \vdots & \vdots & \vdots & \ddots & \vdots \\ C_nA_n^{M-1} & C_nA_n^{M-2}B_n & C_nA_n^{M-3}B_n & \cdots & D_n \end{array}\right] \tag{2.44}$$

and its transfer function matrix as

$$\underline{N}(z) = \begin{bmatrix} n_1 & z^{-1}n_M & \cdots & z^{-1}n_2 \\ n_2 & n_1 & \cdots & z^{-1}n_3 \\ \vdots & \vdots & \ddots & \vdots \\ n_M & n_{M-1} & \cdots & n_1 \end{bmatrix} = \begin{bmatrix} N_1 \\ N_2 \\ \vdots \\ N_M \end{bmatrix},$$

where N_k is the kth row of $\underline{N}$. From the above equation it can be seen that

$$N_k = N_M N_{ik}, \tag{2.45}$$

where

$$N_{ik} = \begin{bmatrix} 0 & z^{-1}I_{(M-k)\times(M-k)} \\ I & 0 \end{bmatrix}_{M\times M}.$$

N_{ik} is an inner function where the subscripts i and k denote inner and the kth row of $\underline{N}$ respectively. Similarly, the lifted plant transfer function matrix is as:

$$\underline{P}(z) = \begin{bmatrix} p_1 & z^{-1}p_{nM} & \cdots & z^{-1}p_2 \\ p_2 & p_1 & \cdots & z^{-1}p_3 \\ \vdots & \vdots & \ddots & \vdots \\ p_M & p_{M-1} & \cdots & p_1 \end{bmatrix} = \begin{bmatrix} P_1 \\ P_2 \\ \vdots \\ P_M \end{bmatrix}, \tag{2.46}$$

where P_k represents the kth row of $\underline{P}$.

To prove that $J_{dual} \geqslant J_{fast}$, we will first investigate the minimum variance of each branch of the lifted output. The first sampled output y_{f1}, which is also the control feedback signal at the slow rate, can be obtained from (2.43) as

$$y_{f1} = N_1 a + P_1 \underline{K_d} y_{f1},$$

where $\underline{K_d} = \begin{bmatrix} K_1 & K_2 & \cdots & K_M \end{bmatrix}^T$ is the lifted dual-rate controller in Fig. 2.4. Thus we have

$$y_{f1} = \frac{N_1 a}{1 - P_1 \underline{K_d}}. \tag{2.47}$$

From (2.45) we can see that N_M is an outer factor of N_1, thus designing a minimum variance dual-rate controller against the disturbance N_1 is the same as against N_M. The Diophantine decomposition of N_M is as

$$N_M = \begin{bmatrix} n_M & \cdots & n_1 \end{bmatrix} = F_M + z^{-d_{dual}} R_M, \tag{2.48}$$

where

$$F_M = \begin{bmatrix} f_M & \cdots & f_1 \end{bmatrix}, \; R_M = \begin{bmatrix} r_M & \cdots & r_1 \end{bmatrix}. \tag{2.49}$$

Substituting (2.49) into (2.47) and noticing $P_1 = z^{-d_{dual}} \tilde{P}_1$ where $\tilde{P}_1$ is the delay-free transfer function of P_1, (2.47) can be written as

$$y_{f1} = F_M a + z^{-d_{dual}} \left(\frac{R_M + \tilde{P}_1 \underline{K_d} F_M}{1 - P_1 \underline{K_d}} \right) a. \tag{2.50}$$

Supposing there exists an optimal controller which could cancel the second term of the above equation, and noticing that $a_1, \cdots, a_M$ are independent white noises, we have

$$\begin{aligned} & R_M + \tilde{P}_1 \underline{K_d} F_M \\ & = \begin{bmatrix} r_M & \cdots & r_1 \end{bmatrix} + (p_1 K_1 + z^{-1} p_M K_2 + \cdots + z^{-1} p_2 K_M) \begin{bmatrix} f_M & \cdots & f_1 \end{bmatrix} = 0, \end{aligned}$$

which leads to

$$\frac{r_1}{f_1} = \frac{r_2}{f_2} = \cdots = \frac{r_M}{f_M}.$$

Unfortunately in (2.48) n_i is generally different from n_j $(i \neq j)$, thus this equation cannot be satisfied, which means that the optimal controller can not make the second term of (2.50) zero but can minimize its $\mathcal{H}_2$ norm instead. So the minimum variance of y_{f1} can be written as

$$J_{y_{f1}} = Var(F_M a) + c_1 \tag{2.51}$$

where $c_1 = \min \left\| \frac{R_M + \tilde{P}_1 \underline{K_d} F_M}{1 - P_1 \underline{K_d}} \right\|^2$. $Var(F_M a)$ will be derived by the following analysis. When $\frac{d_f}{M} = k$, from (2.44) the impulse response of N_M is

$$H_{N_M} = \{\ h_{N_M 0},\ \cdots\ h_{N_n(k-1)}\ ,\ \cdots\}$$

where

$$h_{N_M 0} = \left[\ C_n A_n^{M-2} B_n \quad C_n A_n^{M-3} B_n \quad \cdots \quad D_n\ \right], \tag{2.52}$$

$$\vdots$$

$$h_{N_M(k-1)} = \left[\ C_n A_n^{d_f-2} B_n \quad C_n A_n^{d_f-3} B_n \quad \cdots \quad C_n A_n^{d_f-M-1} B_n\ \right], \tag{2.53}$$

$$\vdots$$

From (2.48) we can see that F_M is a transfer function of order $z^{-d_{dual}}$, hence $\left[\ f_M \quad \cdots \quad f_1\ \right] \begin{bmatrix} a_1 \\ \vdots \\ a_M \end{bmatrix}$ are the first d_{dual} items of the impulse response sequence of N_M, which gives

$$F_M a = \left[\ f_M \quad \cdots \quad f_1\ \right] \begin{bmatrix} a_1 \\ \vdots \\ a_M \end{bmatrix} = \left[\ h_{N_M 0} \quad \cdots \quad h_{N_M(k-1)}\ \right] \begin{bmatrix} a(0) \\ \vdots \\ a(k-1) \end{bmatrix}$$

where $a(m)$ is the lifted standard white noise signal at different sampling time, i.e., $a(m) = z^{-m} a(0)$ and m is an integer. Considering J_{fast} shown in (2.41), (2.51) can be revised as

$$\begin{aligned} J_{y_{f1}} &= \left\| \left[\ h_{N_M 0} \quad \cdots \quad h_{N_M(k-1)}\ \right] \begin{bmatrix} a(0) \\ \vdots \\ a(k-1) \end{bmatrix} \right\|^2 + c_1 \\ &= D_n^2 + (C_n B_n)^2 + (C_n A_n B_n)^2 + \cdots + (C_n A_n^{d_f-2} B_n)^2 + c_1 \\ &= J_{fast} + c_1 \geqslant J_{fast}. \end{aligned}$$

Till now we have shown the components of $J_{y_{f1}}$. Let us consider the minimum variance $J_{y_{fi}}$ of the ith $(2 \leqslant i \leqslant n)$ row of the lifted output $\underline{y_f}$. In the fast single rate control loop we have $\min_{\underline{u_f}} Var(y_{fi}) = J_{fast}$, where $\underline{u_f} = \underline{K_f}\left[\ y_{f1} \quad \cdots \quad y_{fM}\ \right]^T$ and $\underline{K_f}$ is the lifted fast rate controller. But in the lifted dual rate control loop $J_{y_{fi}} = \min_{\underline{u_d}} Var(y_{fi})$, where $\underline{u_d} = \underline{K_d} S\left[\ y_{f1} \quad \cdots \quad y_{fM}\ \right]^T = \underline{K_d} y_{f1}$. It can be seen

that $\min_{\underline{u_d}} Var(y_{fi}) \geqslant \min_{\underline{u_f}} Var(y_{fi})$, i.e., $J_{y_{fi}} \geqslant J_{fast}$. According to (2.10), we have

$$
\begin{aligned}
J_{dual} &= \min_{K_d} trace\left[\frac{Var(\underline{y_f})}{M}\right] = \min_{K_d}\left[\frac{1}{M}E\left\{trace\left(\begin{bmatrix} y_{f1} \\ \vdots \\ y_{fM} \end{bmatrix}\begin{bmatrix} y_{f1} \\ \vdots \\ y_{fM} \end{bmatrix}^T\right)\right\}\right] \\
&= \frac{J_{y_{f1}} + J_{y_{f2}} + \cdots + J_{y_{fM}}}{M} \geqslant \frac{J_{fast} + c_1 + J_{fast} + \cdots + J_{fast}}{M} \\
&= J_{fast} + c \geqslant J_{fast},
\end{aligned}
$$

where c is positive number usually presenting a minimized $\mathcal{H}_2$ norm of a certain transfer function matrix. When $\frac{d_f}{M} = k + \frac{i}{M}$, following the exactly same proof as in the case when $\frac{d_f}{M} = k$, we can still prove $J_{dual} \geqslant J_{fast}$ since the first k terms of the output are control independent. Thus, we have shown that $J_{dual} \geqslant J_{fast}$. Combining this conclusion and that of the previous subsection: $J_{dual} \leqslant J_{slow}$, it has been proved that the conjecture $J_{fast} \leqslant J_{dual} \leqslant J_{slow}$ holds.

2.6 Simulation examples

The key results are illustrated by two univariate examples: Example 1 is a numerical one; Example 2 is a case study of a stirred tank heater. In the examples, the continuous disturbances are discretized via the proposed discretization method, and then the optimal controllers are designed for the control loops of three rates : the MVC law is employed to the FSR control loops; the LMI $\mathcal{H}_2$ optimal controller design method is applied to the DR and SSR control loops. The simulation results of both examples show that: the performance of the optimal DR controller is better than that of the optimal SSR controller but worse than that of the optimal FSR controller. In addition, Example 1 illustrates the optimal controllers derived by the fast-rate criterion obtain smaller inter-sample ripples than the optimal controllers derived by the slow-rate criterion.

2.6.1 Example 1

A continuous plant and a continuous disturbance models are given as:

$$
P_c = e^{-2s}\frac{s^2 + 0.7s + 0.3}{s^2 + 0.36s + 0.24}, \quad N_c = \frac{2s + 0.2}{s^2 + 0.36s + 0.24}. \tag{2.54}
$$

We adopt the fast and slow sampling periods as $T_f = 1\text{sec}$ and $T_s = 2\text{sec}$ respectively. Thus the dual-rate factor $M = 2$. In the FSR control loop, using the zero-order-hold discretization, the discrete-time plant is acquired as:

$$P_f = z^{-2}\frac{1 - 1.2z^{-1} + 0.4466z^{-2}}{1 - 1.5z^{-1} + 0.6977z^{-2}}.$$

By the proposed discretization method, the fast-rate noise model is:

$$N_f = \begin{bmatrix} \frac{1.709z^{-1}-1.53z^{-2}}{1-1.5z^{-1}+0.6977z^{-2}} & \frac{0.0585z^{-1}-0.1486z^{-2}}{1-1.5z^{-1}+0.6977z^{-2}} \end{bmatrix}.$$

Since the co-inner-outer factorization of N_f can be obtained as:

$$N_f = N_{co}N_{ci} = \frac{1.723 - 1.523z^{-1}}{1 - 1.5z^{-1} + 0.6977z^{-2}} \begin{bmatrix} \frac{0.9919z^{-1}-0.888z^{-2}}{1-0.8837z^{-1}} & \frac{0.03395z^{-1}-0.08625z^{-2}}{1-0.8837z^{-1}} \end{bmatrix},$$

the outer-factor N_{co} is an equivalent of N_f, such that

$$N_f \Leftrightarrow N_{co} = \frac{1.723 - 1.523z^{-1}}{1 - 1.5z^{-1} + 0.6977z^{-2}}.$$

In the lifted DR and SSR control loops, after lifting by L_2, we can calculate the lifted plant and disturbance transfer function matrices from (2.15) and (2.44) as

$$\underline{P} = \begin{bmatrix} \frac{z^{-1}(1-0.6553z^{-1}+0.3116z^{-2})}{1-0.855z^{-1}+0.4868z^{-2}} & \frac{z^{-2}(0.3005-0.167z^{-1})}{1-0.855z^{-1}+0.4868z^{-2}} \\ \frac{z^{-1}(0.3005-0.167z^{-1})}{1-0.855z^{-1}+0.4868z^{-2}} & \frac{z^{-1}(1-0.6553z^{-1}+0.3116z^{-2})}{1-0.855z^{-1}+0.4868z^{-2}} \end{bmatrix},$$

$$\underline{N} = \begin{bmatrix} \frac{1.723-1.0824z^{-1}}{1-0.855z^{-1}+0.4868z^{-2}} & \frac{z^{-1}(1.0615-1.06264z^{-1})}{1-0.855z^{-1}+0.4868z^{-2}} \\ \frac{1.0615-1.06264z^{-1}}{1-0.855z^{-1}+0.4868z^{-2}} & \frac{1.723-1.0824z^{-1}}{1-0.855z^{-1}+0.4868z^{-2}} \end{bmatrix},$$

and S, H in (2.9) and (2.11) as

$$S = \begin{bmatrix} 1 & 0 \end{bmatrix}, H = \begin{bmatrix} 1 & 1 \end{bmatrix}^T.$$

We design the FSR, DR and SSR optimal controllers: K_f, K_d and K_s to minimize the variance in the sense of the fast sampled output. To show the advantage of adopting the fast-rate cost function as criterion, we design controller K_d^s (for the DR case) and K_s^s (for the SSR case) minimizing the variances of the slow sampled outputs. The simulation results are shown in Table 1, where y_{f1}, y_{f2} are the first and second row of the lifted y_f, and Var denotes the variance of a signal. It should be noticed that y_{f1} is the slow sampled output actually. From theoretical minimum

Table 2.1: Results of Example 1

Optimal controllers	K_f	K_d	K_d^s	K_s	K_s^s
Fast-rate minimum cost function	4.0955	4.4094	–	4.5273	–
Slow-rate minimum cost function	–	–	4.3264	–	4.3264
Simulated $Var(y_{f1})$	–	4.3509	4.3509	4.4895	4.3509
Simulated $Var(y_{f2})$	–	4.4364	5.1377	4.5362	5.1180
Simulated minimum cost function	4.0966	4.3937	4.7445	4.5078	4.7344

cost functions and the consistent simulation results one can see that $J_{fast} \leqslant J_{dual} \leqslant J_{slow}$. One can also see that the variances of y_f under K_d and K_s are smaller than those under K_d^s and K_s^s respectively, although K_d^s and K_s^s may have even better control effects at some slow sampling instances (y_{f1}). Hence, considering the fast sampled output, controllers by fast-rate criteria achieve better performances than controllers by slow-rate criteria.

2.6.2 Example 2

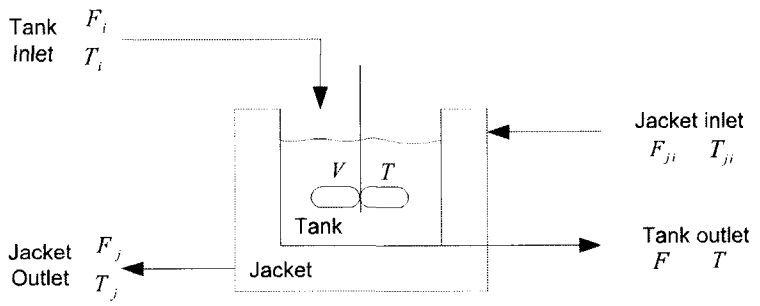

Figure 2.8: The stirred tank heater

In this example, we consider a stirred tank heater shown in Fig. 2.8. Similar examples can be found in [49] and [8]. The stirred tank may serve as a chemical reactor, in which the reaction often occurs at a certain temperature to obtain the desired yield. In this example, saturated steam is circulated through the jacket to heat the fluid in the tank. The assumptions made in writing the dynamic modeling equations to find the tank temperature are as follows:

(1) Perfect mixing in both the tank and the jacket.

(2) The steam and liquids have constant density and heat capacity.

(3) The temperature and the flow rate of the saturated steam are constant through the jacket.

(4) The tank inlet flow rate F_i, tank outlet flow rate F_o, tank inlet temperature T_i vary with time.

Neglecting the work done by the impeller, we use energy balance around the tank to obtain the modeling equation given by

$$\frac{dT_o}{dt} = \frac{F_o}{V}(T_i - T_o) + \frac{Q}{\rho V C_\rho}, \tag{2.55}$$

where ρ is the liquid density, V is the volume of the tank, C_ρ is the heat capacity, Q is the rate of heat transfer from the jacket to the tank. It is governed by the equation

$$Q = UA(T_j - T_o),$$

where U is the overall heat transfer coefficient and A is the area for the heat transfer. The subscripts i and j denote inlet and jacket. Considering F_o, T_o, and T_i as the manipulated variable, the controlled variable and the disturbance respectively, the steady-state can be obtained by solving the dynamic equation $\frac{dT_o}{dt} = 0$. The steady-state variables of this system and some parameters are given as:

F_s=5.0 ft^3/min, $\rho C_\rho = 61.3$ $\text{Btu}/^\circ\text{F} \cdot \text{ft}^3$, V=20 ft^3, $T_{is} = 50^\circ F$, $T_s = 125^\circ$F,
$F_{js} = 1.5$ ft^3/min, $\rho_j C_{\rho j} = 61.3$ $\text{Btu}/^\circ\text{F} \cdot \text{ft}^3$, $V_j = 1\text{ft}^3$, $T_{jis} = 200^\circ$F,
$T_{js} = 150^\circ$F, $UA = 183.9$, $Var(T_i) = 25$ $(^\circ\text{F})^2$

Linearizing (2.55) and applying Laplace transform yield

$$\tilde{T_o} = \frac{1/V(T_{is} - T_{os})}{s + F_{os}/V + UA/\rho V C_\rho}\tilde{F_o} + \frac{F_{os}/V}{s + F_{os}/V + UA/\rho V C_\rho}\tilde{T_i}. \tag{2.56}$$

Inserting the above parameters values and assuming that the temperature measurement has a time delay of 0.3 sec, (2.56) can be written as

$$\tilde{T_o} = \frac{-7.5e^{-0.3s}}{s + 0.4}\tilde{F_o} + \frac{1.25}{s + 0.4}\tilde{a}$$

where $\tilde{a}$ is a continuous standard white noise signal. The fast and slow sampling periods are chosen as $T_f = 0.1$ min and $T_s = 0.3$ min, respectively. Thus the lifting

Table 2.2: Results of Example 2

Control loops	FSR	DR	SSR
Fast-rate minimum cost function $(°F)^2$	0.5349	0.6411	0.6882
Simulated $Var(y_{f1})$ $(°F)^2$	–	0.7418	0.7573
Simulated $Var(y_{f2})$ $(°F)^2$	–	0.5338	0.6462
Simulated $Var(y_{f3})$ $(°F)^2$	–	0.6392	0.6492
Simulated minimum cost function $(°F)^2$	0.5321	0.6383	0.6842

operator in this example is L_3. After discretization, the fast-rate system can be expressed as

$$T_o = z^{-4}\frac{-0.7352}{1-0.9608z^{-1}}Fo + \frac{0.3875}{1-0.9608z^{-1}}a_k,$$

where a_k is a discrete-time white noise with zero mean and unit variance. The lifted plant and disturbance transfer function matrices can be calculated from (2.15) and (2.44). S, H in (2.9) and (2.11) are as

$$S = \begin{bmatrix} 1 & 0 & 0 \end{bmatrix},\ H = \begin{bmatrix} 1 & 1 & 1 \end{bmatrix}^T.$$

Thus the generalized models of the lifted DR rate and SSR rate can be obtained from (2.9) and (2.11). For the FSR, DR and SSR control loops, we design the optimal controllers, calculate the minimum cost functions and then do simulations. The results are shown in Table 2 where y_{f1}, y_{f2}, and y_{f3} are the first, second and third row of the lifted y_f. It can be seen that the results illustrate the effectiveness of the proposed methods and validate our results again.

2.7 Conclusions

In this chapter we have investigated the MVC problem for single-input single-output linear systems sampled with different rates: fast, dual and slow rates. The minimum variance of the fast sampled output was chosen as the control cost function. A discretization method preserving the mean and auto-correlation of a continuous stochastic disturbance model was developed. The MVC law was directly applied to the design of the optimal controller for the fast-rate control loop. Using the lifting technique, the dual-rate and the slow-rate control loops can be unified under a common structural plant. This kind of plants do not satisfy the regularity assumptions for a general discrete-time $\mathcal{H}_2$ optimal control problem. Hence, a novel linear matrix

inequality approach to solve this problem was developed. Then the new approach was used to derive the optimal controllers for the lifted dual-rate and slow-rate control loops. It was theoretically proved that the performance of a dual-rate controller is superior to that of a slow single rate controller but inferior to that of a fast single rate controller in the sense of MVC. The effectiveness of the proposed methods were illustrated by two simulation examples. The future work is to develop an experimental methodology to estimate the dual-rate minimum variance from data for the assessment of dual-rate control loops.

Chapter 3

Multirate Minimum Variance Control Design and Control Performance Assessment: a Data-driven Subspace Approach[2]

This chapter discusses MVC design and control performance assessment based on the MVC-benchmark for multirate systems. In particular, a dual-rate system with a fast control updating rate and a slow output sampling rate is considered, which is not uncommon in practice. A lifted model is used to analyze the multirate system in a state-space framework and the lifting technique is applied to derive a subspace equation for multirate systems. From the subspace equation the multirate MVC law and the algorithm to estimate the multirate MVC-benchmark variance or performance index are developed. The multirate optimal controller is calculated from a set of input/output open-loop experimental data and thus this approach is data-driven since it does not involve an explicit model. In parallel, the presented MVC-benchmark estimation algorithm requires a set of open-loop experimental data and closed-loop routine operating data. No explicit models, namely, transfer function matrices, Markov parameters or interactor matrices, are needed. This is in contrast to traditional control performance assessment algorithms. The proposed

[2]The materials in this chapter will be published in "X. Wang, B. Huang, and T. Chen. Multirate minimum variance control design and control performance assessment: A data-driven subspace approach. IEEE Trans. Contr. Syst. Technol., 15(1): 65-74, 2007".

methods are illustrated through a simulation example.

3.1 Introduction

In this chapter we consider a dual-rate system where the sampling frequency of the controller output is M (a positive integer) times that of the plant output. There exist other cases of dual-rate systems, e.g., those systems where the plant output is fast sampled and the controller output is slow sampled. However, the former one is more common in practice. For example, polymer reactors [48], fermentation processes [20] and octane quality control [43] are this kind of multirate systems, where the manipulated variables are sampled faster than the output measurements. This is because the composition, density and molecular weight distribution measurements are typically obtained after several minutes of analysis, whereas the manipulated variables can be adjusted at relatively fast rates.

The first objective of this work is to explore a dual-rate MVC law, when only the input-output data of a given dual-rate system are available. Unlike the traditional methods, where Diophantine or Riccati equations are solved to achieve this goal, we follow a novel approach based on results from the area of subspace system identification [58, 59]. Subspace identification methods, which were developed in the late 80's and early 90's, allow the identification of a system's state space model directly from input-output data [41, 51, 73]. Subspace identification algorithms contain two steps. The first step is making data projections to obtain subspace matrices; the second step is to extract the state space model from the subspace matrices [52]. The idea of designing predictive controllers using subspace system identification techniques has been around for a few years. For instance, subspace matrices are used in the model-free LQG design [14] and subspace predictive control design [15]. In addition, the extended state space model is used to obtain predictive controllers [60]. The subspace approach to designing a predictive controller with all the important predictive control features is investigated in [34]. The model-free design approach presented in the literature so far has been limited to single-rate systems. In this work, we will consider the MVC design for dual-rate systems. As it will be shown, a subspace equation will be proposed with the lifting technique. This subspace equation is of importance because as soon as the subspace matrices in it are determined, the dual-rate MVC law can be obtained without relying on an

explicit model. It should be noticed that the determination of subspace matrices is different from subspace identification. The former does not identify an explicit state space model, but the latter does. This is why the method we use is so-called model-free or data-driven in the literature.

The second objective of this work is to assess dual-rate control-loop performance using input-output data. Control performance assessment is an important technology used to assist high efficiency process operations. There are many ways to assess the quality of process controllers, but in general they explicitly or implicitly involve comparing the current control quality against some standard. To the best of our knowledge, little work has been done in multirate control performance assessment, even though multirate sampling or operations are not uncommon in industry. Due to the lack of published work on multirate control performance assessment, we will only review the important research which has been done for single-rate control loops. For linear systems, it is known that the MVC is the best possible control in the sense that no controllers can provide a lower closed-loop variance [5]. Many papers [22, 12, 68, 46, 28] have shown that MVC is a useful benchmark to assess control-loop performance. A comprehensive overview of research up to 1998 on control performance assessment using minimum variance principles can be found in [55]. A significant work is [22] by Harris, who presented a new direction and framework for the control performance-assessment area. It applies time-series analysis to find a suitable expression for the feedback controller-invariant terms from closed-loop routine operating data, and subsequently uses it as a benchmark to assess SISO control-loop performance. The filtering and correlation analysis in [28] extends the method in [22] to MIMO processes. Other MIMO performance assessment work can also be found in [23]. To estimate the MVC-benchmark variance from routine operating data, the time delay (SISO case) or the interactor matrix (MIMO case) must be known a priori. This is a common point in these aforementioned traditional methods. The factorization of the interactor matrix by singular value decomposition is one of the main contributions in [29]. A similar result is given in [38], which presents a one-shot solution to estimate the MVC-benchmark variance, but it requires the first few Markov parameters in multivariable feedback control loops. A framework based on subspace matrices is studied for the estimation of the MVC-

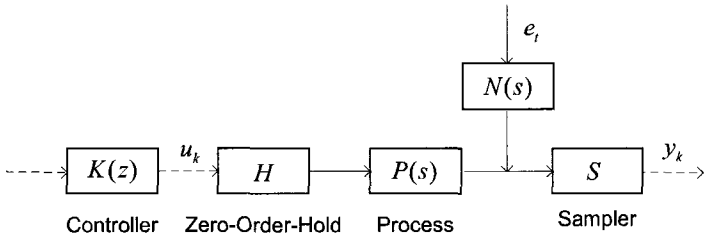

Figure 3.1: Block diagram of a sampled-data system

benchmark variance for multivariate feedback control systems [27]. This algorithm consolidates the traditional three-step procedure, model identification, closed-loop time series analysis, and extraction of the MVC benchmark, into a single shot. No prior knowledge, such as Markov parameters and interactor matrices are needed in the algorithm. The second objective of our work, estimation of the dual-rate MVC-benchmark variance, is an extension of the work in [27] to dual-rate systems by using a novel multirate subspace algorithm [59, 62].

The remainder of this chapter is organized as follows. The system and the problem formulation are described in detail in Section 3.2. Section 3.3 presents the derivation of the dual-rate subspace equation via the lifting technique. In Section 3.4, a model-free approach which is based on the subspace equation, is investigated to design the dual-rate MVC controllers. Section 3.5 presents a data-driven framework to estimate the dual-rate MVC-benchmark variance. An illustrative numerical example is provided in Section 3.6, followed by conclusions in Section 3.7.

3.2 System description and problem statement

Consider the following discrete-time, time-invariant, linear state space model of the form

$$x_{k+1} = Ax_k + Bu_k + Ee_k \tag{3.1}$$

$$y_k = Cx_k + Du_k + Fe_k \tag{3.2}$$

where k is a discrete-time instance, $x_k \in R^n$ is the state vector, $y_k \in R^m$ is the system output, $u_k \in R^r$ is the system input, and $e_k \in R^m$ is white noise with zero mean and identity covariance matrix. A, B, C, D, E, F are system matrices with appropriate dimensions. We assume that (C, A) is observable, (A, B) is controllable, and u and e

are independent signals. The system is shown in Figure 3.1, where H and S denote a zero-order-hold and an output sampler with interval T, respectively, the solid line represents continuous-time signals, and the dashed line indicates discrete-time signals. Thus the discrete-time state space model of the system SPH is (A, B, C, D), and the discretized state space model of the disturbance SN is (A, E, C, F). In certain industrial applications [43], it is common that the control updating rate is faster than the output sampling rate by a certain factor, which leads to dual-rate systems. Assume that the input variable is sampled with a fast sampling rate $T_{\text{fast}} = T$ and the output variable is sampled with a slow sampling rate $T_{\text{slow}} = MT_{\text{fast}}$, where $M = \frac{T_{\text{slow}}}{T_{\text{fast}}}$ is the lifting factor. The problem investigated in this chapter is to design the dual-rate MVC law, and then estimate the MVC-benchmark variance directly from the input-output data defined as

$$\begin{cases} u_k, \ k = i + k_0, \ \forall i = 0, 1, \cdots, N_u - 1, \\ y_k, \ k = jM + k_0, \ \forall j = 0, 1, \cdots, N_y - 1, \end{cases}$$

where $k_0 \geq 1$ is the first discrete-time instance when y_k is available. The lengths of input and output data satisfy $N_u = Ny \times M$, which means that the last time instance when u_k is available equals to the last time instance when y_k is available.

3.3 A dual-rate subspace equation with the lifting approach

The two objectives of this work, dual-rate MVC design and dual-rate control performance assessment via data-driven approaches, are both based on a dual-rate subspace equation. This input-output subspace equation is also named as extended state space model in the DSR algorithm [59, 62] and the related predictive control algorithm [60]. Here, we will derive it for dual-rate systems with the lifting technique, which makes it possible to follow the conventional subspace approach in solving multirate problem, and, most importantly, facilitates the derivation of the model-free multirate control performance assessment algorithm.

3.3.1 Definitions

For the sake of presentation, the following definitions are adopted. In this chapter, $\{\cdots\}$ is used to represent a data set, and $[\cdots]$ is used to denote a vector. For a

sequence of data

$$s_t \in R^{n_r \times n_c},\ \forall t = 0, 1, \cdots, k, k+1, \cdots$$

with n_r being the number of the rows and n_c the number of the columns in s_t, given positive integers k, J, L and K, the extended signal sequence $s_{k|L} \in R^{(L \times n_r) \times n_c}$ is defined as

$$s_{k|L} \stackrel{\text{def}}{=} \begin{bmatrix} s_k \\ s_{k+1} \\ \vdots \\ s_{k+L-1} \end{bmatrix}, \tag{3.3}$$

and the Hankel matrix $S_{k|L} \in R^{(L \times n_r) \times K n_c}$ is defined as

$$S_{k|L} \stackrel{\text{def}}{=} \begin{bmatrix} s_k & s_{k+1} & \cdots & s_{k+K-1} \\ s_{k+1} & s_{k+2} & \cdots & s_{k+K} \\ \vdots & \vdots & \ddots & \vdots \\ s_{k+L-1} & s_{k+L} & \cdots & s_{k+K+L-2} \end{bmatrix}, \tag{3.4}$$

where k is the starting index and $k = k_0 + JM$; L, the number of n_r-block rows in $s_{k|L}$ and $S_{k|L}$, is defined as the prediction horizon. K is the number of n_c-block columns in $S_{k|L}$. In this chapter we work with vector sequences, i.e., s_k is a vector ($n_c = 1$) in this case. The number of block columns in $S_{k|L}$ is chosen as $K = N_y - L - J$ [62], where J is the past horizon to define the instrumental variable matrix.

3.3.2 Lifting and input-output subspace equation

In the dual-rate control loop in Figure 3.1 the slow sampled output signal is $y = \{y_{k_0}, \cdots, y_k, y_{k+M}, \cdots\}$, and the fast sampled input signal is $u = \{u_{k_0}, \cdots, u_k, u_{k+1}, \cdots\}$. The dual-rate controller is time-varying due to the presence of the fast-rate hold and the slow-rate sampler. To avoid dealing with the time-varying system directly, we introduce the lifting technique. By the definition in equation (3.3), the control signals can be stacked as vector-valued sequences as follows:

$$\underline{u} = \left\{ u_{k_0|M}, \cdots, u_{k|M}, u_{k+M|M}, \cdots \right\}.$$

For instance, if $M = 2$, the lifted control signal is as

$$\underline{u} = \left\{ \begin{bmatrix} u_{k_0} \\ u_{k_0+1} \end{bmatrix}, \cdots, \begin{bmatrix} u_k \\ u_{k+1} \end{bmatrix}, \begin{bmatrix} u_{k+2} \\ u_{k+3} \end{bmatrix}, \cdots \right\}.$$

The map from u to $\underline{u}$ is defined as the lifting operator L_M [40]. The inverse lifting operator L_M^{-1} is the reverse of the mapping. It can be seen that $L_M^{-1} L_M = I$ and

$L_M L_M^{-1} = I$. After lifting, both the signal dimension and the underlying period are increased by a factor of M. The system from $\underline{u}$ to y is the lifted system which is single-rate and linear time-invariant. Recall that the state space model for the system SPH in Figure 3.1 is (A, B, C, D). The systems we are studying in this work have at least one time delay, hence matrix D can be set to a zero matrix without loss of generality. From the known state space model of the fast-rate plant, the lifted system G_M can be written as [10]:

$$x_{k+M} = A^M x_k + \underline{B} u_{k|M} \,, \tag{3.5}$$

$$y_k = C x_k + D_M u_{k|M} \tag{3.6}$$

where $\underline{B} = [\ A^{M-1}B \ \cdots \ AB \ \ B\ ] \in R^{n\times(M\times r)}$ is the lifted external input matrix, and $D_M = [\ 0 \ \cdots \ 0\ ] \in R^{m\times(M\times r)}$ is the lifted direct control input-to-output matrix. Again, by lifting y_k and $u_{k|M}$ with the user chosen prediction horizon L, equation (3.6) can be written as

$$\begin{bmatrix} y_k \\ y_{k+M} \\ \vdots \\ y_{k+(L-1)M} \end{bmatrix} = \begin{bmatrix} C \\ CA^M \\ \vdots \\ CA^{(L-1)M} \end{bmatrix} x_k + \begin{bmatrix} D_M & \cdots & 0 \\ C\underline{B} & \cdots & 0 \\ \vdots & \ddots & 0 \\ CA^{(L-2)M}\underline{B} & \cdots & D_M \end{bmatrix} \begin{bmatrix} u_{k|M} \\ u_{k+M|M} \\ \vdots \\ u_{k+(L-1)M|M} \end{bmatrix}. \tag{3.7}$$

Let us make the following matrix definitions. The dual-rate extended observability matrix O_L for the pair $(C,\ A^M)$ is defined as

$$O_L \stackrel{\text{def}}{=} \begin{bmatrix} C \\ CA^M \\ \vdots \\ CA^{M(L-1)} \end{bmatrix} \in R^{(L\times m)\times n}, \tag{3.8}$$

and the lower block triangular Toeplitz matrix H_L is defined as

$$H_L \stackrel{\text{def}}{=} \begin{bmatrix} D_M & \cdots & 0 & 0 \\ C\underline{B} & \cdots & 0 & 0 \\ CA^M\underline{B} & \cdots & 0 & 0 \\ \vdots & \ddots & \vdots & 0 \\ CA^{(L-2)M}\underline{B} & \cdots & C\underline{B} & D_M \end{bmatrix} \in R^{(L\times m)\times(L\times M\times r)}. \tag{3.9}$$

Then (3.7) can be expressed as

$$y_{k|L} = O_L x_k + H_L u_{k|LM}. \tag{3.10}$$

Then it can be obtained from (3.5, 3.10) that [58]

$$\begin{aligned}
y_{k+M|L} &= O_L x_{k+M} + H_L u_{k+M|LM} \\
&= O_L(A^M x_k + \underline{B} u_{k|M}) + H_L u_{k+M|LM} \\
&= O_L A^M (O_L^T O_L)^{-1} O_L^T O_L O_L^{-1} (y_{k|L} - H_L u_{k|LM}) + O_L \underline{B} u_{k|M} + H_L u_{k+M|LM} \\
&= \tilde{M}(y_{k|L} - H_L u_{k|LM}) + O_L \underline{B} u_{k|M} + H_L u_{k+M|LM} \\
&= \tilde{M} y_{k|L} - \tilde{M} \left[\begin{array}{cc} H_L & 0_{(L\times m)\times(M\times r)} \end{array} \right] u_{k|(L+1)M} \\
&+ \left[\begin{array}{cc} O_L\underline{B} & 0_{(L\times m)\times(L\times M\times r)} \end{array} \right] u_{k|(L+1)M} + \left[\begin{array}{cc} 0_{(L\times m)\times(M\times r)} & H_L \end{array} \right] u_{k|(L+1)M} \\
&= \tilde{M} y_{k|L} + (\left[\begin{array}{cc} O_L\underline{B} & H_L \end{array} \right] - \tilde{M}[H_L \;\; 0_{(L\times m)\times(M\times r)}]) u_{k|(L+1)M} \\
&= \tilde{M} y_{k|L} + \tilde{N} u_{k|(L+1)M} \qquad (3.11)
\end{aligned}$$

where $\tilde{M}$ and $\tilde{N}$ are defined as

$$\begin{aligned}
&\tilde{M} \stackrel{\text{def}}{=} O_L A^M (O_L^T O_L)^{-1} O_L^T, \\
&\tilde{N} \stackrel{\text{def}}{=} \left[\begin{array}{cc} O_L\underline{B} & H_L \end{array} \right] - \tilde{M} \left[\begin{array}{cc} H_L & 0_{(L\times m)\times(M\times r)} \end{array} \right]. \qquad (3.12)
\end{aligned}$$

The subspace model in (3.11) is disturbance free. Now let us consider the noisy part of the model. The disturbance model is in the slow sampling rate and the corresponding discrete-time state space model is as (A^M, E_s, C, F_s), where the subscript s denotes the slow sampling rate. Actually, this model can also be obtained from the fast-rate noise model (A, E, C, F) by lifting. The relationship between these two models is discussed in detail in [82]. So by taking into account the disturbance, via similar derivation as shown in (3.11), it can be seen that

$$y_{k+M|L} = \tilde{M} y_{k|L} + \tilde{N} u_{k|(L+1)M} + \tilde{T} e_{k|L+1} \qquad (3.13)$$

where $e_{k|L+1}$ is defined in (3.3), $\tilde{T} \stackrel{\text{def}}{=} \left[\begin{array}{cc} O_L E_s & H_L^s \end{array} \right] - \tilde{M} \left[\begin{array}{cc} H_L^s & 0_{(L\times m)\times m} \end{array} \right]$, and H_L^s is defined as

$$H_L^s \stackrel{\text{def}}{=} \left[\begin{array}{cccc} F_s & \cdots & 0 & 0 \\ CE_s & \cdots & 0 & 0 \\ CA^M E_s & \cdots & 0 & 0 \\ \vdots & \ddots & \vdots & 0 \\ CA^{(L-2)M} E_s & \cdots & CE_s & F_s \end{array} \right] \in R^{(L\times m)\times(L\times m)}. \qquad (3.14)$$

From (3.13), it can be observed that

$$Y_{k+M|L} = \tilde{M} Y_{k|L} + \tilde{N} U_{k|(L+1)M} + \tilde{T} E_{k|L+1} \qquad (3.15)$$

where the data matrices $Y_{k+M|L}$, $Y_{k|L}$, $U_{k|(L+1)M}$ and $E_{k|L+1}$ are defined as in (3.4). Equations (3.13) and (3.15) are equivalent, and they both are input-output equations for dual-rate systems. Though in [62] equation (3.13), named as the extended state space model, is derived by an M-step predictor approach, our alternative method approaches the problem from a different way, i.e. lifting, which makes it possible to use conventional subspace approach to solve multirate problem.

3.3.3 Determination of subspace matrices

Since the subspace matrices $\tilde{M}$, $\tilde{N}$ and $\tilde{T}$ in (3.13) and (3.15) will play important roles in the later dual-rate MVC controller design and MVC variance estimation, in this part we will show how to determine them directly from the open-loop input-output data. It is important to mention that estimating the subspace matrices is not equivalent to estimating state space matrices of the lifted system, although the steps which will be presented here are clearly based on techniques from the area of subspace identification. Using the subspace matrices calculated from the input-output data we can directly design the control law as well as assess the control loop performance, while the lifted dual-rate system parameters A^M, $\underline{B}$, C, D_M, E_s and F_s are never explicitly calculated. The sketch to determine the subspace matrices is shown in the following by using a QR decomposition from DSR algorithm [59, 62]. The first step is to structure the data matrix in the left-hand side of (3.16) from the open-loop input-output data set. Then, the QR decomposition of the data matrix can be defined as

$$\frac{1}{\sqrt{K}}\begin{bmatrix} U_{k|(L+1)M} \\ W \\ Y_{k|L} \\ Y_{k+M|L} \end{bmatrix} = RQ = \begin{bmatrix} R_{11} & 0 & 0 & 0 \\ R_{21} & R_{22} & 0 & 0 \\ R_{31} & R_{32} & R_{33} & 0 \\ R_{41} & R_{42} & R_{43} & R_{44} \end{bmatrix}\begin{bmatrix} Q_1 \\ Q_2 \\ Q_3 \\ Q_4 \end{bmatrix} \tag{3.16}$$

where $W = \begin{bmatrix} Y_{k_0|J}^T & U_{k_0|JM}^T \end{bmatrix}^T$ denotes the past information including the past input and output data. The QR decomposition can be treated as a data compression step, i.e., the data matrix in the left-hand side of (3.16) can be compressed to a usually much smaller lower triangular matrix R which contains the relevant information of the system. By certain derivations [59], the subspace matrices can

be obtained as follows:

$$\tilde{M} = R_{42}R_{32}^{\dagger} \tag{3.17}$$

$$\tilde{N} = (R_{41} - \tilde{M}R_{31})R_{11}^{T}(R_{11}R_{11}^{T})^{-1} \tag{3.18}$$

$$\tilde{T} = R_{43} - \tilde{M}R_{33} \tag{3.19}$$

where the superscript † means the Moore-Penrose pseudo inverse.

3.4 Data-driven MVC law design

3.4.1 Control objective

For linear systems, it is known that MVC is the best possible control in the sense of variance control because no controllers could provide a lower closed-loop variance. The control objective for the system in Figure 3.1 can be expressed as

$$\min\ E[y_k^T y_k] = \min \lim_{N\to\infty} \frac{1}{N}\sum_{k=1}^{N} y_k^T y_k \tag{3.20}$$

Given the transfer function of a system, e.g., an ARMAX model, the principle of MVC can be obtained by solving a Diophantine equation [6]. A more explicit solution can be found in [29]. Also, if the system state-space model is known, the MVC problem can be reformulated into an $\mathcal{H}_2$ optimal problem. For the $\mathcal{H}_2$ optimal problem, an elegant solution is developed by solving two Riccati equations [10]. Numerical solutions can also be found by solving a group of linear matrix inequalities [63, 82].

3.4.2 Prediction model

What inspired one to develop MVC law via subspace approach is the following idea. It can be seen that the subspace input-output equations (3.13) and (3.15) contain inherent relationship between the past and the future control/output signals. Then by setting the future predicted output variance to the minimum, the optimal future control signals will be expressed as a certain combination of the past control and past output signals. Hence, we can obtain the feedback MVC law. Next, it will be shown how to present the explicit relationship between the past and the future control/output signals by the subspace equations.

Proposition 3.1 *The prediction model for the future outputs is*

$$\hat{y}_{k+M|L} = P_y y_{k-(L-1)M|L} + P_{L-1} u_{k-(L-1)M|(L-1)M} + F_{L+1} u_{k|(L+1)M}, \tag{3.21}$$

and the terms are given by

$$\begin{aligned} P_y &= \tilde{M}^L, \\ P_{L-1} &= [\ p_1 \quad p_2 \quad \cdots \quad p_{L-1}\ ], \\ F_{L+1} &= [\ f_1 \quad f_2 \quad \cdots \quad f_{L+1}\ ], \end{aligned} \tag{3.22}$$

where

$$p_i = \sum_{j=1}^{i} H_{j+L-i,j} \ \forall i = 1, \cdots, L-1, \tag{3.23}$$

$$f_i = \sum_{j=1}^{L-i+2} H_{j,j+i-1} \ \forall i = 2, \cdots, L+1, \ f_1 = \sum_{j=1}^{L} H_{j,j}. \tag{3.24}$$

$H_{i,j}$ denotes the sub-block of the Hankel Matrix H, which is structured by the subspace matrices $\tilde{M}$ and $\tilde{N}$:

$$H \stackrel{def}{=} \begin{bmatrix} \tilde{N} \\ \tilde{M}\tilde{N} \\ \vdots \\ \tilde{M}^{L-1}\tilde{N} \end{bmatrix} = \begin{bmatrix} H_{11} & \cdots & H_{1,L+1} \\ H_{21} & \cdots & H_{2,L+1} \\ \vdots & \ddots & \vdots \\ H_{L1} & \cdots & H_{L,L+1} \end{bmatrix}. \tag{3.25}$$

Proof. By noting that $e_{k|L+1}$ is a white noise sequence, it follows from (3.13) that an optimal prediction of $y_{k+M|L}$ can be written as

$$\hat{y}_{k+M|L} = \tilde{M} y_{k|L} + \tilde{N} u_{k|(L+1)M}. \tag{3.26}$$

It can be derived from this equation that

$$\hat{y}_{k+2M|L} = \tilde{M}^2 y_{k|L} + [\ \tilde{M}\tilde{N} \quad \tilde{N}\ ] \begin{bmatrix} u_{k|(L+1)M} \\ u_{k+M|(L+1)M} \end{bmatrix}$$

$$\vdots$$

$$\hat{y}_{k+LM|L} = \tilde{M}^L y_{k|L} + [\ \tilde{M}^{L-1}\tilde{N} \quad \tilde{M}^{L-2}\tilde{N} \quad \cdots \quad \tilde{N}\ ] \begin{bmatrix} u_{k|(L+1)M} \\ u_{k+M|(L+1)M} \\ \vdots \\ u_{k+(L-1)M|(L+1)M} \end{bmatrix}.$$

By letting $k' = k + (L-1)M$ and then substituting k' with k, the above equation can be written as

$$\hat{y}_{k+M|L} = \tilde{M}^L y_{k|L} + \begin{bmatrix} \tilde{M}^{L-1}\tilde{N} & \tilde{M}^{L-2}\tilde{N} & \cdots & \tilde{N} \end{bmatrix} \begin{bmatrix} u_{k-(L-1)M|(L+1)M} \\ u_{k-(L-2)M|(L+1)M} \\ \vdots \\ u_{k|(L+1)M} \end{bmatrix}. \tag{3.27}$$

From equations (3.26) and (3.27) it can be seen that $P_y = \tilde{M}^L$. To prove that (3.23) and (3.24) hold, we first rewrite the term $P_{L-1}u_{k-(L-1)M|(L-1)M} + F_{L+1}u_{k|(L+1)M}$ as follows:

$$\begin{aligned} &P_{L-1}u_{k-(L-1)M|(L-1)M} + F_{L+1}u_{k|(L+1)M} \\ &= \begin{bmatrix} p_1 & p_2 & \cdots & p_{L-1} \end{bmatrix} \begin{bmatrix} u_{k-(L-1)M|M} \\ u_{k-(L-2)M|M} \\ \vdots \\ u_{k-M|M} \end{bmatrix} + \begin{bmatrix} f_1 & f_2 & \cdots & f_{L+1} \end{bmatrix} \begin{bmatrix} u_{k|M} \\ u_{k+M|M} \\ \vdots \\ u_{k+LM|M} \end{bmatrix}. \end{aligned} \tag{3.28}$$

Then the second term in (3.27) can be reformulated as

$$\begin{aligned} &\begin{bmatrix} \tilde{M}^{L-1}\tilde{N} & \tilde{M}^{L-2}\tilde{N} & \cdots & \tilde{N} \end{bmatrix} \begin{bmatrix} u_{k-(L-1)M|(L+1)M} \\ u_{k-(L-2)M|(L+1)M} \\ \vdots \\ u_{k|(L+1)M} \end{bmatrix} \\ &= \tilde{N} \begin{bmatrix} u_{k|M} \\ u_{k+M|M} \\ \vdots \\ u_{k+LM|M} \end{bmatrix} + \tilde{M}\tilde{N} \begin{bmatrix} u_{k-M|M} \\ u_{k|M} \\ \vdots \\ u_{k+(L-1)M|M} \end{bmatrix} + \cdots + \tilde{M}^{L-1}\tilde{N} \begin{bmatrix} u_{k-(L-1)M|M} \\ u_{k-(L-2)M|M} \\ \vdots \\ u_{k+M|M} \end{bmatrix}. \end{aligned} \tag{3.29}$$

Considering the Hankel Matrix

$$\begin{bmatrix} \tilde{N} \\ \tilde{M}\tilde{N} \\ \vdots \\ \tilde{M}^{L-1}\tilde{N} \end{bmatrix} = \begin{bmatrix} H_{11} & H_{12} & \cdots & H_{1,L+1} \\ H_{21} & H_{22} & \cdots & H_{2,L+1} \\ \vdots & \vdots & \ddots & \vdots \\ H_{L1} & H_{L2} & \cdots & H_{L,L+1} \end{bmatrix},$$

from (3.28) and (3.29) it can be seen that

the coefficient of $u_{k|M}$: $f_1 = H_{11} + H_{22} + \cdots + H_{LL}$,

the coefficient of $u_{k+M|M}$: $f_2 = H_{12} + H_{23} + \cdots + H_{L,L+1}$,

$\vdots$

the coefficient of $u_{k+LM|M}$: $f_{L+1} = H_{1,L+1}$.

Then equation (3.24) is proven. Similarly, by collecting and comparing the coefficients of the past control signals in (3.28) and (3.29), we can obtain that

the coefficient of $u_{k-(L-1)M|M}$: $p_1 = H_{L1}$,

the coefficient of $u_{k-(L-2)M|(L+1)M}$: $p_2 = H_{L-1,1} + H_{L2}$,

the coefficient of $u_{k-M|M}$: $p_{L-1} = H_{21} + H_{32} + \cdots + H_{L,L-1}$.

Thus, equation (3.23) holds. The similar prediction model for single-rate case can be found in [60]. ■

3.4.3 Computing MVC control law

Proposition 3.2 *Considering the prediction model in (3.21), the L-step ahead optimal control variables, which minimize the control cost function*

$$J_L \stackrel{def}{=} \hat{y}^T_{k+M|L}\hat{y}_{k+M|L}, \tag{3.30}$$

can be computed as

$$u_{k|(L+1)M} = -(F^T_{L+1}F_{L+1})^{\dagger}F^T_{L+1}(\tilde{M}^L y_{k-(L-1)M|L} + P_{L-1}u_{k-(L-1)M|(L-1)M}). \tag{3.31}$$

Proof. Inserting $\hat{y}_{k+M|L}$ shown in (3.21) into the control objective function (3.30), it can be shown that

$$\begin{aligned}\frac{\partial J_L}{\partial u_{k|(L+1)M}} &= 2F^T_{L+1}(\tilde{M}^L y_{k-(L-1)M|L} \\ &\quad + P_{L-1}u_{k-(L-1)M|(L-1)M} + F_{L+1}u_{k|(L+1)M}).\end{aligned}$$

By setting $\frac{\partial J_L}{\partial u_{k|(L+1)M}} = 0$, the optimal control variables can be obtained as

$$\begin{aligned}u_{k|(L+1)M} &= -(F^T_{L+1}F_{L+1})^{\dagger}F^T_{L+1} \\ &\quad \times (\tilde{M}^L y_{k-(L-1)M|L} + P_{L-1}u_{k-(L-1)M|(L-1)M}).\end{aligned}$$

■

After the optimal control sequence $u_{k|(L+1)M}$ is calculated, only the first block row of $u_{k|(L+1)M}$, $u_{k|M}$, is implemented as the receding horizon MVC law. Observing equation (3.31) we can make some important remarks:

- The data-driven MVC law avoids the system identification step in the traditional MVC design. Moreover, the lifted system matrices A^M, $\underline{B}$, C, D_M, E_s and F_s do not have to be calculated. The only parameters of importance are $\tilde{M}$ and $\tilde{N}$. The Riccati equation or Diophantine equation is replaced by one single QR decomposition of data block matrices (see (3.16)).

- Although only the first control action is implemented, it has been shown [14] as the horizon being increased, the receding horizon implementation converges to the true optimal control. This fact will be further elaborated next.

- Looking at both, the data-driven MVC law derived via the subspace approach and the classic MVC law, one might wonder what the link between these two is, and if they are equivalent. The answer to the latter question is positive. The reason is that as discussed in [39], the minimum variance controllers designed for ARMAX systems using Diophantine equations are identical to the LQG controllers for any system delay. Thus, the MVC problem is a special case of the LQG problem. Also, it is proved that a subspace-based LQG approach is equivalent to the classical LQG when the horizon is infinite [14]. Due to the equivalence of the subspace identification methods, we can conclude that the data-driven MVC controllers approach the classical MVC controllers when the prediction horizon goes to infinity ($L \rightarrow \infty$). This fact has also been verified from our simulation studies.

- The prediction horizon L must be chosen greater than or equal to the order of the interactor of the lifted system d. Recall H and $\tilde{N}$ are defined in (3.25) and (3.12) as

$$H \stackrel{\text{def}}{=} \begin{bmatrix} \tilde{N} \\ \tilde{M}\tilde{N} \\ \vdots \\ \tilde{M}^{L-1}\tilde{N} \end{bmatrix}$$

and

$$\tilde{N} \stackrel{\text{def}}{=} [\ O_L\underline{B} \quad H_L\ ] - \tilde{M}[\ H_L \quad 0_{(L\times m)\times(M\times r)}\ ].$$

When $L \leqslant d-1$, from (3.8) and (3.9) it can be seen that $O_L\underline{B}$ and H_L are zero matrices, thus $\tilde{N}$ and H are zero matrices. In addition, the optimal future

control signals in (3.31) are zeroes. Therefore the minimum prediction horizon $L_{\min}$ should be chosen as $L_{\min} = d$ [60].

- A dual-rate system where the outputs are sampled at the same rate is considered in this chapter, to make the exposition simple and clear. Notice that a multirate system where the outputs are sampled at different rates can also be handled within the framework, if the proper lifting operators are applied. Considering a system where $y = \begin{bmatrix} y_1^T & y_2^T \end{bmatrix}^T$, y_1 is sampled at n_1T, y_2 is sampled at n_2T, and the input u is fast-updated with period T, to apply the designed algorithms we need to lift the input signal u by the lifting operator L_M (M is the least common multiple of $n_1$and n_2), lift y_1 by L_{N_1} ($N_1 = \frac{M}{n_1}$) and lift y_2 by L_{N_2} ($N_2 = \frac{M}{n_2}$). The lifted system from the lifted input $\underline{u} = L_M u$ to the lifted output $\underline{y} = \begin{bmatrix} (L_{N_1}y_1)^T & (L_{N_2}y_2)^T \end{bmatrix}^T$ is a single-rate linear time-invariant system with sampling period MT. Thus our algorithms can be applied.

3.5 Estimation of the MVC-benchmark variance directly from input-output data

3.5.1 Estimation of the single-rate MVC-benchmark variance

In [27], a data-driven approach is developed for multivariate feedback control performance assessment for any structure of time delays. It presents the extended output $y_{k|L}$ of the process (in Figure 3.1) as

$$y_{k|L} = O_L x_t + H_L u_{k|L} + H_L^s e_{k|L},$$

and the output variance under MVC can be written as

$$\begin{aligned} J_{\text{mvc}} &= \min\ E[y_k^T y_k] = \text{trace}(\min\ E[y_k y_k^T]) \\ &= \text{trace}\ (I - H_L H_L^\dagger) H_{L,1}^s H_{L,1}^{sT} (I - H_L H_L^\dagger)^T \end{aligned} \tag{3.32}$$

where H_L is defined as in (3.9) with $M = 1$ as it addressed in the single-rate case; H_L^s is defined as in (3.14), and $H_{L,1}^s$ denotes the first block column of H_L^s. The important contribution of this algorithm is that "it consolidates the traditional three-step procedure, model identification, closed-loop time series analysis, and extraction of the MVC benchmark into a single shot". Thus "no concepts, such as transfer function matrices, state space matrices, Markov parameters, interactor matrices, etc. are

needed anymore in the algorithm" [27]. In the following subsection we will introduce the estimation of the dual-rate MVC-benchmark variance based on this method.

3.5.2 Estimation of the dual-rate MVC-benchmark variance

It is shown in (3.32) that the J_{mvc} can be estimated if H_L and $H^s_{L,1}$ are known. In the following, we will discuss how to estimate these two matrices. From (3.21, 3.22) it can be seen that

$$\begin{aligned}\hat{y}_{k|L} &= \tilde{M}^L y_{k-LM|L} + P_{L-1} u_{k-LM|(L-1)M} + F_{L+1} u_{k-M|(L+1)M} \\ &= L_w W_p + H_L u_{k|LM},\end{aligned}$$

where $W_p = \begin{bmatrix} y^T_{k-LM|L} & u^T_{k-LM|LM} \end{bmatrix}^T$ denotes the past information (output and control signals), and $L_w = [\ \tilde{M}^L \quad P_{L-1} \quad F_{L+1}(:, 1 : M \times r)\ ]$. Then $\hat{H}_L$, the estimation of H_L, can be determined as

$$\hat{H}_L = [\ h_1 \quad h_2 \quad \cdots \quad h_L\ ] \tag{3.33}$$

where

$$h_i = \sum_{j=1}^{L-i+1} \hat{H}_{j,j+i},\ \forall i = 1, \cdots L, \tag{3.34}$$

and $\hat{H}$ is the estimation of the Hankel Matrix defined in (3.25). To estimate $H^s_{L,1}$, we need first define another Hankel matrix

$$\Lambda = \begin{bmatrix} \tilde{T} \\ \tilde{M}\tilde{T} \\ \vdots \\ \tilde{M}^{L-1}\tilde{T} \end{bmatrix} = \begin{bmatrix} \Lambda_{11} & \cdots & \Lambda_{1,L+1} \\ \Lambda_{21} & \cdots & \Lambda_{2,L+1} \\ \vdots & \ddots & \vdots \\ \Lambda_{L1} & \cdots & \Lambda_{L,L+1} \end{bmatrix}, \tag{3.35}$$

then $\hat{H}^s_{L,1}$ can be obtained as

$$\hat{H}^s_{L,1} = \sum_{j=1}^{L} \Lambda_{j,j+1}. \tag{3.36}$$

The proof of (3.33), (3.34) and (3.36) is omitted since the procedure is the same as that in Proposition 3.1. Therefore, the estimated MVC-benchmark variance can be computed as

$$\hat{J}_{\text{mvc}} = \text{trace}\ (I - \hat{H}_L \hat{H}^\dagger_L)\hat{H}^s_{L,1}\hat{H}^{sT}_{L,1}(I - \hat{H}_L \hat{H}^\dagger_L)^T. \tag{3.37}$$

So far we have shown the procedure to estimate the dual-rate MVC-benchmark variance: the first step is to arrange the data matrix in the left-hand side of (3.16) from the open-loop input-output data; then the subspace matrices $\tilde{M}$, $\tilde{N}$ and $\tilde{T}$ should be determined by a QR decomposition; finally the dual-rate MVC-benchmark variance can be calculated by (3.37), where $\hat{H}_L$ and $\hat{H}^s_{L,1}$ are obtained from Hankel Matrices (3.25) and (3.35). Notice that $H^s_{L,1}$ is preferably estimated from a set of representative closed-loop routine operating data to reflect control performance assessment under routine operating condition. With the estimated MVC-benchmark variance, the closed-loop performance index can be computed as the ratio between the estimated MVC-benchmark variance and the current output variance:

$$\eta = \frac{\hat{J}_{\text{mvc}}}{\text{var}(y_k)}.$$

3.6 A simulation example

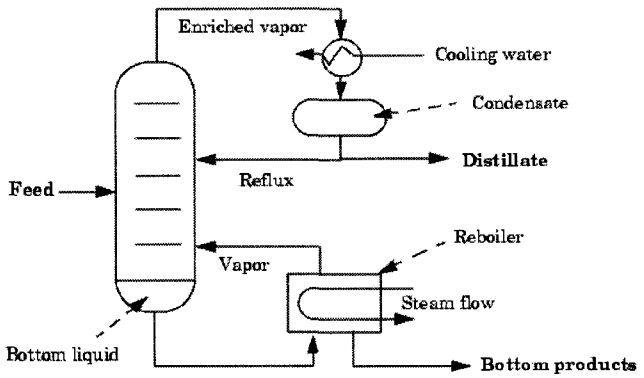

Figure 3.2: The distillation column [1]

This distillation column example is adopted from [83] and illustrated in Figure 3.2. Similar examples can be found in [34] and MATLAB/Control Toolbox User's Guide [1]. This distillation column is used to separate a mix of methanol and water (the feed) into bottom products (mostly water) and a methanol-saturated distillate. The linearized transfer function model around the steady-state operation condition is:

$$\begin{bmatrix} y_1(s) \\ y_2(s) \end{bmatrix} = \begin{bmatrix} \frac{12.8e^{-s}}{16.7s+1} & \frac{-18.9e^{-3s}}{21.0s+1} \\ \frac{6.6e^{-7s}}{10.9s+1} & \frac{-19.4e^{-3s}}{14.4s+1} \end{bmatrix} \begin{bmatrix} u_1(s) \\ u_2(s) \end{bmatrix},$$

where the regulated output variables y_1 and y_2 are the percentage of methanol in the distillate and in the bottom products, respectively; the manipulated variable u_1 is the reflux flow rate, and u_2 is the steam flow rate in the reboiler. We assume the control signals are fast sampled while the output signals are slow sampled. The fast and slow sampling periods are chosen as $T_f = 1$ sec and $T_s = 2$ sec; therefore the lifting factor $M = 2$ in this example. By discretization and lifting [10], we can obtain the lifted dual-rate system model as

$$\begin{bmatrix} y_1(z) \\ y_2(z) \end{bmatrix} = \begin{bmatrix} \frac{0.744z^{-1}}{1-0.8871z^{-1}} & \frac{-0.8789z^{-2}}{1-0.9092z^{-1}} & \frac{0.7077z^{-2}}{1-0.8871z^{-1}} & \frac{-0.838z^{-3}}{1-0.9092z^{-1}} \\ \frac{0.5786z^{-4}}{1-0.8324z^{-1}} & \frac{-1.302z^{-2}}{1-0.8703z^{-1}} & \frac{0.5278z^{-5}}{1-0.8324z^{-1}} & \frac{-1.214z^{-3}}{1-0.8703z^{-1}} \end{bmatrix} \begin{bmatrix} \underline{u_1}(z) \\ \underline{u_2}(z) \end{bmatrix},$$

where $\underline{u_1}$ and $\underline{u_2}$ are lifted control signals. We assume the slow-rate transfer function model of the disturbance, under which the dual-rate system works, is as

$$N_s(z) = \begin{bmatrix} \frac{1}{1-0.4z^{-1}} & \frac{0.7}{1-0.3z^{-1}} \\ \frac{-0.3}{1-0.6z^{-1}} & \frac{1}{1-0.5z^{-1}} \end{bmatrix} \begin{bmatrix} e_1(z) \\ e_2(z) \end{bmatrix},$$

where e_1 and e_2 are independent white noises with unit variance in slow rate. The unitary interactor matrix of the lifted dual-rate system is calculated [29] as

$$D_{in} = \begin{bmatrix} -z & \\ & -z^2 \end{bmatrix},$$

and the order of the interactor matrix $d = 2$. As stated in Theorem 6.2.1 in [29], the interactor-filtered disturbance model can be separated as

$$\begin{aligned} z^{-d} D_{in} N_s &= z^{-2} \begin{bmatrix} -z & \\ & -z^2 \end{bmatrix} \begin{bmatrix} \frac{1}{1-0.4z^{-1}} & \frac{0.7}{1-0.3z^{-1}} \\ \frac{-0.3}{1-0.6z^{-1}} & \frac{1}{1-0.5z^{-1}} \end{bmatrix} \\ &= N_F + z^{-2} N_R, \end{aligned}$$

where

$$N_F = \begin{bmatrix} -z^{-1} & -0.7z^{-1} \\ 0.3 + 0.18z^{-1} & -1 - 0.5z^{-1} \end{bmatrix}$$

and

$$N_R = \begin{bmatrix} \frac{-0.4z^{-2}}{1-0.4z^{-1}} & \frac{-0.21z^{-2}}{1-0.3z^{-1}} \\ \frac{0.108z^{-2}}{1-0.6z^{-1}} & \frac{-0.25z^{-2}}{1-0.5z^{-1}} \end{bmatrix}.$$

Thus, the theoretical minimum variance can be calculated as

$$J_{\text{mvc}} = \text{trace}(a_t a_t^T) = 2.8624,$$

where $a_t = N_F \begin{bmatrix} e_1^T & e_2^T \end{bmatrix}^T$.

In the following part, we are going to use this distillation column example to illustrate both the dual-rate data-driven MVC algorithm and the control performance assessment algorithm. To design the data-driven dual-rate MVC, the open-loop input-output data are required to identify the subspace matrices. Open loop input-output data are obtained by exciting the open loop dual-rate system using a designed random binary signal of magnitude 1 for the inputs, and random numbers with unit variance for the white noise sequences. The input and output data are collected over 600 seconds with their respective sampling rates. The data are plotted in Figure 3.3. After estimating the subspace matrices from the input-output data by equations (3.17) and (3.18), the optimal control signal series are computed from (3.31). Notice that only the first $2M$ rows of the optimal control signal are implemented because of the receding horizon MVC control law. According to Remark 3, the longer prediction horizon L we choose, the better control performance we could obtain. Using the same group of open loop data, we design different MVC controllers with different prediction horizons for the dual-rate system, such that L changes from 10 to 20 and the past horizon $J = 2$. The simulation results are shown in Table 3.1, where $\text{var}(y_k)$ is the simulated output variance, and the relative error between the simulated and the theoretical minimum variances $O_e = \frac{var(y_k) - J_{\text{mvc}}}{J_{\text{mvc}}}$. Table 3.1 shows that the error between $\text{var}(y_k)$ and the J_{mvc} is small, which verifies the dual-rate data-driven algorithm. Also, it can be observed that when L increases, $\text{var}(y_k)$ approaches the theoretical minimum variance J_{mvc}. This validates Remark 3. The fast-rate optimal control signals and slow-rate regulated outputs are shown in Figure 3.4 when $L = 20$.

Table 3.1: Simulation results of the distillation column under the designed data-driven dual-rate MVC controllers

Prediction horizon L	10	11	12	13	14	15	20
$\text{var}(y_k)$	2.9906	2.9756	2.9750	2.9360	2.9025	2.8931	2.8915
O_e	0.0448	0.0395	0.0393	0.0257	0.0140	0.0107	0.0102

Now let us look at simulations for the data-driven dual-rate MVC-benchmark

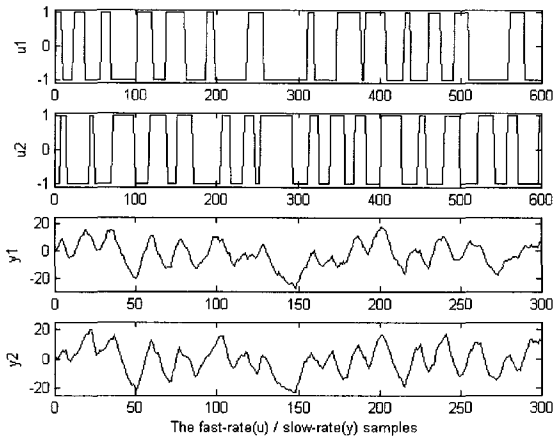

Figure 3.3: The open loop input-output data from simulations

Table 3.2: Simulation results of the distillation column for the data-driven dual-rate MVC-benchmark performance assessment

Control law	Prediction horizon L	$\text{var}(y_k)$	J_{mvc}	$\hat{J}_{\text{mvc}}$	η_e
Non-optimal	13	3.2510	2.8624	2.8339	0.0100
Non-optimal	14	3.2018	2.8624	2.7751	0.0305
Optimal	10	2.9872	2.8624	2.8040	0.0204
Optimal	11	2.9721	2.8624	2.9931	0.0457

performance assessment algorithm. Open-loop and closed-loop input-output data sets are needed to estimate $\hat{H}_L$ and $\hat{H}^s_{L,1}$, respectively. Then the MVC-benchmark variance is calculated according to equation (3.37). The open-loop data set is generated in the same way as in the dual-rate MVC design simulations. The closed-loop data sets are collected under two kinds of control laws: the non-optimal and the optimal. The non-optimal control law is computed by multiplying the optimal receding horizon MVC control signals by 1.5. For each of the cases listed in Table 3.2, we run the simulations for 1000 seconds. The simulation results are listed in Table 3.2, where $\text{var}(y_k)$ is the simulated output variance, J_{mvc} is the theoretical minimum variance, $\hat{J}_{\text{mvc}}$ is the estimated minimum variance from each simulation, and $\eta_e = \left| \frac{J_{\text{mvc}}}{\text{var}(y_k)} - \frac{\hat{J}_{\text{mvc}}}{\text{var}(y_k)} \right|$ is the absolute value of the performance index estimation error. We can see that η_e is small, which verifies the derived dual-rate MVC-benchmark performance assessment algorithm.

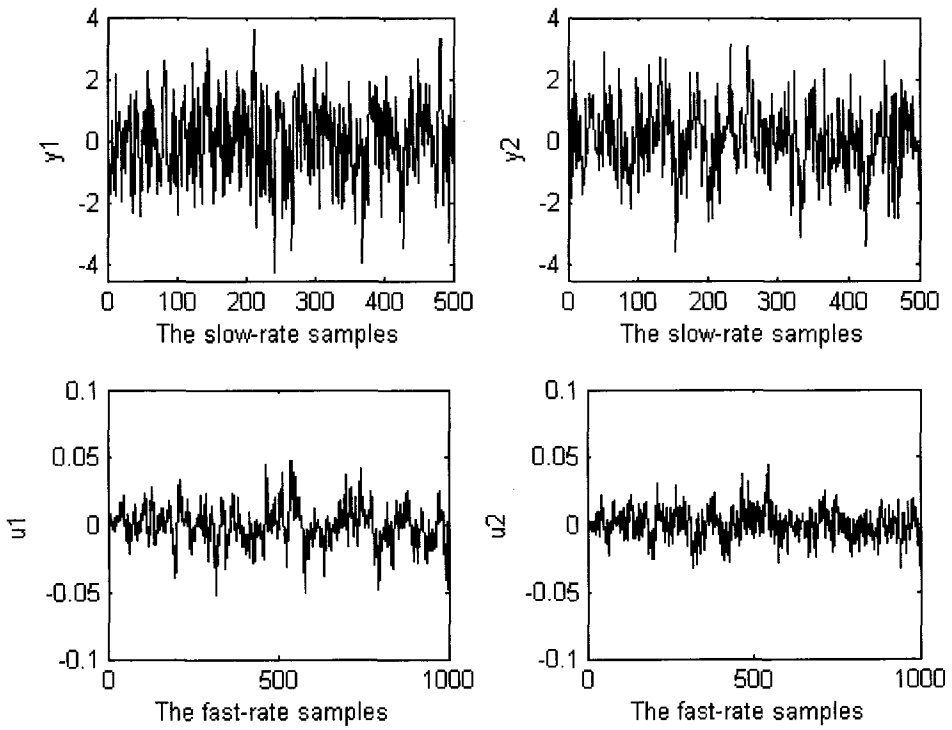

Figure 3.4: The closed-loop control/output signals when $L = 20$

3.7 Conclusions

In this chapter, the data-driven minimum variance control and the MVC-benchmark variance estimation have been discussed for a dual-rate system. A subspace input-output equation is derived by the lifting technique to obtain a prediction model. The dual-rate optimal controller design is data-driven since it only requires a set of input-output open-loop experimental data and the explicit process model is not needed. The presented MVC-benchmark estimation algorithm requires a set of open-loop experimental data plus a set of closed-loop routine operating data. The proposed algorithms were illustrated through a distillation column simulation example. In this chapter we consider a dual-rate system where the outputs are sampled at the same rate, to make the exposition simple and clear. Notice that a multirate system where the outputs are sampled at different rates can also be handled within the framework, if the proper lifting operators are applied.

Chapter 4

A Data-driven Predictive Control for Single-rate Systems[3]

This chapter is concerned with some outstanding problems in predictive control of single-rate systems. The predictive control applied is completely data based and does not need an explicit model. In addition, unlike other data-driven predictive control designs, the proposed approach can deal with systems without complete on-line measurement of all output variables. The proposed data-driven predictive control approach is applied to solving the control problem of a solid oxide fuel cell (SOFC) system, which is challenging owing to its slow response and tight operating constraints. Simulation results have demonstrated the feasibility of the control application.

[3]The materials in this chapter will be published in "X. Wang, B. Huang, and T. Chen. Data-driven predictive control for solid oxide fuel cells. J. of Process Contr., to be published, 2007".

4.1 Introduction

One of the objectives of this chapter is to explore a data-driven predictive control law for single-rate systems, when only open-loop input-output data are available. Unlike the model-based approach, where the system model is required to achieve this goal, we follow a novel approach based on results from subspace system identification [58, 59]. The data-driven design approach presented in the literature so far has been derived under the condition that all outputs measurements are measured on-line in closed-loop systems. However, in reality, some outputs may not be measured in real time, or are too costly to be measured on-line although they may be measured in some off-line model identification experiments in a laboratory. For example, it may be difficult and costly to on-line measure the fuel utilization which is the ratio between the reacted fuel flow rate and the inlet fuel flow rate which is a component of total inlet flow in the SOFC system [53, 85]. To circumvent this problem, we consider the data-driven predictive control design based on only partially available output measurements.

In this chapter we propose a predictive control method via subspace approach. The predictive control has usually been studied under the heading of MPC. This is because MPC has considerable advantages relative to other conventional control strategies: the ability to handle input and state constraints for large scale multi-variable plants, the capability of dealing with variables interaction, and the ease of adaptation to new operating conditions [17, 32]. Like any other model-based control, conventional MPC relies heavily on process models. An accurate process model is required if the process is to be regulated tightly. Usually there are two ways to obtain process models: the analytic approach where certain process knowledge (such as fundamental physical laws) is required to derive the model and the experimental approach by fitting a model to the input-output data through system identification. In this chapter the proposed predictive control is completely data based and does not need an explicit model. It can explicitly deal with constraints and incomplete on-line measurements.

The remainder of this chapter is organized as follows. The system description and the problem formulation are described in Section 4.2. In Section 4.3, a data-driven

approach is investigated to design the predictive controller using partial closed-loop output measurements. The SOFC dynamic model and operating conditions are given in Section 4.4. SOFC control simulation is provided in Section 4.5, followed by conclusions in Section 4.6.

4.2 System description and problem statement

As it can be seen later in Section 4.4, the SOFC model of concern is linear in its dynamics but nonlinear in its output equation (due to the Nernst equation). In this chapter, we restrict to a linear predictive control strategy. The model is not linearized from the original nonlinear model. Instead, we assume that the nonlinear model is not available, but an off-line experiment can be performed by varying fuel and oxygen inlet flows. In classical system identification, a linear state space model can be identified. Note that in the proposed method only certain subspace matrices, not an explicit system model, need to be determined. To formulate the problem, we consider a general linear time-invariant system which can be described by the following discrete-time state-space model

$$x_{k+1} = Ax_k + Bu_k + Ee_k \tag{4.1}$$

$$y_k = Cx_k + Du_k + Fe_k \tag{4.2}$$

where k is a discrete-time instance, $x_k \in R^n$ the state vector, $y_k \in R^m$ the system output, $u_k \in R^r$ the system input, and $e_k \in R^m$ a white noise sequence with zero mean and identity covariance matrix. A, B, C, D, E, F are system matrices with appropriate dimensions. We assume that (C, A) is observable, (A, B) is controllable, and u and e are independent signals. Due to time-delay, it is generally assumed that $D = 0$.

For the sake of presentation, the following definitions are adopted. $\{\cdots\}$ is used to present a data set, and $[\cdots]$ is used to denote a vector. The problem investigated in this chapter is to design the data-driven predictive control law directly from the experimental input-output data defined as

$$\{u_k,\ y_k\colon\ k = 0, 1, \cdots, N-1\}.$$

The lengths of input and output data equal to N. Particularly, the controller to

be designed needs to work in control-loops where only partial measurements are available, i.e., the output can be described as $y_k = [(y_k^s)^T\ (y_k^u)^T]^T \in R^m$, where $y_k^s \in R^a$ denotes the measurable outputs and $y_k^u \in R^b$ indicates the unmeasurable outputs. The superscript s means "sampled" and u indicates "unmeasured" respectively. It is obvious that $a + b = m$.

4.3 Data-driven predictive control algorithm

Recall that in this work the extended signal sequence $s_{k|L} \in R^{L \times n_r}$ is defined as

$$s_{k|L} \stackrel{\text{def}}{=} [s_k^T\ s_{k+1}^T\ \cdots\ s_{k+L-1}^T]^T,$$

where $s_t \in R^{n_r}$ $(t = k_0, \cdots, k, k+1, \cdots)$ is a sequence of data with n_r being the number of the rows; k is the starting index; L is the number of n_r-block rows in $s_{k|L}$. The control objective of this work is to minimize a standard cost function in model-based predictive control subject to certain constraints. This can be re-written in vector form for convenience as follows:

$$\min_{\Delta u_{k|J_c}} J_k = \min(\hat{y}_{k+1|L} - r_{k+1|L})^T Q(\hat{y}_{k+1|L} - r_{k+1|L}) + \Delta u_{k|J_c}^T R_{J_c} \Delta u_{k|J_c} + u_{k|J_c}^T P_{J_c} u_{k|J_c}, \tag{4.3}$$

subject to

$$u_{k|J_c}^{\min} \leqslant u_{k|J_c} \leqslant u_{k|J_c}^{\max}, \tag{4.4}$$

$$\Delta u_{k|J_c}^{\min} \leqslant \Delta u_{k|J_c} \leqslant \Delta u_{k|J_c}^{\max}, \tag{4.5}$$

$$y_{k+1|L}^{\min} \leqslant \hat{y}_{k+1|L} \leqslant y_{k+1|L}^{\max}, \tag{4.6}$$

where L is defined as the prediction horizon; J_c $(J_c \leqslant L)$ is the control horizon; $\hat{y}_{k+1|L}$ is a vector of the prediction of future output; $r_{k+1|L}$ is a vector of future reference signals; $u_{k|J_c}$ is a vector of future manipulated signal; $\Delta \stackrel{\text{def}}{=} 1 - z^{-1}$ with z^{-1} being the back shift operator; hence $\Delta u_k = u_k - u_{k-1}$ is the incremental input or control move, and $\Delta u_{k|J_c}$ is a vector of future incremental inputs over the next J_c samples. Δu_k is introduced to ensure zero steady state error in the case of non-zero constant reference or load step changes [9]. $Q \in R^{(L \times m) \times (L \times m)}$, $R_{J_c} \in R^{(J_c \times r) \times (J_c \times r)}$ and $P_{J_c} \in R^{(J_c \times r) \times (J_c \times r)}$ are weighting matrices with block diagonal

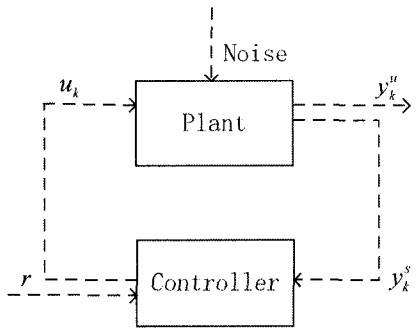

Figure 4.1: Block diagram of the closed-loop system

structure on the error between the predictive outputs and the future references, the future incremental inputs and the future control efforts respectively. Note that Q, R_{J_c}, and P_{J_c} can be time-varying in general. Different from [60, 61] where the prediction horizon and the control horizon are both chosen to be L, we set the control horizon to J_c to make the predictive control law more flexible. The closed-loop system diagram is shown in Figure 4.1, where u_k is the control signal to make $y_k = [(y_k^s)^T \ (y_k^u)^T]^T$ follow the reference r or satisfy certain constraints, while only partial measurements, y_k^s, are available on line.

Given the measured output as $y = \{y_{k_0}^s, \ \cdots, \ y_k^s, \ y_{k+1}^s, \ \cdots\}$, and the input as $u = \{u_{k_0}, \ \cdots, \ u_k, \ u_{k+1}, \ \cdots\}$, the subspace predictive equation of the measured outputs can be written as [60]

$$\hat{y}_{k+1|L}^s = (\tilde{M}^s)^L y_{k-(L-1)|L}^s + P_{L-1}^s u_{k-(L-1)|L-1} + F_L^s u_{k|L}, \tag{4.7}$$

where $\tilde{M}^s$, $P_{L-1}^s$and F_L^s are subspace matrices which can be obtained from the experimental input-output data [60].

Proposition 4.1 *It can be obtained that the predictive equation for the unmeasured outputs is*

$$\hat{y}_{k+1|L}^u = P_{L-1}^u u_{k-(L-1)|L-1} + F_L^u u_{k|L} + U_p, \tag{4.8}$$

where P_{L-1}^u and F_L^u are subspace matrices obtained in the same way that P_{L-1}^s and F_L^s are formed, respectively, in [60], and U_p is a constant matrix in terms of past inputs.

Proof. By iteratively substituting $y^u_{k-jL+1|L}$ where $j = 1, \cdots, i$, it can be obtained [60]

$$\begin{aligned}
\hat{y}^u_{k+1|L} &= (\tilde{M}^u)^L y^u_{k-(L-1)|L} + P^u_{L-1} u_{k-(L-1)|L-1} + F^u_L u_{k|L} \\
&= (\tilde{M}^u)^L [(\tilde{M}^u)^L y^u_{k-2L+1|L} + P^u_{L-1} u_{k-2L+1|L-1} + F^u_L u_{k-L|L}] \\
&+ P^u_{L-1} u_{k-(L-1)|L-1} + F^u_L u_{k|L} \\
&= \cdots \\
&= [(\tilde{M}^u)^{i\times L} y^u_{k-i\times L+1|L} + (\tilde{M}^u)^{(i-1)L} P^u_{L-1} u_{k-i\times L+1|L-1} \\
&+ (\tilde{M}^u)^{(i-1)L} F^u_L u_{k-(i-1)L+1|L} + \cdots + (\tilde{M}^u)^L P^u_{L-1} u_{k-2L+1|L-1} \\
&+ (\tilde{M}^u)^L F^u_L u_{k-L|L}] + P^u_{L-1} u_{k-(L-1)|L-1} + F^u_L u_{k|L} \\
&= (\tilde{M}^u)^{i\times L} y^u_{k-i\times L+1|L} + P^u_{L-1} u_{k-(L-1)|L-1} + F^u_L u_{k|L} + U_p \qquad (4.9)
\end{aligned}$$

where

$$U_p = \begin{bmatrix} (\tilde{M}^u)^{(i-1)L} P^u_{L-1} & \cdots & (\tilde{M}^u)^L P^u_{L-1} \end{bmatrix} \begin{bmatrix} u_{k-i\times L+1|L-1} \\ \vdots \\ u_{k-2L+1|L-1} \end{bmatrix} +$$

$$\begin{bmatrix} (\tilde{M}^u)^{(i-1)L} F^u_L & \cdots & (\tilde{M}^u)^L F^u_L \end{bmatrix} \begin{bmatrix} u_{k-(i-1)L+1|L} \\ \vdots \\ u_{k-L|L} \end{bmatrix}.$$

It will be proven below that $(\tilde{M}^u)^{i\times L} \to 0$ when $i \times L \to \infty$. Assuming that in the operating control loop some measurements are unavailable, we can re-write (4.1) and (4.2) as

$$\begin{aligned}
x_{k+1} &= Ax_k + Bu_k + Ee_k, \\
y_k &= \begin{bmatrix} y^s_k \\ y^u_k \end{bmatrix} = \begin{bmatrix} C^s \\ C^u \end{bmatrix} x_k + \begin{bmatrix} D_s \\ D_u \end{bmatrix} u_k + \begin{bmatrix} F_s \\ F_u \end{bmatrix} e_k,
\end{aligned}$$

where the superscripts s and u indicate "sampled"and "unmeasured". Thus, the state-space model from u to y^u is

$$\begin{aligned}
x_{k+1} &= Ax_k + Bu_k + Ee_k \\
y^u_k &= C^u x_k + D_u u_k + F_u e_k
\end{aligned}$$

and O_L^u, the extended observability matrix for the pair (C^u, A) is defined as

$$O_L^u \stackrel{\text{def}}{=} \begin{bmatrix} C^u \\ C^u A \\ \vdots \\ C^u (A)^{L-1} \end{bmatrix} \in R^{(L\times b)\times n}.$$

It can be obtained that [59]

$$\tilde{M}^u = O_L^u A[(O_L^u)^T O_{L]}^u]^{-1}(O_L^u)^T.$$

Noting that

$$\text{eig}(AB) = \text{eig}(BA);$$

hence

$$\begin{aligned} \text{eig}(\tilde{M}^u) &= \text{eig}\{O_L^u A[(O_L^u)^T O_L^u]^{-1}(O_L^u)^T\} \\ &= \text{eig}\{A[(O_L^u)^T O_L^u]^{-1}(O_L^u)^T O_L^u\} \\ &= \text{eig}(A). \end{aligned}$$

Because the identified discrete-time open-loop system is stable, i.e., $\text{eig}(A) < 1$, thus when $i \times L$ goes to infinity,

$$\begin{aligned} \text{eig}[(\tilde{M}^u)^{i\times L}] &= \text{eig}[(A)^{i\times L}] \\ &= [\text{eig}(A)]^{i\times L} \to 0 \\ &\Rightarrow (\tilde{M}^u)^{i\times L} \to 0. \end{aligned}$$

Therefore, it can be seen that when $i \times L$ is large enough to make $(\tilde{M}^u)^{i\times L} \to 0$, (4.9) can be written as

$$\hat{y}_{k+1|L}^u = P_{L-1}^u u_{k-(L-1)|L-1} + F_L^u u_{k|L} + U_p.$$

■

Proposition 4.2 *Combining (4.7) and (4.8), it can be obtained the prediction of the future outputs presented by the past available measurements and past input signals as*

$$\hat{y}_{k+1|L} = \tilde{M}^L y_{k-(L-1)|L} + P_{L-1} u_{k-(L-1)|L-1} + F_L u_{k|L} + \Psi_p. \qquad (4.10)$$

Proof. The matrices in equation (4.10) are as follows:

$$\tilde{M}^L = \begin{bmatrix} (\tilde{M}^s)^L(1,1) & 0 & \cdots & (\tilde{M}^s)^L(1:L) & 0 \\ 0 & 0 & \cdots & 0 & 0 \\ \vdots & \vdots & \vdots & \vdots & \vdots \\ (\tilde{M}^s)^L(L,1) & 0 & \cdots & (\tilde{M}^s)^L(L,L) & 0 \\ 0 & 0 & \cdots & 0 & 0 \end{bmatrix},$$

$$P_{L-1} = \begin{bmatrix} P^s_{L-1}(1,:)^T & P^u_{L-1}(1,:)^T & \cdots & P^s_{L-1}(L,:)^T & P^u_{L-1}(L,:)^T \end{bmatrix}^T,$$

$$F_L = \begin{bmatrix} F^s_L(1,:)^T & F^u_L(1,:)^T & \cdots & F^s_L(L,:)^T & F^u_L(L,:)^T \end{bmatrix}^T,$$

and

$$\Psi_p = \begin{bmatrix} 0 & U_p(1,:)^T & \cdots & 0 & U_p(L,:)^T \end{bmatrix}^T.$$

In the above equations, each block is with appropriate dimension, such as for $j = 1, 2, \cdots, L$,

$$(\tilde{M}^s)^L(j,k) \in R^{a\times a},\ P^s_{L-1}(j,:) \in R^{a\times(L-1)r},\ P^u_{L-1}(j,:) \in R^{b\times(L-1)r},$$
$$F^s_L(j,:) \in R^{a\times(L\times r)},\ F^u_L(j,:) \in R^{b\times(L\times r)},\ U_p(j,:) \in R^b.$$

■

Proposition 4.3 *Substituting (4.10) into (4.3) to predict the future measured and unmeasured outputs, one can formulate the control objective as a Quadratic Programming (QP) problem [61], i.e.,*

$$\min_{\Delta u_{k|L}} J_k = \Delta u^T_{k|L} H \Delta u_{k|L} + 2 f^T_k \Delta u_{k|L}, \tag{4.11}$$

subject to constraints:

$$\widetilde{A} \Delta u_{k|L} \leqslant b_k. \tag{4.12}$$

Proof. Defining matrices S and c as

$$S \stackrel{\text{def}}{=} \begin{bmatrix} I_r & 0_r & \cdots & 0_r \\ I_r & I_r & \cdots & 0_r \\ \vdots & \vdots & \ddots & \vdots \\ I_r & I_r & \cdots & I_r \end{bmatrix} \in R^{(L\times r)\times(L\times r)},$$

and

$$c \stackrel{\text{def}}{=} \begin{bmatrix} I_r & I_r & \cdots & I_r \end{bmatrix}^T \in R^{(L\times r)\times r},$$

we can obtain

$$u_{k|L} = S\Delta u_{k|L} + cu_{k-1}. \tag{4.13}$$

Thus, equation (4.10) can be re-written as

$$\begin{aligned}\hat{y}_{k+1|L} &= \tilde{M}^L y_{k-(L-1)|L} + P_{L-1}u_{k-(L-1)|L-1} + F_L u_{k|L} + \Psi_p \\ &= \Phi_L(k) + F_L u_{k|L} \\ &= \Phi_L(k) + F_L(S\Delta u_{k|L} + cu_{k-1}) \\ &= \Phi_L^{\Delta}(k) + F_L^{\Delta}\Delta u_{k|L}\end{aligned} \tag{4.14}$$

where

$$\begin{aligned}\Phi_L(k) &= \tilde{M}^L y_{k-(L-1)|L} + P_{L-1}u_{k-(L-1)|L-1} + \Psi_p, \\ \Phi_L^{\Delta}(k) &= \Phi_L(k) + F_L cu_{k-1}, \\ F_L^{\Delta} &= F_L S.\end{aligned} \tag{4.15}$$

It can be seen that (4.3) is equivalent to (4.16) with the future control moves being zero after $k + J_c$ step, i.e. $\Delta u_{k+J_c+1|(L-J_c)} = 0$. Thus (4.3)–(4.6) can be re-formulated as

$$\min_{\Delta u_{k|L}} J_k = \min(\hat{y}_{k+1|L} - r_{k+1|L})^T Q(\hat{y}_{k+1|L} - r_{k+1|L}) + \Delta u_{k|L}^T R\Delta u_{k|L} + u_{k|L}^T P u_{k|L}, \tag{4.16}$$

subject to

$$\begin{aligned} u_{k|L}^{\min} \leqslant u_{k|L} \leqslant u_{k|L}^{\max}, \\ \Delta u_{k|L}^{\min} \leqslant \Delta u_{k|L} \leqslant \Delta u_{k|L}^{\max}, \\ y_{k+1|L}^{\min} \leqslant \hat{y}_{k+1|L} \leqslant y_{k+1|L}^{\max}, \\ \Delta u_{k+J_c+1|(L-J_c)} = 0. \end{aligned}$$

Control signal related weighting matrices and constraints are all extended from original ones to those with proper dimensions. Substituting (4.13) and (4.14) into

(4.16), we have

$$
\begin{aligned}
J_k &= (\hat{y}_{k+1|L} - r_{k+1|L})^T Q(\hat{y}_{k+1|L} - r_{k+1|L}) + \Delta u_{k|L}^T R \Delta u_{k|L} + u_{k|L}^T P u_{k|L} \\
&= \left(\Phi_L^{\Delta}(k) + F_L^{\Delta}\Delta u_{k|L} - r_{k+1|L}\right)^T Q \left(\Phi_L^{\Delta}(k) + F_L^{\Delta}\Delta u_{k|L} - r_{k+1|L}\right) \\
&+ \Delta u_{k|L}^T R \Delta u_{k|L} + \left(S\Delta u_{k|L} + cu_{k-1}\right)^T P \left(S\Delta u_{k|L} + cu_{k-1}\right) \\
&= \Delta u_{k|L}^T (F_L^{\Delta} Q F_L^{\Delta} + R + S^T P S)\Delta u_{k|L} + 2\left(\Phi_L^{\Delta}(k) - r_{k+1|L}\right)^T Q F_L^{\Delta} \Delta u_{k|L} \\
&+ 2\left(cu_{k-1}\right)^T P S \Delta u_{k|L} + \left(\Phi_L^{\Delta}(k) - r_{k+1|L}\right)^T Q \left(\Phi_L^{\Delta}(k) - r_{k+1|L}\right) + \left(cu_{k-1}\right)^T P \left(cu_{k-1}\right) \\
&= \Delta u_{k|L}^T H \Delta u_{k|L} + 2 f_k^T \Delta u_{k|L} + J_k^0,
\end{aligned}
$$

where

$$
\begin{aligned}
H &= F_L^{\Delta} Q F_L^{\Delta} + R + S^T P S, \\
f_k &= F_L^{\Delta T} Q \left(\Phi_L^{\Delta}(k) - r_{k+1|L}\right) + S^T P c u_{k-1}, \\
J_k^0 &= \left(\Phi_L^{\Delta}(k) - r_{k+1|L}\right)^T Q \left(\Phi_L^{\Delta}(k) - r_{k+1|L}\right) + u_{k-1} c^T P c u_{k-1}.
\end{aligned}
$$

The constraints on control are

$$
\begin{aligned}
u_{k|L}^{\min} \leqslant u_{k|L} \leqslant u_{k|L}^{\max} &\Leftrightarrow \\
u_{k|L}^{\min} \leqslant S\Delta u_{k|L} + cu_{k-1} \leqslant u_{k|L}^{\max} &\Leftrightarrow \\
S\Delta u_{k|L} \leqslant u_{k|L}^{\max} - cu_{k-1}, & \\
-S\Delta u_{k|L} \leqslant -u_{k|L}^{\min} + cu_{k-1}. &
\end{aligned}
$$

The control rate constraints are

$$
\begin{aligned}
\Delta u_{k|L}^{\min} \leqslant \Delta u_{k|L} \leqslant \Delta u_{k|L}^{\max} &\Leftrightarrow \\
I_{L\times r}\Delta u_{k|L} \leqslant \Delta u_{k|L}^{\max}, & \\
-I_{L\times r}\Delta u_{k|L} \leqslant -\Delta u_{k|L}^{\min}. &
\end{aligned}
$$

The output constraints are

$$
\begin{aligned}
y_{k+1|L}^{\min} \leqslant y_{k+1|L} \leqslant y_{k+1|L}^{\max} &\Leftrightarrow \\
y_{k+1|L}^{\min} \leqslant \Phi_L^{\Delta}(k) + F_L^{\Delta}\Delta u_{k|L} \leqslant y_{k+1|L}^{\max} &\Leftrightarrow \\
F_L^{\Delta}\Delta u_{k|L} \leqslant y_{k+1|L}^{\max} - \Phi_L^{\Delta}(k), & \\
-F_L^{\Delta}\Delta u_{k|L} \leqslant -y_{k+1|L}^{\min} + \Phi_L^{\Delta}(k). &
\end{aligned}
$$

To change the control horizon from L to J_c ($J_c \leqslant L$) we set $\Delta u_{k+J_c+1|(L-J_c)} = 0$. Thus

$$I_{(L-J_c)r}\Delta u_{k+J_c+1|(L-J_c)} \leqslant 0 \text{ and } -I_{(L-J_c)r}\Delta u_{k+J_c+1|(L-J_c)} \leqslant 0 \Leftrightarrow$$
$$M_{J_c}\Delta u_{k|L} \leqslant 0 \text{ and } -M_{J_c}\Delta u_{k|L} \leqslant 0$$

where

$$M_{J_c} = \begin{bmatrix} 0^{(J_c\times r)\times(L\times r)} \\ 0^{(L-J_c)r\times(J_c\times r)} \quad I^{(L-J_c)r} \end{bmatrix}.$$

All these constraints above can be written as an equivalent linear inequality:

$$\tilde{A}\Delta u_{k|L} \leqslant b_k \tag{4.17}$$

where

$$\tilde{A} = \begin{bmatrix} S \\ -S \\ I_{L\times r} \\ -I_{L\times r} \\ F_L^{\Delta} \\ -F_L^{\Delta} \\ M_{J_c} \\ -M_{J_c} \end{bmatrix}, \text{and } b_k = \begin{bmatrix} u_{k|L}^{\max} - cu_{k-1} \\ -u_{k|L}^{\min} + cu_{k-1} \\ \Delta u_{k|L}^{\max} \\ -\Delta u_{k|L}^{\min} \\ y_{k+1|L}^{\max} - \Phi_L^{\Delta}(k) \\ -y_{k+1|L}^{\min} + \Phi_L^{\Delta}(k) \\ 0 \\ 0 \end{bmatrix}$$

Thus the predictive control law can be solved by the following QP problem

$$\min_{\Delta u_{k|L}} (\Delta u_{k|L}^T H \Delta u_{k|L} + 2f_k^T \Delta u_{k|L}),$$
$$\text{subject to } \tilde{A}\Delta u_{k|L} \leqslant b_k,$$

which can be solved in MATLAB as

$$\Delta u_{k|L}^* = qp(H, f_k, \tilde{A}, b_k).$$

■

After the optimal control sequence $u_{k|L}$ is calculated, only the first block row, u_k, is implemented in the receding horizon predictive control law.

4.4 Dynamic model of SOFC and operating conditions

A fuel cell is an electrochemical device that converts the chemical energy of a fuel directly into electricity and heat without combustion. The electricity produced has

all kinds of applications such as residential power stations, portable devices, military services and transportation. The byproduct heat is also used in some applications, e.g., for space heating. Though certain problems still remain, fuel cells have shown their potential for high energy conversion efficiency, low to zero emissions, quiet operation, and high reliability over conventional power generation equipment [24]. Depending on the electrolytes used, there are different types of fuel cells:

- Alkaline fuel cell (AFC)
- Direct methanol fuel cell (DMFC)
- Molten carbonate fuel cell (MCFC)
- Phosphoric acid fuel cell (PAFC)
- Polymer electrolyte/ Proton exchange membrane fuel cell (PEMFC)
- SOFC

They are all based on a central design that consists of two electrodes, a positive cathode and a negative anode. Almost all the research that has been conducted in fuel cell control is model-based [54, 85, 72, 19, 69, 3, 36], i.e., an explicit model of the fuel cell system is required to design controllers. In [54] a combination of a nonlinear feedforward and a linear feedback controller was designed to improve the transient oxygen response. An SOFC dynamic model that has been well studied lately is originally presented in [53]. Its dynamic performance is analyzed and evaluated in [85]. A model predictive controller is developed in [72] for a hybrid PEMFC system with ultracapacitors as an auxiliary source of power. A feedforward controller is utilized to solve the "oxygen starvation" problem in [19]. A nonlinear model-based controller is developed for the regulation for a PEMFC system. A detailed dynamic model is presented and a multi-loop control strategy is proposed for a simple SOFC hybrid system in [69]. In [3], a master controller which maintains constant fuel utilization and air ratio and a typical feedback proportional-integral-derivative temperature controller are implemented for an SOFC model. In [36], two robust controllers, which are synthesized by solving an $\mathscr{H}_\infty$ mixed-sensitivity optimization, are designed for a linearized SOFC power plant that is originally developed in [53].

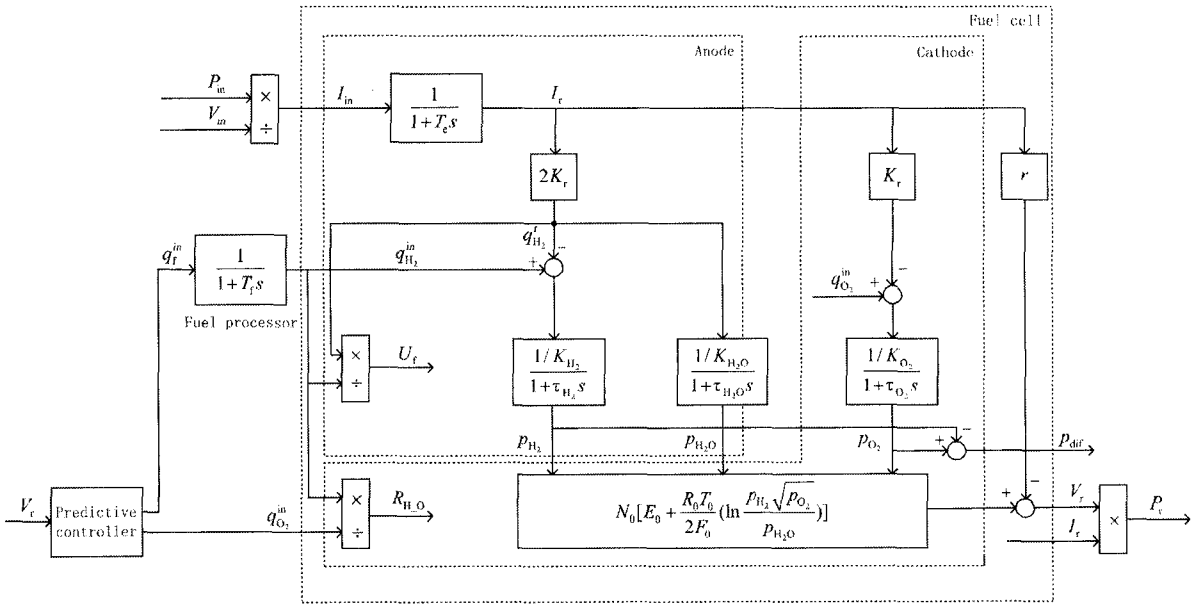

Figure 4.2: SOFC system dynamic model

The SOFC model that is selected for control study in this chapter has been investigated by several researchers for dynamic modeling and control [53, 85, 33, 36]. Although the model is a simplified dynamic model of SOFC systems, it has been shown to be a challenging control problem owing to the SOFC's slow dynamics and tight operating constraints [36]. The solid oxide fuel cell (SOFC) system dynamic model [53, 85] is shown in Figure 4.2. This SOFC system includes three main parts:

- Power section (fuel cells), which generates electricity. There are numerous individual fuel cells in the power section. The SOFC stack dynamic model is based on the following assumptions [53]: ideal gas and isothermal operation. The only source of losses is ohmic loss, as the working conditions of interest are not close to the upper and lower extremes of current. The channels that transport gases along the electrodes have a small and fixed volume; thus it is only necessary to define one single pressure value in the interior. The exhaust of each channel is via a single orifice, which can be considered choked. The Nernst equation can be applied to calculate the voltage.

- Fuel processor, which converts fuels such as natural gas to hydrogen and byproduct gases. The chemical response in the fuel processor is generally

slow. It is associated with the time to change the chemical reaction parameters after a change in the flow of reactants. This dynamic response function of the fuel processor is modeled as a first-order transfer function with a time constant of 5 s [85].

- Data driven predictive controller, which is to be designed via the subspace approach. There are four variables to be controlled including the voltage (to be given later). The only on-line measurement is fuel cell stack output voltage. Other three controlled variables are assumed not to be measured in real time.

The electrochemical reaction in the triple phase boundary is

$$H_2 + \frac{1}{2}O_2 \rightarrow H_2O.$$

- The manipulated variables are $[q_f^{in}\ q_{O_2}^{in}]^T$, where q_f^{in} is the input fuel flow and $q_{O_2}^{in}$ is the input oxygen flow. The steady state of the inputs is $[0.7023\ 0.6134]^T$ mol/s, and the constraints are

$$[0\ 0]^T \text{ mol/s} \leqslant [q_f^{in}\ q_{O_2}^{in}]^T \leqslant [1.7023\ 1.6134]^T \text{ mol/s}.$$

- The fuel cell current demand I_{in} is considered as the disturbance. The power output of the fuel cell system is 100kW, under which the nominal value of the voltage demand V_{in} is 333.8 V and the current demand is 300 A. The dynamic response function from I_{in} to the fuel cell current I_r is modeled as a first order transfer function with a time constant of 0.8 s. This electrical response time in fuel cells is usually fast, and it is mainly associated with the speed at which the chemical reaction is capable of restoring the charge that has been drained by the load.

- The controlled variables are$[V_r\ U_f\ R_{H_O}\ p_{dif}]^T$, where

  - V_r is the fuel cell stack output voltage. Applying Nernst's equation and Ohm's law (to consider ohmic losses), the stack output voltage is represented by the following expression [53]:

$$V_r = N_0 \left[E_0 + \frac{R_0 T_0}{2F_0} \left(\ln \frac{p_{H_2} \sqrt{p_{O_2}}}{p_{H_2O}} \right) \right] - rI_r$$

where p_{H_2}, p_{O_2} and p_{H_2O} are hydrogen, oxygen and water partial pressure. The constraint on V_r is 328.8 V$\leqslant V_r \leqslant$ 338.8 V, and 333.8 V is chosen as the operating point. In the closed-loop simulation, we assume that only V_r is measurable.

- U_f is fuel utilization, which is defined as the ratio between the H_2 flow that reacts and the input H_2 flow, i.e.,

$$U_f \stackrel{\text{def}}{=} q^r_{H_2}/q^{in}_{H_2}.$$

Typically, an $80\% - 90\%$ fuel utilization is desired [53]. We choose the operating point of U_f as 85%.

- R_{H_O} is the ratio between inlet H_2 and O_2 flows, which is defined as

$$R_{H\_O} \stackrel{\text{def}}{=} q^{in}_{H_2}/q^{in}_{O_2}.$$

In the simulation, the constraint on R_{H_O} is set as $0 \leqslant R_{H\_O} \leqslant 2$, and the operating point is as $R_{H\_O} = 1.145$ [85].

- p_{dif} is the fuel cell pressure difference between the hydrogen and oxygen passing through the anode and cathode gas compartments, i.e., $p_{dif} = p_{H_2} - p_{O_2}$. By taking Laplace transform, it can be derived that [53]

$$p_{H_2} = \frac{1/K_{H_2}}{1 + \tau_{H_2} s}(q^{in}_{H_2} - 2K_r I_r).$$

$\tau_{H_2} = \frac{V_{an}}{K_{H_2} R_0 T_0}$ is the value of the system pole associated with the hydrogen flow, where V_{an} is the volume of the anode. Similar expressions can be obtained for all the reactants and products such as p_{O_2} and p_{H_2O}. To prevent damage to the electrolyte, $|p_{dif}|$ needs to be kept below 8 kPa under transient conditions [85]. The steady operating point of p_{dif} is 0 kPa. All parameters and operating conditions are summarized in Table 4.1 and Table 4.2, respectively.

4.5 Control of SOFC

In this section we apply the proposed data-driven predictive control to the SOFC problem discussed in Section 4.4 to achieve optimal fuel utilization and maintain operation constraints when only the voltage output is measurable online. The sampling

Table 4.1: Parameters in the SOFC system model

Parameter	Value	Unit	Representation
T_0	1273	K	Absolute temperature
F_0	96485	C/mol	Faraday's constant
R_0	8.314	J/(mol K)	Universal gas constant
E_0	1.18	V	Ideal standard potential
N_0	384	–	Number of cells in series in the stack
K_r	0.996×10^{-3}	mol/(s A)	Constant, $K_r = N_0/4F_0$
K_{H_2}	8.32×10^{-6}	mol/(s Pa)	Valve molar constant for hydrogen
K_{H_2O}	2.77×10^{-6}	mol/(s Pa)	Valve molar constant for water
K_{O_2}	2.49×10^{-5}	mol/(s Pa)	Valve molar constant for oxygen
τ_{H_2}	26.1	s	Response time of hydrogen flow
τ_{H_2O}	78.3	s	Response time of water flow
τ_{O_2}	2.91	s	Response time of oxygen flow
r	0.126	Ω	Ohmic loss
T_e	0.8	s	Electrical response time
T_f	5	s	Fuel processor response time

Table 4.2: Operating conditions of the SOFC system model

Variable	Nominal Value	Constraint	Unit
$q_{H_2}^{in}$	0.7023	$0 \leqslant q_{H_2}^{in} \leqslant 1.7023$	mol/s
$q_{O_2}^{in}$	0.6134	$0 \leqslant q_{O_2}^{in} \leqslant 1.6134$	mol/s
V_r	333.8	$328.8 \leqslant V_r \leqslant 338.8$	V
I_{in}	300	–	A
U_f	85%	$80\% \leqslant U_f \leqslant 90\%$	–
R_{H_O}	1.145	$0 \leqslant R_{H\_O} \leqslant 2$	–
$\lvert p_{dif}\rvert$	0	$0 \leqslant \lvert p_{dif}\rvert \leqslant 8$	kPa

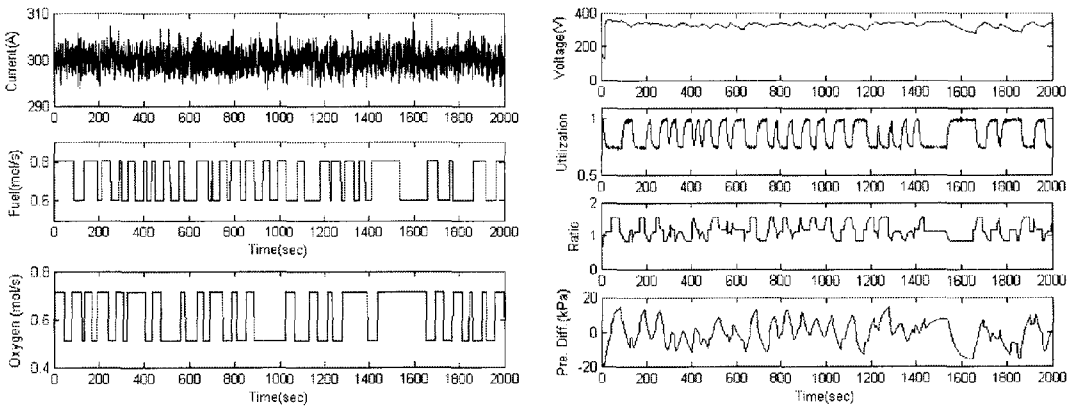

Figure 4.3: The open-loop SOFC disturbance, input and output signals

rate of the SOFC and the predictive controller is chosen as $T = 1$ s mainly targeting the system's dominant dynamics (see Table 4.1). To design the data-driven predictive controllers, open-loop input-output data are required to determine the subspace matrices. Open loop input-output data are obtained by exciting the open loop SOFC system using a designed random binary signal of magnitude 0.1 mol/s for the fuel and oxygen inlet flows, and a white noise with variance 5 A^2 for the current demand disturbance (see the generated disturbance signal in Figure 4.3). The input and output data are collected over 2000 seconds, and they are plotted in Figure 4.3. In the control objective function in (4.3), the weighting matrices are selected as Q =diag$(Q_1, \cdots, Q_L)$, Q_q =diag$(10^4, 10^4, 0, 10^3)$, where $q = 1, \cdots, L$, R_{J_c} =0.1$\times I$, and $P_{J_c} = I$. The predictive control is applied to the SOFC system after $t = 100$ s.

4.5.1 The effect of prediction of the unmeasured outputs

To demonstrate the effect of prediction of the unmeasured outputs, we did the closed-loop simulations with two different predictive control laws – without and with prediction of the unmeasured outputs $U_{\rm f}$, $R_{\rm H\_O}$ and $p_{\rm dif}$. In this example, the best control tuning with prediction horizon $L = 9$ and the control horizon $J_c = 9$ for the developed predictive control with prediction of the unmeasured outputs is chosen. For the control without prediction, the best tuning with prediction horizon $L = 3$ and the control horizon $J_c = 1$ is chosen. It can be seen that the optimal prediction

horizon selected through simulations is not very large. Since the actual system is nonlinear but the prediction based on subspace matrices is linear, larger prediction horizons may also introduce larger prediction error. In addition, not all outputs are measured and they need to be predicted from data and the subspace matrices, a longer prediction horizon also introduces larger prediction error. We performed several simulations to determine the best prediction horizon. In Table 4.3 we listed the integral absolute errors (IAE) of the SOFC outputs under the developed data-driven predictive control with a number of different prediction horizons. In terms of the IAEs of the output voltage and fuel utilization (while both the H/O ratio and pressure difference are controlled within their constraints), we find that $L = 9$ is the optimal prediction horizon length for the control law obtained for this example. As for the control without prediction of the unmeasured outputs, the simulation results show that with $2 \leqslant L \leqslant 5$, the controller works better than with longer prediction horizons. In this latter case, there is neither measurement nor prediction of the unmeasured outputs that are assumed to be available for the feedback when the control is designed. This is equivalent to an additional model-plant mismatch and thus a longer prediction horizon yields larger error.

The fuel cell current demand disturbance is a multiple step signal which increases from 300 A to 330 A when $t = 200$ s, changes from 330 A to 270 A when $t = 300$ s, and goes back to 300 A after $t = 350$ s. The closed-loop outputs and inputs are shown in Figure 4.4 and Figure 4.5, where the signals under the controller without prediction of the unmeasured outputs are plotted in the left-hand side, and the signals under the controller with prediction are drawn in the right-hand side. The errors between the SOFC outputs and their respective operating points are shown in Figure 4.6, and the integral absolute errors (IAE) of the SOFC outputs from time 101 to 500 s are listed in the first two rows of Table 4.4. It can be seen from both Figure 4.6 and Table 4.4 that the regulatory errors with prediction of the unmeasured outputs are smaller than those without prediction. In addition, from Figure 4.6 it can be seen that the errors of voltage and utilization are kept close to zero steady state under large current load step changes, which is the effect of the integral control. Furthermore, we compare the control results in terms of electrical power of the SOFC system in Figure 4.7. The power demand of the SOFC is defined

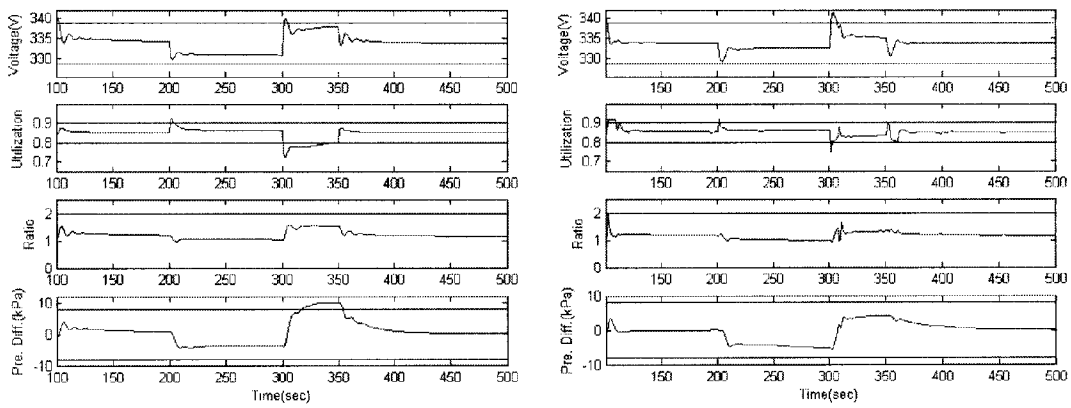

Figure 4.4: The SOFC output signals without and with prediction of the unmeasured outputs

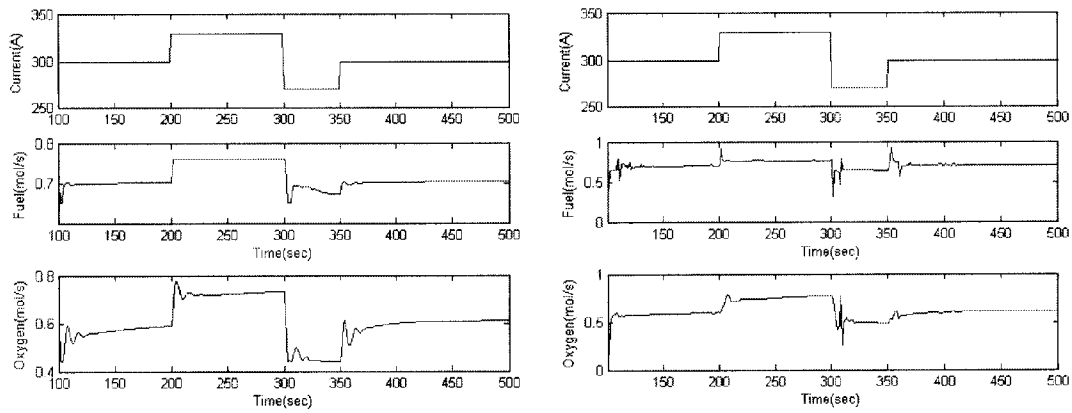

Figure 4.5: The SOFC disturbance and control signals without and with prediction of the unmeasured outputs

as $P_{\text{in}} = V_{\text{in}} I_{\text{in}}$ and the real power is as $P_{\text{r}} = V_{\text{r}} I_{\text{r}}$. The results show that under the control with prediction of the unmeasured outputs, the real power provided by the SOFC tracks the power demand better. All the above comparisons show that the predictive control with prediction of the unmeasured outputs yields higher control performance.

4.5.2 Robustness test

To test whether the proposed predictive controller performs well under different operating conditions, we perform simulations as follows: a group of open-loop data

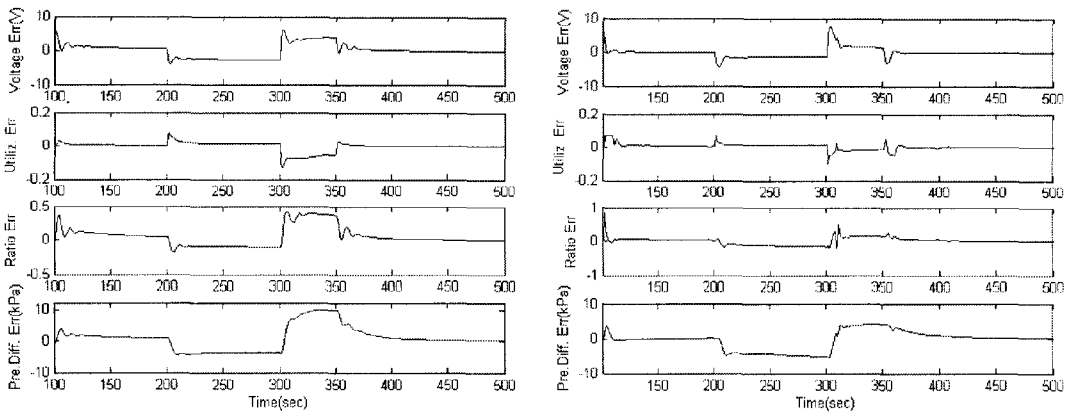

Figure 4.6: The errors of SOFC outputs without and with prediction of the unmeasured outputs

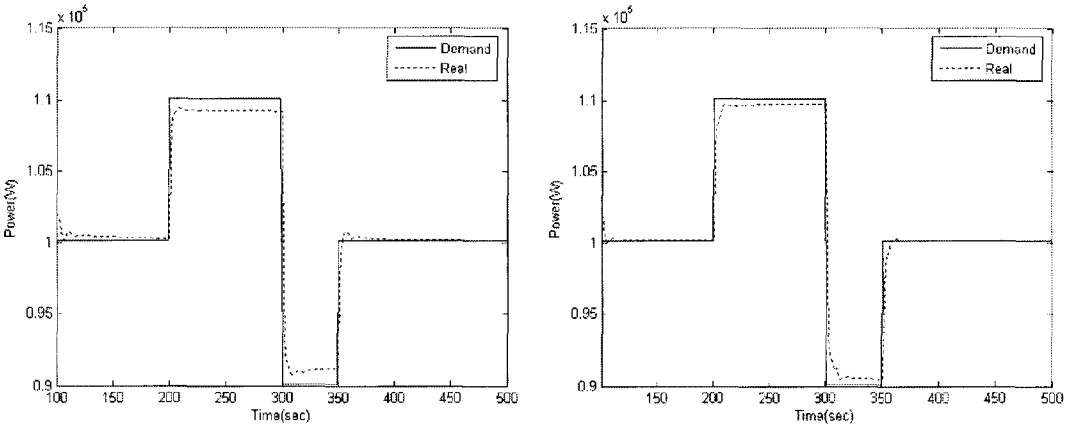

Figure 4.7: The SOFC demand and real power without and with prediction of the unmeasured outputs

Table 4.3: IAE of the SOFC outputs with different prediction horizons

Prediction and control horizon	IAE(V_r) (V)	IAE(U_f)	IAE(R_{H_O})	IAE(p_{dif}) (kPa)
$L = J_c = 8$	5.457×10^2	5.414	2.613×10	7.548×10^3
$L = J_c = 9$	3.037×10^2	4.430	3.097×10	7.847×10^2
$L = J_c = 10$	3.477×10^2	4.973	3.308×10	8.661×10^2
$L = J_c = 15$	5.714×10^2	6.169	3.176×10	9.017×10^2

Table 4.4: IAE of the SOFC outputs without and with prediction of the unmeasured outputs

IAE	I_{in}^{0} (A)	IAE(V_r) (V)	IAE(U_f)	IAE(R_{H_O})	IAE(p_{dif}) (kPa)
Without prediction	300	6.027×10^{2}	6.204	4.172×10	1.110×10^{3}
With prediction	300	3.037×10^{2}	4.430	3.097×10	7.847×10^{2}
Robustness test	350	3.593×10^{2}	4.738	3.188×10	8.656×10^{2}
Robustness test	250	3.649×10^{2}	8.003	4.532×10	7.957×10^{2}

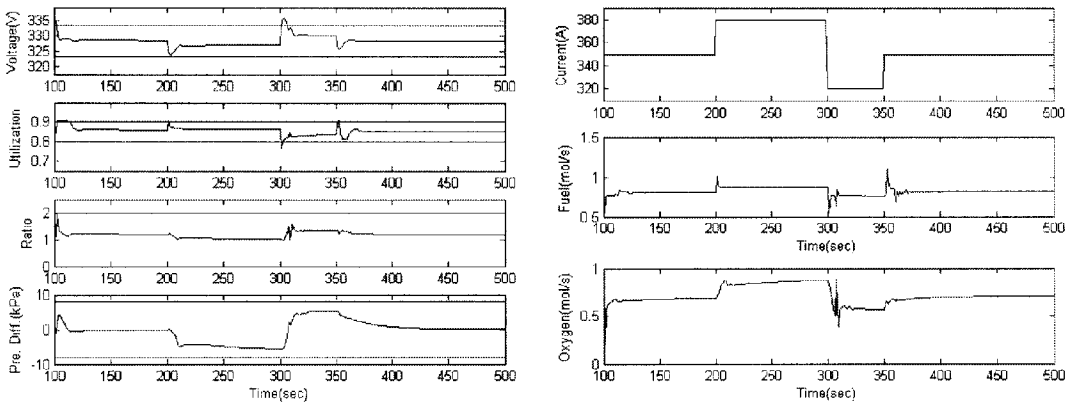

Figure 4.8: The SOFC output signals, disturbance and control signals of Case 1

is collected under the nominal condition $I_r = 300$ A and $V_r = 333.8$ V (the open-loop disturbance is a white noise signal with variance of 5); this group of open-loop data are applied to determine subspace matrices and then design the predictive controller; the designed controller are run in the closed-loop SOFC system under two different operating conditions shown in Cases 1 and 2.

Case 1 The operating condition in this case is as $I_r = 350$ A with corresponding $V_r = 328.4$ V; $[q_f^{in}\ q_{O_2}^{in}]^T = [0.8202\ 0.7163]^T$ mol/s; $[U_f\ R_{H\_O}\ p_{dif}]^T = [0.85\ 1.145\ 0]^T$. The constraint on V_r is 323.4 V$\leqslant V_r \leqslant$ 333.4 V. The current disturbance is a multiple step signal which increases from 350 A to 380 A when $t = 200$ s, changes from 380 A to 320 A when $t = 300$ s, and goes back to 350 A after $t = 350$ s. Simulation results are plotted in Figures 4.8 and 4.9, and the IAEs of the SOFC outputs from time 101 to 500 s are shown in the third row of Table 4.4, from where it can be seen that the power generated by the SOFC can track the power demand well, and the SOFC outputs errors under the designed controller are negligibly small under this non-nominal condition.

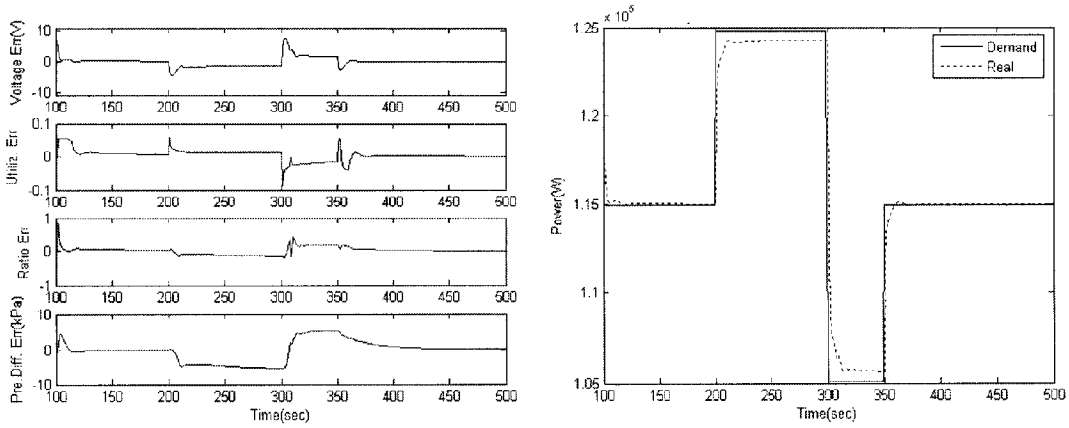

Figure 4.9: The SOFC outputs errors, demand and real power of Case 1

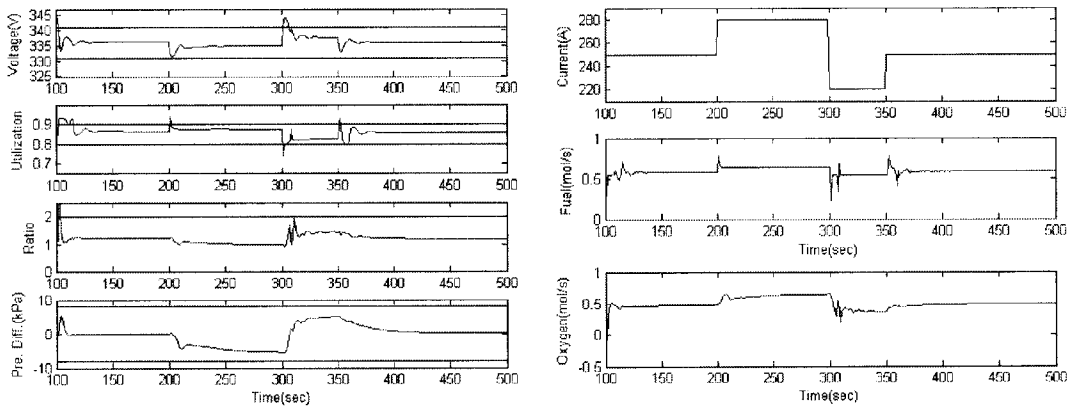

Figure 4.10: The SOFC output signals, disturbance and control signals of Case 2

Case 2 The operating condition in this case is as $I_r = 250$ A with corresponding $V_r = 335.9$ V; $[q_{\rm f}^{\rm in}\ q_{\rm O_2}^{\rm in}]^T = [0.5859\ 0.5117]^T$ mol/s; $[U_{\rm f}\ R_{\rm H\_O}\ p_{\rm dif}]^T = [0.851\ 1.1450]^T$. The constraint on $V_{\rm r}$ is 330.9 V$\leqslant V_{\rm r} \leqslant$ 340.9 V. The current disturbance is a multiple step signal which increases from 250 A to 280 A when $t = 200$ s, changes from 280 A to 220 A when $t = 300$ s and goes back to 250 A after $t = 350$ s. Simulation results can be found in Figures 4.10 and 4.11, and the IAE of the SOFC outputs from time 101 to 500 s are shown in the fourth row of Table 4.4. Similar conclusions can be obtained as in Case 1.

Here, we make some important remarks about the proposed data-driven predictive control for the SOFC system:

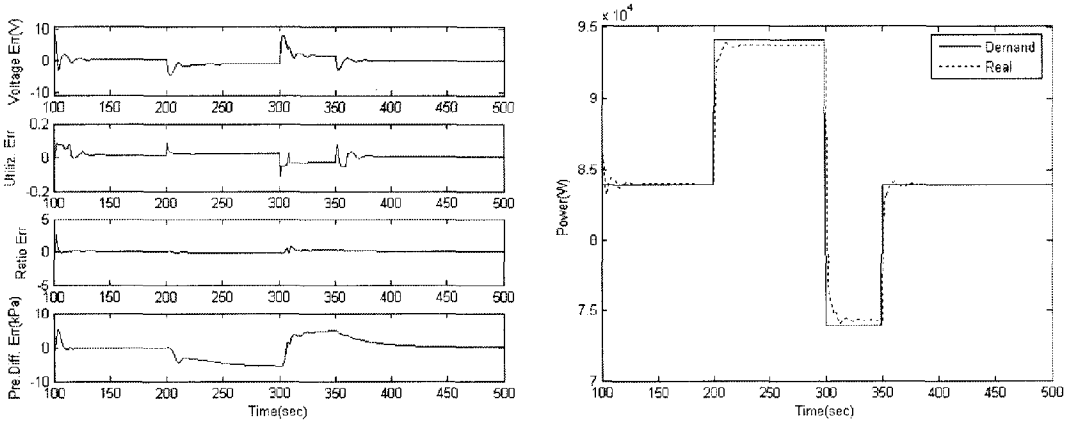

Figure 4.11: The SOFC outputs errors, demand and real power of Case 2

- In the simulations, certain subspace matrices are calculated from open-loop input-output data. It is important to mention that estimating the subspace matrices is not equivalent to estimating state space matrices of the SOFC system. Using the subspace matrices calculated from the input-output data we can directly design the control law, while the system matrices A, B, C, D, E, and F are never explicitly calculated.

- Although only the first control action is implemented, it has been shown in [14] that as the horizon increases, the data-driven receding horizon implementation converges to the true optimal control, i.e., the data-driven predictive controllers approach the classical MPC controllers when the prediction horizon L goes to infinity.

- The problem of stability of the subspace-based data-driven controllers is still open [13, 84]. There is no explicit model used in the proposed data-driven approach. Intuitively, one would expect that the longer the prediction horizon, the greater the probability that the closed-loop system is stable [13, 84]. However, since the actual system is nonlinear but the prediction based on subspace matrices is linear, larger prediction horizons may also introduce larger prediction error. Thus, the choice of prediction horizon length is a design parameter which must be selected by the designer.

- If a model is obtained from experimental data, the model is only valid within

the experimental region if the system of concern is nonlinear. The first-principle models represent nonlinear systems better, but this type of models are typically difficult to obtain and, even if available, difficult for control design. The proposed method is data driven; thus it is subject to the same limitation as using models identified through experiments. However, since SOFC control is mainly regulatory and the system is expected to operate around an operating point, a carefully designed experiment around the operating point can provide a good dynamic model for control purpose as we did in this chapter. In general, however, if the system needs to operate in several distinguished operating points, a nonlinear control or a multiple model control should be applied. In this case, several experiments or an experiment that cover a large operating region must be considered.

- The previous studies have shown that control of SOFC is challenging due to the slow response and tight operation constraints [36]. Any feasible control must take into account of hard constraints of the manipulated variables. Thus, constraint predictive control appears to be the most appropriate control strategy. Comparable control strategies for a similar SOFC model, such as $\mathscr{H}_2$ or $\mathscr{H}_\infty$ control [36], have been shown not satisfactory.

4.6 Conclusions

An SOFC model has been commonly investigated in the dynamic SOFC modeling/control literature lately. The previous studies have shown that control of SOFC is challenging due to the slow response and tight operation constraints. In this chapter, a predictive control strategy that can handle constraints and optimize control performance has been developed via the subspace approach for the SOFC system. Unlike model-based approaches, the proposed predictive controller is data-driven since it only requires a set of input-output open-loop data; thus it provides an alternative to SOFC control problem. This is particularly effective for SOFC since the explicit dynamic model of SOFC is generally difficult to develop. Comparing with the previous data-driven predictive control approach, the developed predictive controller can handle systems where only partial on-line outputs measurements are

available. This solution is important when, for example, the fuel utilization in the SOFC system may not be measured in real-time control applications. The simulation results validate the proposed data-driven predictive control algorithm. The robustness of the proposed predictive controller is verified by simulation.

Chapter 5

A Data-driven Predictive Control for Multirate Systems

This chapter discusses predictive control of multirate systems. The multirate prediction strategy that can handle constraints and optimize control performance is developed via the subspace approach. The proposed multirate predictive control is data-driven since it only requires a set of input-output open-loop experimental data and the explicit process model is not needed. This algorithm is effective for multirate systems where some measurements are difficult to sample at the fast rate. The proposed algorithm is illustrated through simulations of a distillation column and an SOFC control.

5.1 Introduction

The objective of this work is to explore a data-driven predictive control law for multirate systems, when only the open-loop input-output data are available. Unlike the model-based approach, where the system model is required to achieve this goal, we follow an approach based on results from multirate subspace system identification [59, 81]. The data-driven approach presented in the literature so far has been derived for single-rate systems. However, in reality, some outputs may not be measured or too costly to be measured at the fast sampling rate, leading to multirate systems. In many applications of electrical, mechanical and chemical engineering, control signals and output measurements need to be sampled at different rates. For example, in control of solid oxide fuel cell it may be difficult and costly to measure the fuel utilization at the fast sampling rate because the fuel utilization is the ratio between the reacted fuel flow rate and the inlet fuel flow rate which is a component of total inlet flow [53, 85]. To circumvent this problem, we consider the data-driven predictive control design for multirate systems. Instead of treating general multirate systems, in this chapter we consider a dual-rate system where the sampling frequency of some signals is M (a positive integer) times that of the rest signals. Polymer reactors [48], fermentation processes [20] and octane quality control [43] are examples of this kind of multirate systems, where the manipulated variables are faster than the output measurements. Particularly, the developed dual-rate predictive control is verified by a distillation column system and a solid oxide fuel cell system [53, 85].

The remainder of this chapter is organized as follows. The system and the problem formulation are described in detail in Section 5.2. Section 5.3 presents the derivation of the dual-rate predictive control algorithm. Two illustrative examples are provided in Section 5.4, followed by conclusions in Section 5.5.

5.2 System description and problem statement

Consider a multirate system shown in Figure 5.1, where H denotes a zero-order-hold; S_f and S_s are fast-rate and slow-rate samplers with interval T and MT respectively; the superscript f denotes fast rate, s means slow rate, and M is the lifting factor which is an integer; $P(s)$ and $N(s)$ are the continuous-time process and disturbance;

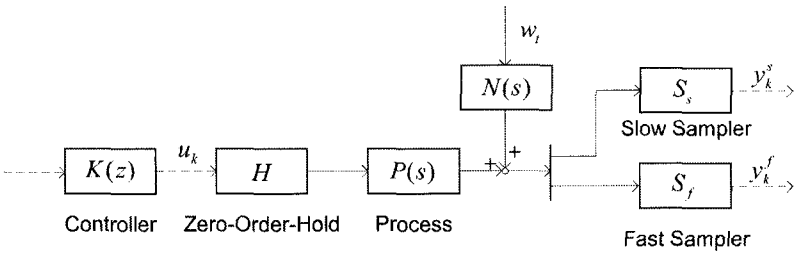

Figure 5.1: Block diagram of the described multi-rate system

$K(z)$ is the discrete-time predictive controller; solid lines represent continuous-time signals, and dashed lines indicate discrete-time signals. Assume that the control input variable $u_k \in R^r$, the measurable disturbance $w_k \in R^{r_w}$ and some output variables $y_k^f \in R^{m_f}$ are sampled with a fast sampling rate at sampling period T, and the remaining output variables $y_k^s \in R^m$ are sampled with a slow sampling rate with sampling period MT. The problem investigated in this paper is to design the data-driven dual-rate predictive law directly from the input/output data defined as

$$\begin{cases} u_k^c, w_k, y_k^f, \ k = i + k_0, \ \forall i = 0, 1, \cdots, N_u - 1, \\ y_k^s, \ k = jM + k_0, \ \forall j = 0, 1, \cdots, N_y - 1 \end{cases}$$

where $k_0 \geq 1$ is the first discrete-time instance when the data is available, and $N_u = Ny \times M$.

5.3 Multirate data-driven predictive control algorithm

5.3.1 Description

For the sake of presentation, the following definitions are adopted. $\{\cdots\}$ is used to present a data set, and $[\cdots]$ is used to denote a vector. Recall that the extended signal sequence $s_{k|L} \in R^{L \times n_r}$ is defined as

$$s_{k|L} \stackrel{\text{def}}{=} [s_k^T \ s_{k+1}^T \ \cdots \ s_{k+L-1}^T]^T, \tag{5.1}$$

where $s_t \in R^{n_r}$ $(t = k_0, \cdots, k, k+1, \cdots)$ is a sequence of data with n_r being the number of the rows; k is the starting index; L is the number of n_r-block rows in $s_{k|L}$.

5.3.2 Control objective

The control objective of this work is to minimize a standard cost function in model-based predictive control subject to certain constraints. This can be re-written in vector form for convenience as follows:

$$\min_{\Delta u_{k|JM}} J_k = \min(\hat{y}^s_{k+M|L} - r_{k+M|L})^T Q(\hat{y}^s_{k+M|L} - r_{k+M|L}) + \Delta u^T_{k|J_cM} R_{J_cM} \Delta u_{k|J_cM} + u^T_{k|J_cM} P_{J_cM} u_{k|J_cM}, \tag{5.2}$$

subject to

$$u^{\min}_{k|J_cM} \leqslant u_{k|J_cM} \leqslant u^{\max}_{k|J_cM}, \tag{5.3}$$

$$\Delta u^{\min}_{k|J_cM} \leqslant \Delta u_{k|J_cM} \leqslant \Delta u^{\max}_{k|J_cM}, \tag{5.4}$$

$$y^{s\,\min}_{k+M|L} \leqslant \hat{y}^s_{k+M|L} \leqslant y^{s\,\max}_{k+M|L}, \tag{5.5}$$

$$y^{f\,\min}_{k+1|LM} \leqslant \hat{y}^f_{k+1|LM} \leqslant y^{f\,\max}_{k+1|LM} \tag{5.6}$$

where L is defined as the prediction horizon on the slowly sampled output (thus LM is the prediction horizon on the fast sampled output); J_cM ($J_c \leqslant L$) is the control horizon defined on the fast sampled control signal; $\hat{y}^s_{k+M|L}$ and $\hat{y}^f_{k+1|LM}$ are vectors of the predictions of future slowly sampled and fast sampled outputs, respectively; $r_{k+M|L}$ is a vector of future reference signals in slow rate; $u_{k|J_cM}$ is a vector of future manipulated signal; $\Delta \stackrel{\text{def}}{=} 1 - z^{-1}$ with z^{-1} being the back shift operator; hence $\Delta u_k = u_k - u_{k-1}$ is the incremental input or control move, and $\Delta u_{k|J_cM}$ is a vector of future incremental inputs over next J_cM samples. Δu_k is introduced to ensure zero steady state error in the case of non-zero constant reference or load step changes [9]. Q, R_{J_cM} and P_{J_cM} are weighting matrices with block diagonal structure on the error between the predicted outputs and the future references, the future incremental inputs and the future control efforts respectively. Q, R_{J_cM}, and P_{J_cM} can be time-varying in general. Note that here we set the control horizon to J_cM to make the predictive control law more flexible.

5.3.3 The dual-rate subspace input-output equation

Although the dual-rate subspace input-output equation has been derived in Chapter 3, to keep the continuity of this Chapter, we will review it in the following part.

In the dual-rate control loop shown in Figure 5.1 the slow sampled output signal is $y^s = \{y^s_{k_0}, \cdots, y^s_k, y^s_{k+M}, \cdots\}$, and the fast sampled input signal is $u = \{u_{k_0}, \cdots, u_k, u_{k+1}, \cdots\}$. The dual-rate controller is time-varying due to the presence of the fast-rate hold and the slow-rate sampler. To avoid dealing with the time-varying system directly, we introduce the lifting technique. By the definition in equation (??), the control signals can be stacked as vector-valued sequences as follows:

$$\underline{u} = \left\{u_{k_0|M}, \cdots, u_{k|M}, u_{k+M|M}, \cdots\right\}.$$

For instance, if $M = 2$, the lifted control signal is as

$$\underline{u} = \left\{\begin{bmatrix} u_{k_0} \\ u_{k_0+1} \end{bmatrix}, \cdots, \begin{bmatrix} u_k \\ u_{k+1} \end{bmatrix}, \begin{bmatrix} u_{k+2} \\ u_{k+3} \end{bmatrix}, \cdots\right\}.$$

The map from u to $\underline{u}$ is defined as the lifting operator L_M [40]. The inverse lifting operator L_M^{-1} is the reverse of the mapping. It can be seen that $L_M^{-1}L_M = I$ and $L_M L_M^{-1} = I$. After lifting, both the signal dimension and the underlying period are increased by a factor of M. The system from $\underline{u}$ to y is the lifted system which is single-rate and linear time-invariant. Assume that the fast-rate state space model from u_k to the output that is going to be slowly sampled is

$$x_{k+1} = Ax_k + Bu_k + Ew_k \tag{5.7}$$

$$y^s_k = Cx_k + Du_k + Fw_k \tag{5.8}$$

where $x_k \in R^n$ is the state vector;A, B, C, D, E, F are system matrices with appropriate dimensions. We assume that (C, A) is observable, (A, B) is controllable, and u and w are independent signals. The systems we are studying in this work have at least one time delay due to the hold, hence matrix D can be set to a zero matrix without loss of generality. From the known state space model of the fast-rate plant, the lifted system G_M from the lifted control signal $(u_{k|M}, w_{k|M})$ to the slowly sampled output y^s_k can be written as [10]:

$$x_{k+M} = A^M x_k + \underline{B}u_{k|M} + \underline{E}w_{k|M}, \tag{5.9}$$

$$y^s_k = Cx_k + D_M u_{k|M} + F_M w_{k|M} \tag{5.10}$$

where $\underline{B} = [\ A^{M-1}B \ \cdots \ AB \ \ B\ ]$ and $\underline{E} = [\ A^{M-1}E \ \cdots \ AE \ \ E\ ]$ are the lifted external input matrices, and $D_M = [\ 0 \ \cdots \ 0\ ]$ and $F_M = [\ F \ \ 0 \ \cdots \ 0\ ]$

are the lifted direct control input-to-output matrices. Note the lifted duel-rate system is a linear-time-invariant system. By lifting y_k, $u_{k|M}$ and $w_{k|M}$ with the user chosen prediction horizon L, we can re-write equation (5.10) as [81]

$$y^s_{k+M|L} = \tilde{M} y_{k|L} + \tilde{N} u_{k|(L+1)M} + \tilde{T} w_{k|(L+1)M}. \tag{5.11}$$

$\tilde{M}$, $\tilde{N}$ and $\tilde{T}$ are subspace matrices that are defined as

$$\begin{aligned} \tilde{M} &\stackrel{\text{def}}{=} O_L A^M (O_L^T O_L)^{-1} O_L^T, \\ \tilde{N} &\stackrel{\text{def}}{=} \left[\begin{array}{cc} O_L \underline{B} & H_L \end{array} \right] - \tilde{M} \left[\begin{array}{cc} H_L & 0_{Lm \times Mr} \end{array} \right], \\ \tilde{T} &\stackrel{\text{def}}{=} \left[\begin{array}{cc} O_L \underline{E} & H^s_L \end{array} \right] - \tilde{M} \left[\begin{array}{cc} H^s_L & 0_{Lm \times Mr_w} \end{array} \right] \end{aligned} \tag{5.12}$$

where O_L is the dual-rate extended observability matrix for the pair (C, A^M) defined as

$$O_L \stackrel{\text{def}}{=} \left[\begin{array}{c} C \\ CA^M \\ \vdots \\ CA^{M(L-1)} \end{array} \right] \in R^{(L \times m) \times n}, \tag{5.13}$$

and H_L and H^s_L are lower block triangular Toeplitz matrices defined as

$$H_L \stackrel{\text{def}}{=} \left[\begin{array}{cccc} D_M & \cdots & 0 & 0 \\ C\underline{B} & \cdots & 0 & 0 \\ CA^M \underline{B} & \cdots & 0 & 0 \\ \vdots & \ddots & \vdots & 0 \\ CA^{(L-2)M} \underline{B} & \cdots & C\underline{B} & D_M \end{array} \right] \in R^{(L \times m) \times (L \times M \times r)}, \tag{5.14}$$

$$H^s_L \stackrel{\text{def}}{=} \left[\begin{array}{cccc} F_s & \cdots & 0 & 0 \\ CE_s & \cdots & 0 & 0 \\ CA^M E_s & \cdots & 0 & 0 \\ \vdots & \ddots & \vdots & 0 \\ CA^{(L-2)M} E_s & \cdots & CE_s & F_s \end{array} \right] \in R^{(L \times m) \times (L \times m)}. \tag{5.15}$$

Though in [62], equation (5.11), named the extended state space model, is derived by an M-step predictor approach, our alternative method approaches the problem from a different way, i.e. lifting, which makes it possible to use conventional subspace approach to solve multirate problem. It can be seen that the lifted subspace input-output equation (5.11) contains inherent relationship between the past and the future control/output signals. It can be shown that the explicit relationship between

the past and the future control/output signals is as

$$\hat{y}^s_{k+M|L} = \tilde{M}^L y^s_{k-(L-1)M|L} + P_{L-1} u_{k-(L-1)M|(L-1)M} + F_L u_{k|LM} + P_w w_{k-(L-1)M|(L-1)M} + F_w w_{k|LM}. \tag{5.16}$$

The subspace input-output equation of the fast sampled output y^f is as [58]

$$\hat{y}^f_{k+1|LM} = (\tilde{M}^f)^{LM} y^f_{k-LM+1|LM} + P^f_{LM-1} u_{k-LM+1|LM-1} + F^f_{LM} u_{k|LM} + P^f_w w_{k-LM+1|LM-1} + F^f_w w_{k|LM} \tag{5.17}$$

where $\tilde{M}^s$, P_{L-1}, F_L, P_w and F_w are dual-rate subspace matrices which can be obtained from the experimental input-output data (u_k, w_k, y^s_k) [58, 81], and $\tilde{M}^f$, P^f_{LM-1}, F^f_{LM}, P^f_w and F^f_w are single-rate subspace matrices that can be calculated from the open-loop experimental data(u_k, w_k, y^f_k).

5.3.4 Data-driven dual-rate predictive control law

Proposition 5.1 *Substituting (5.16) and (5.17) into (5.2) and (5.6), one can formulate the control objective as a Quadratic Programming problem [61, 80], i.e.,*

$$\min_{\Delta u_{k|LM}} J_k = \Delta u^T_{k|LM} H \Delta u_{k|LM} + 2 f^T_k \Delta u_{k|LM}, \tag{5.18}$$

subject to constraints:

$$\widetilde{A} \Delta u_{k|LM} \leqslant b_k. \tag{5.19}$$

Proof. In the following we will show how to formulate the problem described in (5.2) under the constraints (5.3)–(5.6) to a QP problem as shown in (5.18) with the constraints in (5.19). Defining matrices S and c as [61, 80]

$$S \stackrel{\text{def}}{=} \begin{bmatrix} I_r & 0_r & \cdots & 0_r \\ I_r & I_r & \cdots & 0_r \\ \vdots & \vdots & \ddots & \vdots \\ I_r & I_r & \cdots & I_r \end{bmatrix} \in R^{(LM\times r)\times(LM\times r)},$$

and

$$c \stackrel{\text{def}}{=} [\ I_r \quad I_r \quad \cdots \quad I_r\ ]^T \in R^{(LM\times r)\times r},$$

we can obtain

$$u_{k|LM} = S \Delta u_{k|LM} + c u_{k-1}. \tag{5.20}$$

Thus, the dual-rate subspace input-output equation (5.16) can be re-written as

$$\begin{aligned}\hat{y}^s_{k+M|L} &= \tilde{M}^L y^s_{k-(L-1)M|L} + P_{L-1}u_{k-(L-1)M|(L-1)M} + F_L u_{k|LM} \qquad (5.21)\\ &+ P_w w_{k-(L-1)M|(L-1)M} + F_w w_{k|LM}\\ &= \Phi_L(k) + F_L u_{k|LM}\\ &= \Phi_L(k) + F_L(S\Delta u_{k|LM} + cu_{k-1})\\ &= \Phi_L(k) + F_L S\Delta u_{k|LM} + F_L c u_{k-1}\\ &= \Phi^{\Delta}_L(k) + F^{\Delta}_L \Delta u_{k|LM} \qquad (5.22)\end{aligned}$$

where

$$\Phi_L(k) = \tilde{M}^L y_{k-(L-1)M|L} + P_{L-1}u_{k-(L-1)M|(L-1)M} + P_w w_{k-(L-1)M|(L-1)M} + F_w w_{k|LM}, \qquad (5.23)$$

$$\Phi^{\Delta}_L(k) = \Phi_L(k) + F_L c u_{k-1},$$

$$F^{\Delta}_L = F_L S.$$

The subspace equation of the fast-rate output y^f is as

$$\begin{aligned}\hat{y}^f_{k+1|LM} &= (\tilde{M}^f)^{LM} y^f_{k-LM+1|LM} + P^f_{LM-1}u_{k-LM+1|LM-1} + F^f_{LM}u_{k|LM} \qquad (5.24)\\ &+ P^f_w w_{k-LM+1|LM-1} + F^f_w w_{k|LM}\\ &= \Phi^f_{LM}(k) + F^f_{LM}u_{k|LM}\\ &= \Phi^f_{LM}(k) + F^f_{LM}(S\Delta u_{k|LM} + cu_{k-1})\\ &= \Phi^{f\Delta}_{LM}(k) + F^{f\Delta}_{LM}\Delta u_{k|LM} \qquad (5.25)\end{aligned}$$

where

$$\Phi^f_{LM}(k) = (\tilde{M}^f)^{LM} y^f_{k-LM+1|LM} + P^f_{LM-1}u_{k-LM+1|LM-1}P^f_w w_{k-LM+1|LM-1} + F^f_w w_{k|LM} \qquad (5.26)$$

$$\Phi^{f\Delta}_{LM}(k) = \Phi^f_L(k) + F^f_{LM} c u_{k-1}$$

$$F^{f\Delta}_{LM} = F^f_{LM} S.$$

It can be seen that (5.2) is equivalent to

$$\min J_k = \min(\hat{y}^s_{k+M|L} - r_{k+M|L})^T Q(\hat{y}^s_{k+M|L} - r_{k+M|L}) + \Delta u^T_{k|LM} R \Delta u_{k|LM} + u^T_{k|LM} P u_{k|LM} \qquad (5.27)$$

with the future control moves being zero after $k+J_cM$ step, i.e. $\Delta u_{k+J_cM+1|(L-J_c)M} = 0$. Thus (5.2)–(5.6) can be re-written as (5.27) subject to

$$
\begin{aligned}
u^{\min}_{k|LM} \leqslant u_{k|LM} \leqslant u^{\max}_{k|LM},\\
\Delta u^{\min}_{k|LM} \leqslant \Delta u_{k|LM} \leqslant \Delta u^{\max}_{k|LM},\\
y^{\min}_{k+M|L} \leqslant \hat{y}_{k+M|L} \leqslant y^{\max}_{k+M|L},\\
y^{f\,\min}_{k+1|LM} \leqslant \hat{y}^{f}_{k+1|LM} \leqslant y^{f\,\max}_{k+1|LM}\\
\Delta u_{k+J_cM+1|(L-J_c)M} = 0.
\end{aligned}
$$

Substituting (5.20) and (5.22) into (5.27), we have

$$
\begin{aligned}
J_k &= (y^s_{k+M|L} - r_{k+M|L})^T Q (y^s_{k+M|L} - r_{k+M|L}) + \Delta u^T_{k|LM} R \Delta u_{k|LM} + u^T_{k|LM} P u_{k|LM}\\
&= \left(\Phi^{\Delta}_L(k) + F^{\Delta}_L \Delta u_{k|LM} - r_{k+M|L}\right)^T Q \left(\Phi^{\Delta}_L(k) + F^{\Delta}_L \Delta u_{k|LM} - r_{k+M|L}\right)\\
&+ \Delta u^T_{k|LM} R \Delta u_{k|LM} + \left(S\Delta u_{k|LM} + cu_{k-1}\right)^T P \left(S\Delta u_{k|LM} + cu_{k-1}\right)\\
&= \Delta u^T_{k|LM} (F^{\Delta}_L Q F^{\Delta}_L + R + S^T P S) \Delta u_{k|LM} + 2\left(\Phi^{\Delta}_L(k) - r_{k+M|L}\right)^T Q F^{\Delta}_L \Delta u_{k|LM}\\
&+ 2\left(cu_{k-1}\right)^T P S \Delta u_{k|LM} + \left(\Phi^{\Delta}_L(k) - r_{k+M|L}\right)^T Q \left(\Phi^{\Delta}_L(k) - r_{k+M|L}\right)\\
&+ \left(cu_{k-1}\right)^T P \left(cu_{k-1}\right)\\
&= \Delta u^T_{k|LM} H \Delta u_{k|LM} + 2 f^T_k \Delta u_{k|LM} + J^0_k,
\end{aligned}
$$

where

$$
\begin{aligned}
H &= F^{\Delta}_L Q F^{\Delta}_L + R + S^T P S,\\
f_k &= F^{\Delta T}_L Q \left(\Phi^{\Delta}_L(k) - r_{k+M|L}\right) + S^T P c u_{k-1},\\
J^0_k &= \left(\Phi^{\Delta}_L(k) - r_{k+M|L}\right)^T Q \left(\Phi^{\Delta}_L(k) - r_{k+M|L}\right) + u_{k-1} c^T P c u_{k-1}.
\end{aligned}
$$

In the following part, we are going to show that the constraints can be written as an equivalent linear inequality:

$$\tilde{A} u_{k|LM} \leqslant b_k$$

where

$$\tilde{A} = \begin{bmatrix} S \\ -S \\ I_{LMr} \\ -I_{LMr} \\ F_L^{\Delta} \\ -F_L^{\Delta} \\ F_{LM}^{f\Delta} \\ -F_{LM}^{f\Delta} \\ M_{J_c} \\ -M_{J_c} \end{bmatrix}, and\ b_k = \begin{bmatrix} u_{k|LM}^{\max} - cu_{k-1} \\ -u_{k|LM}^{\min} + cu_{k-1} \\ \Delta u_{k|LM}^{\max} \\ -\Delta u_{k|LM}^{\min} \\ y_{k+M|L}^{s\max} - \Phi_L^{\Delta}(k) \\ -y_{k+M|L}^{s\min} + \Phi_L^{\Delta}(k) \\ y_{k+1|LM}^{f\max} - \Phi_{LM}^{f\Delta}(k) \\ -y_{k+1|LM}^{f\min} + \Phi_{LM}^{f\Delta}(k) \\ 0 \\ 0 \end{bmatrix}.$$

From equation (5.20), the output amplitude constraints are

$$\begin{aligned} u_{k|LM}^{\min} \leqslant u_{k|LM} \leqslant u_{k|LM}^{\max} \Leftrightarrow \\ u_{k|LM}^{\min} \leqslant S\Delta u_{k|LM} + cu_{k-1} \leqslant u_{k|LM}^{\max} \Leftrightarrow \\ S\Delta u_{k|LM} \leqslant u_{k|LM}^{\max} - cu_{k-1}, \\ -S\Delta u_{k|LM} \leqslant -u_{k|LM}^{\min} + cu_{k-1}. \end{aligned}$$

The control change constraints are

$$\begin{aligned} \Delta u_{k|LM}^{\min} \leqslant \Delta u_{k|LM} \leqslant \Delta u_{k|LM}^{\max} \Leftrightarrow \\ I_{LMr}\Delta u_{k|LM} \leqslant \Delta u_{k|LM}^{\max}, \\ -I_{LMr}\Delta u_{k|LM} \leqslant -\Delta u_{k|LM}^{\min}. \end{aligned}$$

From equation (5.22), the constraints on slowly sampled output are

$$\begin{aligned} y_{k+M|L}^{s\min} \leqslant y_{k+M|L}^{s} \leqslant y_{k+M|L}^{s\max} \Leftrightarrow \\ y_{k+M|L}^{s\min} \leqslant \Phi_L^{\Delta}(k) + F_L^{\Delta}\Delta u_{k|LM} \leqslant y_{k+M|L}^{s\max} \Leftrightarrow \\ F_L^{\Delta}\Delta u_{k|LM} \leqslant y_{k+M|L}^{s\max} - \Phi_L^{\Delta}(k), \\ -F_L^{\Delta}\Delta u_{k|LM} \leqslant -y_{k+M|L}^{s\min} + \Phi_L^{\Delta}(k). \end{aligned}$$

From equation (5.25), the constraints on fast sampled output are

$$\begin{aligned} y_{k+1|LM}^{f\min} \leqslant \hat{y}_{k+1|LM}^{f} \leqslant y_{k+1|LM}^{f\max} \Leftrightarrow \\ y_{k+1|LM}^{f\min} \leqslant \Phi_{LM}^{f\Delta}(k) + F_{LM}^{f\Delta}\Delta u_{k|LM} \leqslant y_{k+1|LM}^{f\max} \Leftrightarrow \\ F_{LM}^{f\Delta}\Delta u_{k|LM} \leqslant y_{k+1|LM}^{f\max} - \Phi_{LM}^{f\Delta}(k), \\ -F_{LM}^{f\Delta}\Delta u_{k|LM} \leqslant -y_{k+1|LM}^{f\min} + \Phi_{LM}^{f\Delta}(k). \end{aligned}$$

To change the control horizon from LM to J_cM $(J_c \leqslant L)$

$$\Delta u_{k+J_cM+1|(L-J_c)M} = 0 \Leftrightarrow$$
$$I_{(L-J_c)Mr}\Delta u_{k+J_cM|(L-J_c)M} \leqslant 0 \text{ and } -I_{(L-J_c)Mr}\Delta u_{k+J_cM|(L-J_c)M} \leqslant 0 \Leftrightarrow$$
$$M_{J_c}u_{k|LM} \leqslant 0 \text{ and } -M_{J_c}u_{k|LM} \leqslant 0$$

where $M_{J_c} = \begin{bmatrix} 0_{(J_cM\times r)\times(LM\times r)} \\ 0_{[(L-J_c)M\times r]\times(J_cM\times r)} \quad I_{(L-J_c)M\times r} \end{bmatrix}$. Thus equation (5.19) is proved.

Thus the control law can be solved by the following QP problem

$$\min_{\Delta u_{k|LM}} (\Delta u_{k|LM}^T H \Delta u_{k|LM} + 2f_k^T \Delta u_{k|LM}),$$
$$\text{subject to } \tilde{A}u_{k|LM} \leqslant b_k,$$

which can be solved as

$$\Delta u_{k|LM}^* = qp(H, f_k, \tilde{A}, b_k).$$

■

After the optimal control sequence $u_{k|L}$ is calculated, only the first block row, u_k, is implemented in the receding horizon predictive control law.

5.3.5 Prediction of future disturbance

It can be seen that in equations (5.16) and (5.17), the vectors $w_{k-(L-1)M|(L-1)M}$ and $w_{k-LM+1|LM-1}$ are past disturbance which are known. $w_{k|LM}$ is a vector which consists of current and future disturbance signals as

$$w_{k|LM} = \begin{bmatrix} w_k \\ w_{k+1} \\ \vdots \\ w_{k+LM-1} \end{bmatrix} = \begin{bmatrix} w_k \\ w_{k+1|LM-1} \end{bmatrix}$$

where the current disturbance w_k is known but disturbances from $w_{k+1}$to w_{k+LM-1} are unknown. In the following part we will discuss how to predict $w_{k+1|LM-1}$ using past to current w data. Note that w is sampled at fast rate. From [60], it can be seen that

$$w_{k+1|L} = \tilde{M}_w^L w_{k-L+1|L} + *$$

where $\tilde{M}_w$ can be estimated by DSR subspace identification method, and $*$ is the future white noise related term. Hence, the optimal prediction of $w_{k+1|L}$ is given by the first term of the above equation, such that

$$\hat{w}_{k+1|L} = \tilde{M}_w^L w_{k-L+1|L}.$$

Thus

$$\hat{w}_{k+1|LM} = \tilde{M}_w^{LM} w_{k-LM+1|LM},$$

and

$$\hat{w}_{k+1|LM-1} = \hat{w}_{k+1|LM}[1 : (LM-1) * r_w].$$

5.4 Simulation examples

5.4.1 Example 1

This distillation column example is adopted from [83] and illustrated in Figure 3.2. Similar examples can be found in [34] and MATLAB/Control Toolbox User's Guide [1]. The linearized transfer function model around the steady-state operation condition is:

$$\begin{bmatrix} y_1(s) \\ y_1(s) \end{bmatrix} = \begin{bmatrix} \frac{12.8e^{-s}}{16.7s+1} & \frac{-18.9e^{-3s}}{21.0s+1} \\ \frac{6.6e^{-7s}}{10.9s+1} & \frac{-19.4e^{-3s}}{14.4s+1} \end{bmatrix} \begin{bmatrix} u_1(s) \\ u_2(s) \end{bmatrix}$$

The control signals are fast sampled with two-time units and the plant outputs are slow sampled with four-time units. So the lifting factor $M = 2$. By discretization and lifting [10], the lifted dual-rate system is a 2-by-4 LTI as:

$$\begin{bmatrix} y_1(z) \\ y_2(z) \end{bmatrix} = \begin{bmatrix} \frac{0.744z^{-1}}{1-0.8871z^{-1}} & \frac{-0.8789z^{-2}}{1-0.9092z^{-1}} & \frac{0.7077z^{-2}}{1-0.8871z^{-1}} & \frac{-0.838z^{-3}}{1-0.9092z^{-1}} \\ \frac{0.5786z^{-4}}{1-0.8324z^{-1}} & \frac{-1.302z^{-2}}{1-0.8703z^{-1}} & \frac{0.5278z^{-5}}{1-0.8324z^{-1}} & \frac{-1.214z^{-3}}{1-0.8703z^{-1}} \end{bmatrix} \begin{bmatrix} \underline{u_1}(z) \\ \underline{u_2}(z) \end{bmatrix},$$

where $\underline{u_1}$ and $\underline{u_2}$ are lifted control signals. The cost function is

$$J_k = (\hat{y}_{k+M|L} - r_{k+M|L})^T Q(\hat{y}_{k+M|L} - r_{k+M|L}) + \Delta u_{k|LM}^T R \Delta u_{k|LM} + u_{k|LM}^T P u_{k|LM}$$

where the weighting matrices are $Q = I$, $R = 0.5I$ and $P = 0.1I$. The constraints are

$$-2I \leqslant u_{k|LM} \leqslant 2I,$$
$$-I \leqslant \Delta u_{k|LM} \leqslant I,$$
$$-6I \leqslant \hat{y}_{k+M|L} \leqslant 6I.$$

By collecting open-loop data (2000 time-units) with designed random binary inputs, we computed the dual-rate data-driven MPC law by the derived algorithm for $L = 4$ and $J_c = 2$, and $L = 5$ and $J_c = 4$, respectively. Also, supposing the lifted model is known, we designed MPC controllers via MATLAB/MPC toolbox with the same prediction horizon and control horizon for a comparison. The set point is multiple step signal which increases from 0 to 5 when t=11 s and goes back to 0 after 20 s. The output and control signals, under dual-rate MPC controllers both from the data-driven algorithm and from MATLAB/MPC toolbox, are shown in the following figures. It can be seen that the difference between the control results under proposed data-driven and MPC control law is minor. Thus, the proposed data-driven predictive control algorithm is comparable to the traditional MPC algorithm in terms of performance, but the proposed approach has the advantage that no parametric model is needed.

The distillation column with disturbances is modeled as [34]:

$$\begin{bmatrix} y_1(s) \\ y_1(s) \end{bmatrix} = \begin{bmatrix} \frac{12.8e^{-s}}{16.7s+1} & \frac{-18.9e^{-3s}}{21.0s+1} \\ \frac{6.6e^{-7s}}{10.9s+1} & \frac{-19.4e^{-3s}}{14.4s+1} \end{bmatrix} \begin{bmatrix} u_1(s) \\ u_2(s) \end{bmatrix} + \begin{bmatrix} \frac{3.8e^{-8s}}{14.9s+1} \\ \frac{4.9e^{-3s}}{13.2s+1} \end{bmatrix} w(s) \qquad (5.28)$$

where w is a measurable disturbance. In the simulation we first set w is a random walk signal such that

$$w = \frac{1}{1 - z^{-1}} a$$

where a is discrete-time white noise with $\sigma^2(a) = 0.5$. The prediction horizon and control horizon are chosen as $L = 4$ and $J_c = 3$. The simulations are done with feedforward control law and without feedforward control law. From control results shown in Figure 5.6 and Figure 5.8, it is obvious that the performance with feedforward plus feedback control strategy is better than that with feedback control only. Also, we did simulation with w as a fast changing dynamical signal as

$$w = \frac{1}{1 - 0.95z^{-1}} a$$

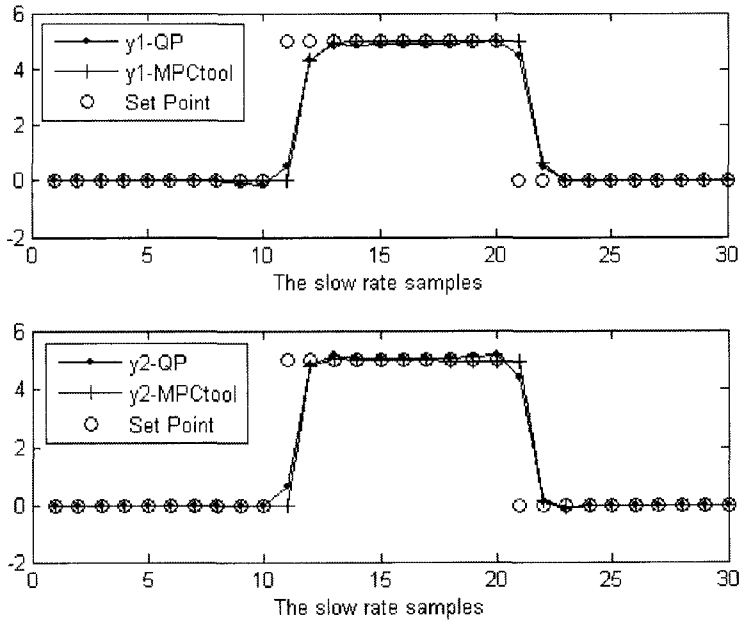

Figure 5.2: The outputs when $L = 4$ and $J_c = 2$

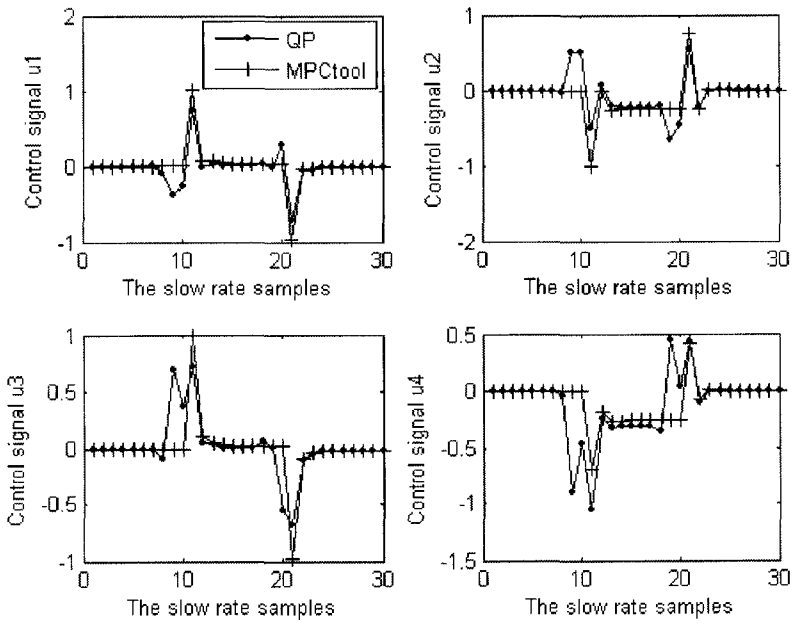

Figure 5.3: The control signals when $L = 4$ and $J_c = 2$

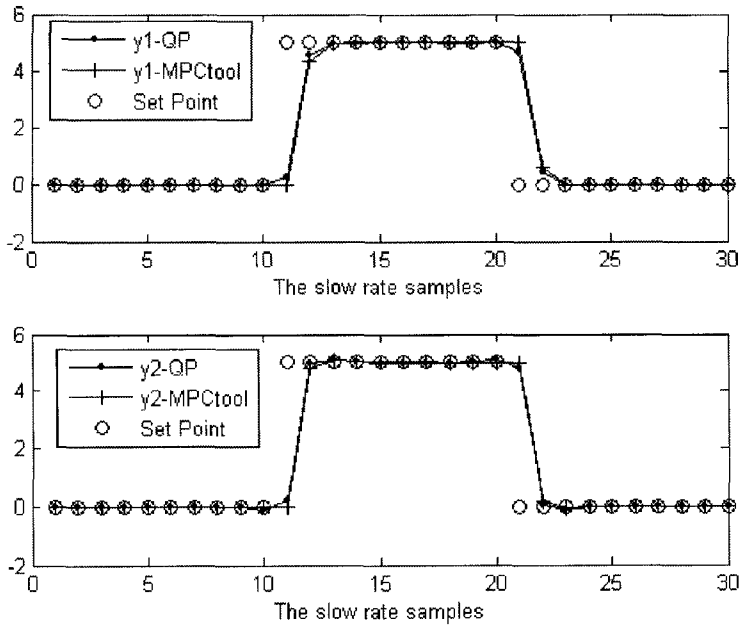

Figure 5.4: The outputs when $L = 5$ and $J_c = 4$

with $\sigma^2(a) = 0.5$. The prediction horizon and control horizon are chosen as $L = 4$ and $J_c = 3$. The controlled variables and manipulated variables are shown in Figure 5.10 and 5.11, respectively. From the figures, we can see that the outputs variables follow the set points well.

5.4.2 Example 2

The solid oxide fuel cell (SOFC) system dynamic model [53, 85] is the same as we used in Chapter 4. Readers are referred to Chapter 4 for details. The problem is briefly summarized below:

- The manipulated variables are $\left[\begin{array}{cc} q_{\mathrm{f}}^{\mathrm{in}} & q_{\mathrm{O}_2}^{\mathrm{in}} \end{array}\right]^T$, where $q_{\mathrm{f}}^{\mathrm{in}}$ is the input fuel flow and $q_{\mathrm{O}_2}^{\mathrm{in}}$ is the input oxygen flow. They are sampled in fast rate. The steady state of the inputs is $\left[\begin{array}{cc} 0.7023 & 0.6134 \end{array}\right]^T$mol/s, and the constraints are

$$\left[\begin{array}{cc} 0 & 0 \end{array}\right]^T mol/s \leqslant \left[\begin{array}{cc} q_{\mathrm{f}}^{\mathrm{in}} & q_{\mathrm{O}_2}^{\mathrm{in}} \end{array}\right]^T \leqslant \left[\begin{array}{cc} 1.7023 & 1.6134 \end{array}\right]^T \text{ mol/s.}$$

- The fuel cell current demand I_{in} is considered as the measurable disturbance which is also sampled in fast rate. The power output of the fuel cell system is

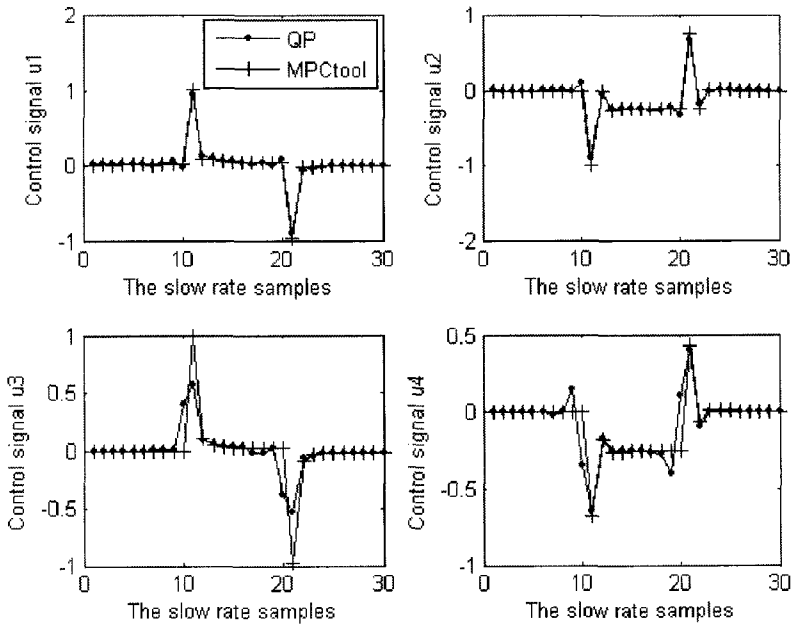

Figure 5.5: The control signals when $L = 5$ and $J_c = 4$

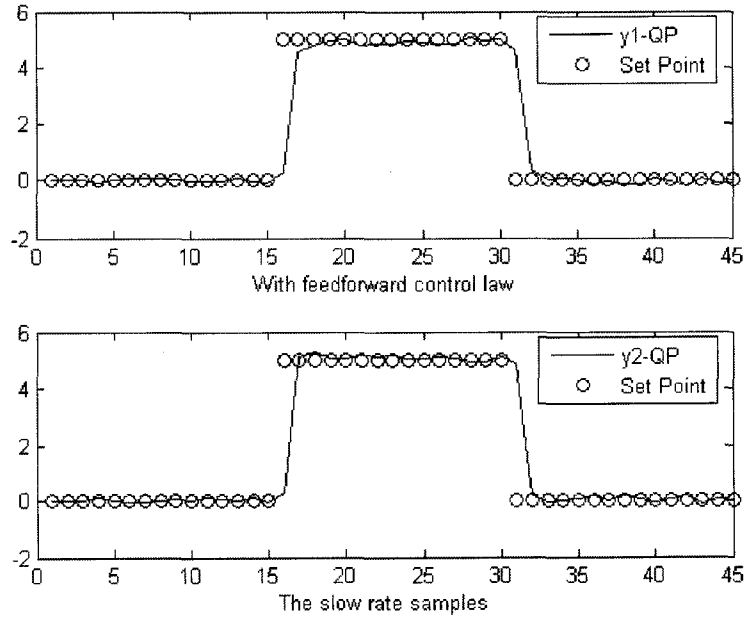

Figure 5.6: The outputs when $L = 4$ and $J_c = 3$ with feedforward

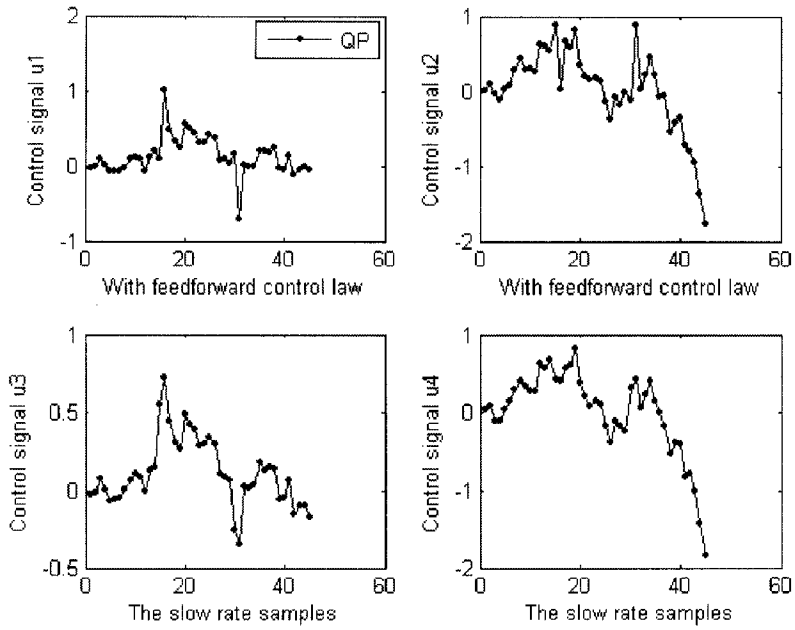

Figure 5.7: The control signals when $L = 4$ and $J_c = 3$ with feedforward

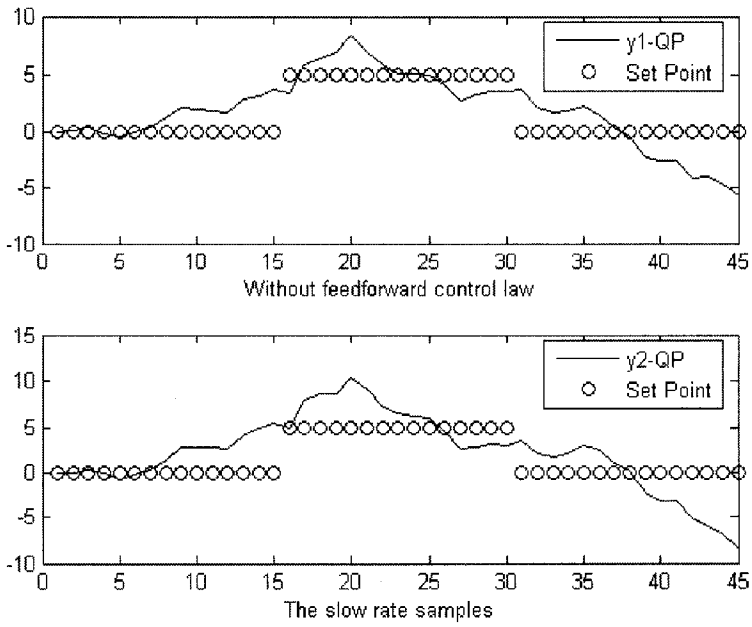

Figure 5.8: The control signals when $L = 4$ and $J_c = 3$ without feedforward

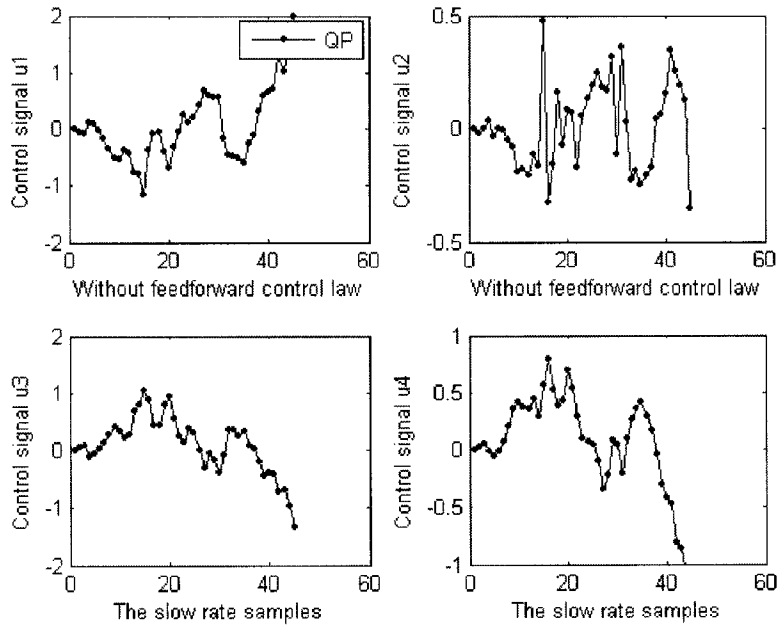

Figure 5.9: The control signals when $L = 4$ and $J_c = 3$ without feedforward

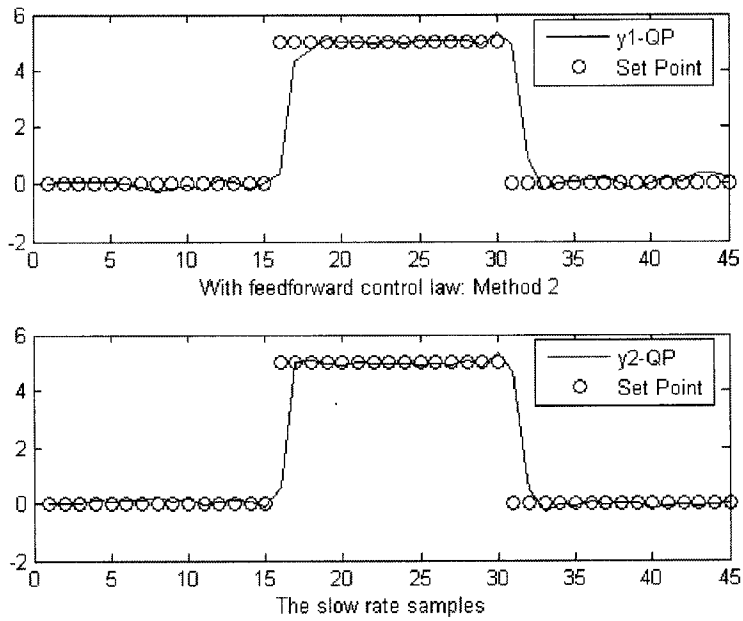

Figure 5.10: The outputs when $L = 4$ and $J_c = 3$

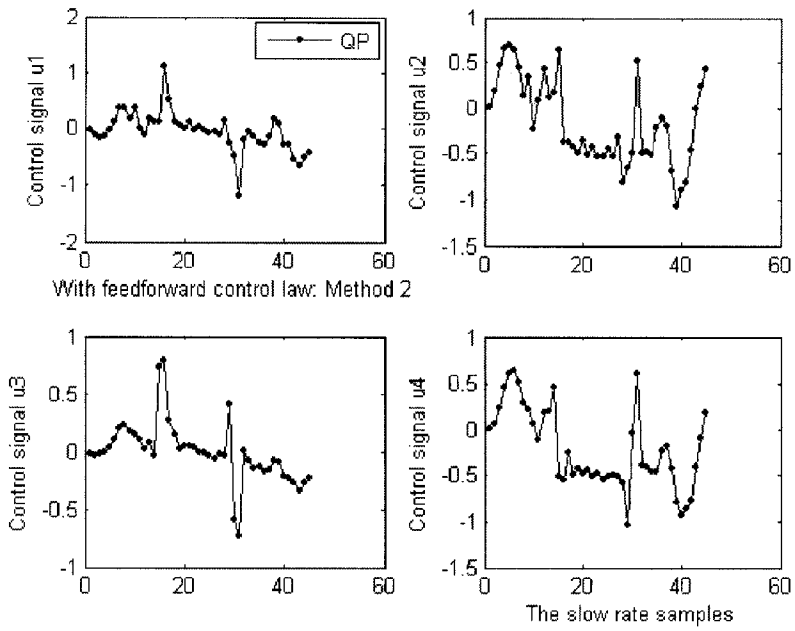

Figure 5.11: The control signals when $L = 4$ and $J_c = 3$

100kW, under which the nominal value of the voltage demand V_{in} is 333.8 V and the current demand is 300 A.

- The controlled variables are$\begin{bmatrix} U_{\text{f}} & V_{\text{r}} & R_{\text{H_O}} & p_{\text{dif}} \end{bmatrix}^T$, where

- U_{f} is fuel utilization, which is defined as the ratio between the H_2 flow that reacts and the input H_2 flow, i.e.,

$$U_{\text{f}} \stackrel{\text{def}}{=} q^{\text{r}}_{\text{H}_2}/q^{\text{in}}_{\text{H}_2}.$$

  Typically, an 80%−90% fuel utilization is desired [53]. We choose the operating point of U_{f} as 85%. It is a component of total inlet flow in the SOFC system [53, 85]. Thus, it is difficult and costly to measure the fuel utilization in the fast rate.

- V_{r} is the fuel cell stack output voltage. The constraint on V_{r} is 313.8 V$\leqslant V_{\text{r}} \leqslant$ 353.8 V, and 333.8 V is chosen as the operating point. In the closed-loop simulation, we assume that only V_{r} is measurable.

- $R_{\text{H\_O}}$ is the ratio between inlet H_2 and O_2 flows, which is defined as

$$R_{\text{H\_O}} \stackrel{\text{def}}{=} q^{\text{in}}_{\text{H}_2}/q^{\text{in}}_{\text{O}_2}.$$

  In the simulation, the constraint on $R_{\text{H\_O}}$ is set as $0 \leqslant R_{\text{H\_O}} \leqslant 2$, and the operating point is as $R_{\text{H\_O}} = 1.145$ [85].

- p_{dif} is the fuel cell pressure difference between the hydrogen and oxygen passing through the anode and cathode gas compartments, i.e., $p_{\text{dif}} = p_{\text{H}_2} - p_{\text{O}_2}$. To prevent damage to the electrolyte, $|p_{\text{dif}}|$ needs to be kept below 8 kPa under transient conditions [85]. The operating point of p_{dif} is 0 kPa. All parameters and operating conditions are summarized in Table 4.1 and Table 4.2, respectively. In the SOFC system, the slowly sample fuel utilization is the controlled variable, the other fast sampled outputs are constraint variables, and the fast sampled current is the measurable disturbance.

We apply the proposed data-driven predictive control to the SOFC problem discussed in the previous subsection to achieve optimal fuel utilization and maintain operation constraints. The fast sampling rate is chosen as $T_{\text{fast}} = 1$ s mainly targeting the system dominant dynamics (see Table 4.1). I_{in}, V_{r}, $R_{\text{H\_O}}$ and p_{dif} are sampled in the fast rate. The slow sampling rate is $T_{\text{slow}} = 5$ s to sample U_{f}. Thus, the lifting factor of the SOFC systems is $M = \frac{T_{\text{slow}}}{T_{\text{fast}}} = 5$. The dual-rate predictive controller updates control inputs and outputs every 1 s. To design the data-driven predictive controllers, the open-loop input-output data are required to determine the subspace matrices. Open loop input-output data are obtained by exciting the open loop SOFC system using a designed random binary signals of magnitude 0.1 for the fuel and oxygen inlet flows. The fuel cell current demand disturbance is a multiple step signal which increases from 300 A to 330 A when $t = 200$ s, and goes back to 300 A after $t = 400$ s. A white noise with variance 5 is added to the current demand as measurement noise (see the generated disturbance signal in Figure 5.12). The input and output data are collected over 1000 seconds, and they are plotted in Figure 5.13. In the control objective function (5.2), the prediction horizon $L = 2$, the control horizon $J_c = 2$, and the weighting matrices are selected as Q =diag(Q_1, Q_2) where $Q_{1,2}$ =diag(10^2), R_M =$0.1 \times I$, and $P_M = 0$. The multirate predictive control is applied to the SOFC system after $t = 100$ s.

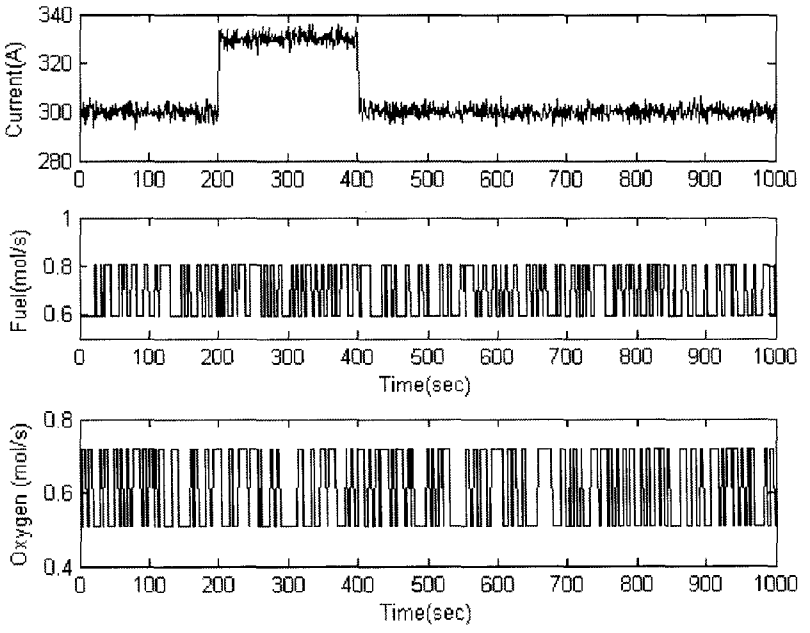

Figure 5.12: The open-loop SOFC disturbance and input signals

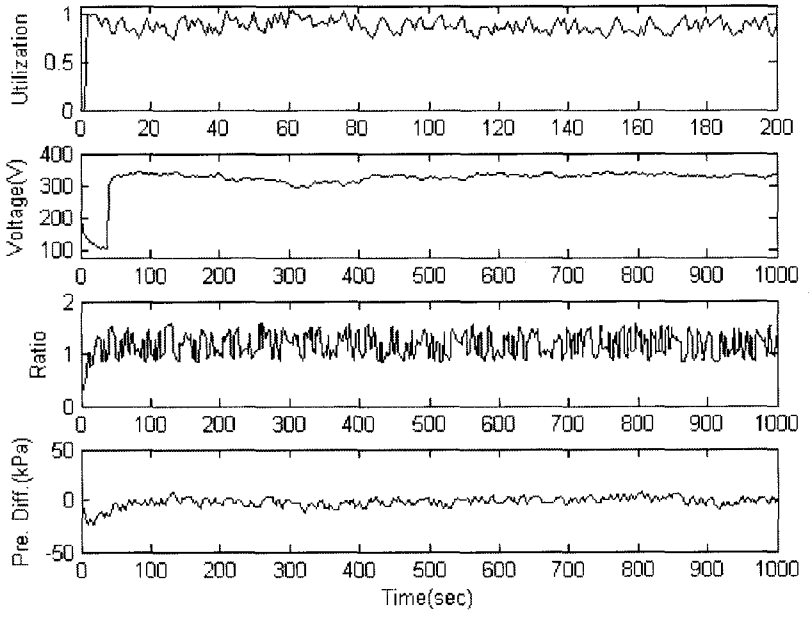

Figure 5.13: The open-loop SOFC output signals

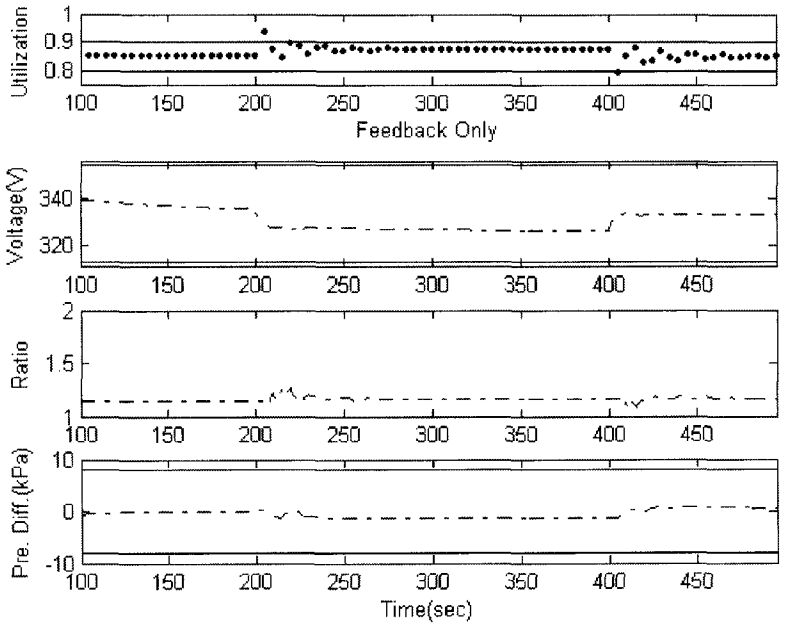

Figure 5.14: The SOFC output signals under feedback control

To demonstrate the effect of feedforward control, we did the closed-loop simulations with two different multirate predictive control laws– feedback control only and feedback plus feedforward control. The closed-loop outputs and inputs under the feedback controller are plotted in Figure 5.14 and Figure 5.15, and the signals under the feedback plus feedforward controller are drawn in Figure 5.16 and Figure 5.17. From Figure 5.14 and Figure 5.16, it can be seen that under both predictive controller, the errors of utilization are kept close to zero at steady state under large current load step changes, which is the effect of the integral control action. Furthermore, we compare the control results in terms of the mean and variance of utilization, $\overline{U_{\mathrm{f}}}$ and $\mathrm{Var}(u_f)$, over closed-loop simulation. Under the feedback control $\overline{U_{\mathrm{f}}} = 0.8660$ and $\mathrm{Var}(u_f) = 0.0028$; under the feedback plus feedforward control, $\overline{U_{\mathrm{f}}} = 0.8577$ (which is closer to the utilization set point 0.85) and $\mathrm{Var}(u_f) = 0.0027$. The results show that under the feedback plus feedforward control, the utilization of the multirate SOFC system tracks the set point better. In other words, the feedforward plus feedback control yields higher control performance.

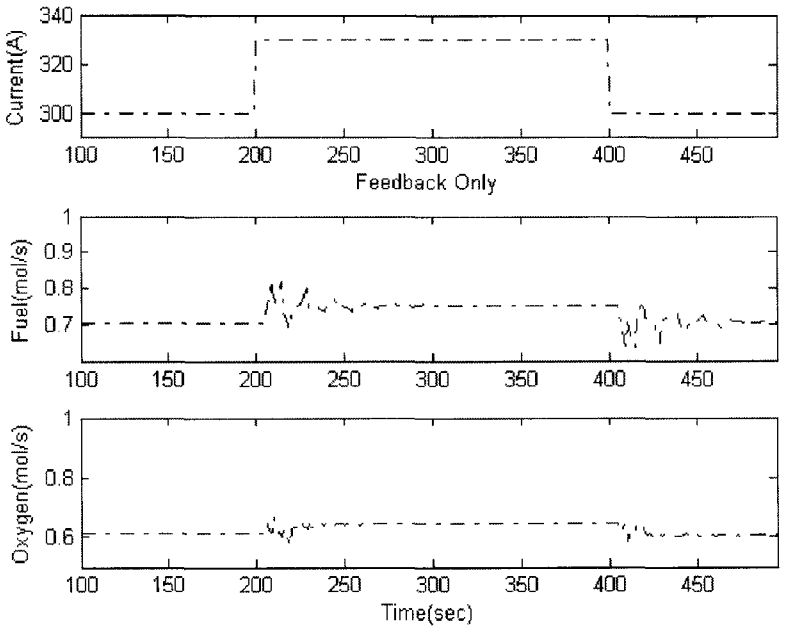

Figure 5.15: The SOFC control signals under feedback control

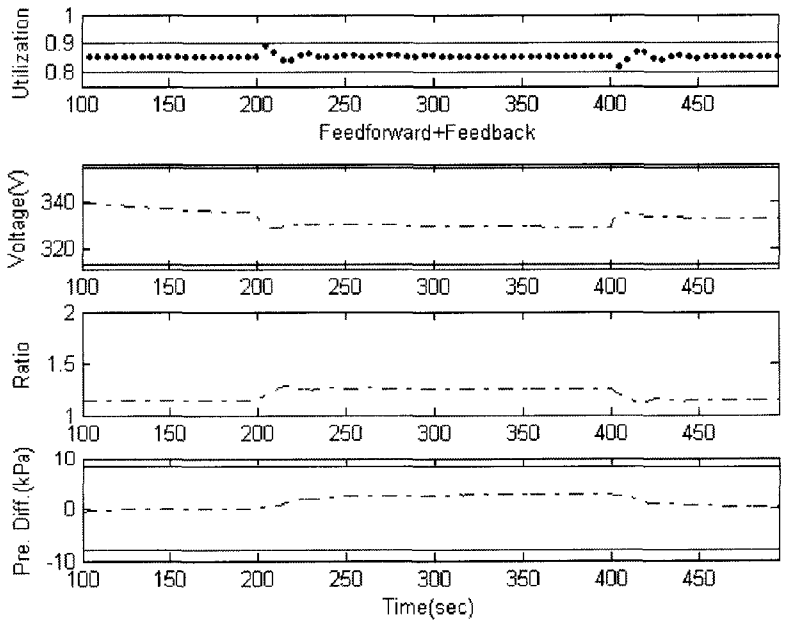

Figure 5.16: The SOFC output signals under feedback plus feedforward control

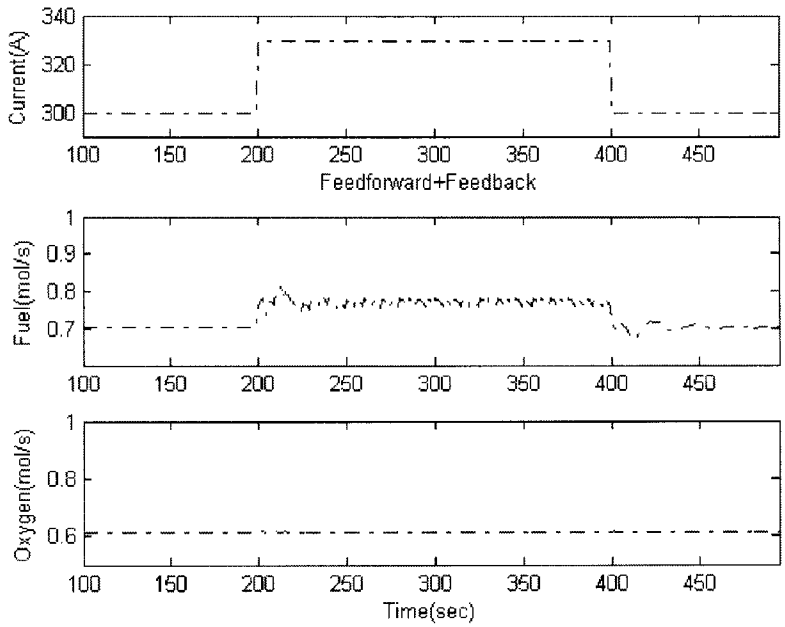

Figure 5.17: The SOFC disturbance and control signals under feedback plus feedforward control

5.5 Conclusions

A data-driven predictive control including feedforward control has been discussed for multirate systems. The multirate predictive strategy that can handle constraints and optimize control performance has been developed via the subspace approach. The proposed multirate predictive control is data-driven since it only requires a set of input-output open-loop experimental data and the explicit parametric process model is not needed. This algorithm is effective for multirate systems where some measurements are difficult to sample in fast rates. The proposed algorithm was illustrated through a distillation column and an SOFC model which have been commonly investigated in the literature. A multirate system where the outputs are sampled with more than two sampling rates can also be handled within the framework, by applying appropriate lifting.

Chapter 6

Conclusions and Future Work

In this chapter, the main contributions of this thesis are summarized and some suggestions for the future research are outlined.

6.1 Conclusions

We have investigated the MVC problem for single-input single-output linear systems sampled at different rates: fast, dual and slow rates. The minimum variance of the fast sampled output was chosen as the control cost function. The MVC law was directly applied to the design of the optimal controller for the fast-rate control loop. Using the lifting technique, the dual-rate and the slow-rate control loops can be unified under a common structural model. A discretization method preserving the mean and auto-correlation of a continuous stochastic disturbance model was developed. A novel linear matrix inequality approach was proposed and then was used to derive the optimal controllers for the lifted dual-rate and slow-rate control loops. It was theoretically proven that the performance of a dual-rate controller is superior to that of a slow single rate controller but inferior to that of a fast single rate controller in the sense of MVC.

We have derived a data-driven MVC and the MVC-benchmark variance estimation has been discussed for dual-rate systems. A subspace input-output equation is derived by the lifting technique to obtain a prediction model for multirate systems. The multirate minimum variance controller is calculated from a set of input-output open-loop experimental data and thus this approach is data-driven since it does not need an explicit model. In parallel, the presented MVC-benchmark estimation algorithm requires a set of open-loop experimental data plus a set of closed-loop routine operating data.

Also, a predictive control strategy that can handle constraints and optimize control performance has been developed via the subspace approach. This algorithm is validated by an SOFC simulation example that has been commonly investigated in the dynamic SOFC modeling/control literature lately. The previous studies have shown that control of SOFC is challenging due to the slow response and tight operation constraints. In this work, unlike model-based approaches, the proposed predictive controller is data-driven; thus it provides an alternative solution to SOFC control problem. This is particularly effective for systems where an explicit dynamic model is generally difficult to develop. Comparing with the previous data-driven predictive control approach, the developed predictive controller can handle systems

where only partial on-line outputs measurements are available.

The proposed data-driven predictive control has been extended to solution of multirate problems. This solution is of importance when, for example, the fuel utilization in the SOFC system may not be measured at the fast rate due to sensor physical limits. The proposed data-driven multirate predictive control only requires a set of input-output open-loop experimental data and an explicit lifted process model is not needed.

6.2 Future work

- In this thesis, we proposed data-driven predictive control laws via subspace approach for both single-rate and multirate systems. The problem of stability of the subspace-based data-driven controllers is still open [13, 84]. Certain terminal constraints can be introduced to achieve the closed-loop stability when the model is an exact representation of the plant. However, in our data-driven approach there is no explicit model used. Thus, considering the terminal constraint without relying on an explicit model in order to prove the closed-loop stability is one of the possible future directions.

- The previous study [14] has shown that the data-driven control laws approach the LQG controllers when the prediction horizon goes to infinity. This fact has also been verified by our simulation studies in Chapters 3 and 4. In addition, the longer the prediction horizon, the greater the probability that the closed-loop system is stable [13, 84]. However, simulation results in Chapter 4 have shown that larger prediction horizons may also introduce larger prediction errors. Thus, how to choose the prediction horizon is an interesting problem to be studied.

- With the lifting technique we can transfer an LPTV system to an LTI system. At the same time the input-output dimensions are enlarged considerably. If a lifted system has an unmanageable dimension, we may not be able to implement the developed data-driven optimal control and control performance algorithms for the system owing to the memory limitation of the computer. Hence, a following problem that needs to be considered is how to reduce the

computation complexity for a high dimensional lifted system.

- To make the exposition simple and clear, a dual-rate system where the outputs are fast sampled and inputs are slowly sampled is considered in this thesis. The next step should be to extend the proposed data-driven MVC, predictive control and control performance algorithms to general multirate systems. Note that the casuality constraint may arise. This condition is induced by the fact that the control signal can only be a function of present and past measurements during the period. The causality constraint on a lifted controller K_d means that K_d must be causal and the direct feedthrough term in K_d, denoted as D_K, must satisfy certain causality constraint, i.e., D_K must be (block) lower-triangular [10]. Hence, it would be interesting to study how to compute data-driven optimal control laws, based on subspace matrices identified from open-loop data, subject to casuality constraints.

Bibliography

[1] *Control System Toolbox for Use with MATLAB.* MathWorks, Natik, MA, 2004.

[2] W. Aangenent, D. Kostic, B. de Jager, R. V. de Molenggraft, and M. Steinbuch. Data-based optimal control. In *Proc. of ACC.*, volume 10, pages 1460–1465, Portland, OR, 2005.

[3] P. Aguiar, C.S. Adjiman, and N.P. Brandon. Anode-supported intermediate-temperature direct internal reforming solid oxide fuel cell II. model-based dynamic performance and control. *J. of Power Sources*, 147:136–147, 2005.

[4] S. Akkarakaran and P. P. Vaidyanathan. Bifrequency and bispectrum maps: A new look at multirate systems with stochastic inputs. *IEEE. Trans. Signal Processing*, 48(3):723–736, 2000.

[5] K. J. Aström. *Introduction to Stochastic Control Theory.* Academic Press, New York, 1970.

[6] K. J. Aström and B. Wittenmark. *Computer-controlled Systems: Theory and Design.* Singular University Press and Prentice Hall, Beijing, 3rd edition, 2002.

[7] T. Barry and L. Wang. A model-free predictive controller with laguerre polynomials. In *Proc. of the 5th Asian Control Conference*, volume 1, pages 177–184, Melbourne, Astralia, July 2004.

[8] B. W. Bequette. *Process Dynamics: Modeling, Analysis and Simulation.* Prentice Hall, Englewood Cliffs, NJ, 1998.

[9] R. R. Bitmead and M. Gevers. *Adaptive Optimal Control: A Thinking Man's GPC.* Prentice Hall, Englewood Cliffs, NJ, 1990.

[10] T. Chen and B. A. Francis. *Optimal Sampled-Data Control Systems.* Springer, Berlin, 1995.

[11] T. Chen and L. Qiu. $\mathscr{H}_\infty$ design of general multirate sampled-data control systems. *Automatica*, 30(7):1139–1152, 1994.

[12] L. Desborough and T. J. Harris. Performance assessment measures for univariate feedback control. *Canadian J. of Chem. Eng.*, 70:1184–1197, 1992.

[13] W. Favoreel. *Subspace methods for identification and control of linear and biliear systems.* PhD thesis, Katholieke Universiteit Leuven, Department of Electrical Engineering, November 1999.

[14] W. Favoreel, B. De Moor, M. Gevers, and P. Van Overschee. Model-free subspace-based LQG-design. Technical Report ESAT-SISTA/TR 1998-34, Department of Electrical Engineering, Katholieke Universiteit Leuven, Leuven, Belgium, 1998.

[15] W. Favoreel, B. De Moor, M. Gevers, and P. Van Overschee. Subspace predictive control. Technical Report ESAT-SISTA/TR 1998-49, Department of Electrical Engineering, Katholieke Universiteit Leuven, Leuven, Belgium, 1998.

[16] B. A. Francis. *Lecture Notes in Control and Information Sciences: A course in $\mathscr{H}_\infty$ Control Theory.* Springer, Berlin.

[17] C. E. Garcia, David M. Prett, and M. Morari. Model predictive control: Theory and practice — a survey. *Automatica*, 25(3):335–348, 1989.

[18] M. J. Grimble. Restricted structure controller tuning and performance assessment. *IEE Proc.-Contr. Theory Appl.*, 149(1):8–16, 2002.

[19] M. Grujicic, K. Chittajallu, E. Law, and J.T. Pukrushpan. Model-based control strategies in the dymanic interaction of air supply and fuel cell. *Proc. of the I MECH E Part A Journal of Power and Energy*, 218(7):487–499, 2004.

[20] R. D. Gudi, S. L. Shah, and M. R. Gray. Adaptive multirate state and parameter estimation strategies with application to a bioreactor. *AIChE*, 41(11):2451–2464, 1995.

[21] T. Harris, C. T. Seppala, and L. D. Desborough. A review of performance monitoring and assessment techniques for univariate and multivariate control systems. *J. of Process Contr.*, 9:1–17, 1999.

[22] T. J. Harris. Assessment of control loop performance. *Canadian J. of Chem. Eng.*, 67:856–861, 1989.

[23] T. J. Harris, T. Boudreau, and J. F. MacGregor. Performance assessment of multivariable feedback controllers. *Automatica*, 32(11):1505–1518, 1996.

[24] W. He. Dynamic model for molten carbonate fuel-cell power-generation systems. *J. of Energy Conv. Manage*, 39(8):775–783, 1998.

[25] B. Huang. A pragmatic approach towards assessment of control loop performance. *An internal technical report*, 2002.

[26] B. Huang, S. X. Ding, and S. J. Qin. Closed-loop subspace identification: an orthogonal projection approach. *J. of Process Contr.*, 15(1):53–66, 2005.

[27] B. Huang, R. Kadali, and S. X. Ding. A direct input/output data-driven approach to multivariate feedback control performance assessment without interactor matrix. Per invitation as a selected paper presented in *IFAC International Symp. on Advanced Control of Chem. Processes 2003,* Hong Kong, China, January 2004.

[28] B. Huang and S. L. Shah. Good, bad or optimal? performance assessment of MIMO process. *Automatica*, 33(6):1175–1183, 1997.

[29] B. Huang and S. L. Shah. *Performance Assessment of Control Loops: Theory and Applications.* Springer, London, 1999.

[30] V. Ionescu and C. Oară. Spectral and inner-outer factorization for discrete-time systems. *IEEE Trans. Automat. Contr.*, 41(12):1840–1845, 1996.

[31] Mohieddine Jelali. An overview of control performance assessment technology and industrial applications. *Control Engineering Practice*, 14(5):441–466, 2006.

[32] R. H. Julien, M. W. Foley, and W. R. Cluett. Performance assessment using a model predictive control benchmark. *J. of Process Contr.*, 14:441–456, 2004.

[33] Francisco Jurado. Modeling sofc plants on the distribution system using identification algorithms. *J. of Power Sources*, 129:205–215, 2004.

[34] R. Kadali, B. Huang, and A. Rossiter. A data driven subspace approach to predictive controller design. *Contr. Eng. Practice*, 11:261–278, 2003.

[35] S. J. Kendra and A. Cinar. Controller performance assessment by frequency domain techniques. *J. of Process Contr.*, 7(3):181–194, 1997.

[36] Valery Knyazkin, Lennart Söder, and Claudio Canizares. Control challenges of fuel cell-driven distributed generation.

[37] B. Ko and T. F. Edgar. Assessment of achievable PI control performance for linear processes with dead time. *American Control. Conf.*, 1998.

[38] B. Ko and T. F. Edgar. Performance assessment of multivariable feedback control systems. *Automatica*, 37(6):899–905, 2001.

[39] R. H. Kong. On the linear quadratic Gaussian problem with correlated noise and its relation to minimum variance control. *SIAM J. Contr. and Optimization*, 29(1):139–152, 1991.

[40] G. M. Kranc. Input-output analysis of multirate feedback systems. *IRE Trans. Automat. Contr.*, 3:21–28, 1957.

[41] W. E. Larimore. Canonical variate analysis in identification, filtering, and adaptive control. In *Proc. of the 29th IEEE Conf. on Desicion and Control*, pages 596–604, Honolulu, Hawaii, December 1990.

[42] D. Li, S. L. Shah, and T. Chen. Identification of fast-rate models from multirate data. *Int. J. Contr.*, 74(7):680–689, 2001.

[43] D. Li, S.L. Shah, T. Chen, and K. Qi. Application of dual-rate modeling to CCR octane quality inferential control. *IEEE Trans. on Contr. Syst. Technol.*, 11(1):43–51, 2003.

[44] Q. Li, J. R. Whiteley, and R. R. Rhinehart. An automated performance monitor for process controllers. *J. of Process Contr.*, 12:537–553, 2004.

[45] W. P. Lu and D. G. Fisher. Output estimation with multi-rate sampling. *Int. J. Contr.*, 48:149–160, 1988.

[46] C. B. Lynch and G. A. Dumont. Control loop performance monitoring. *IEEE Trans. Contr. Syst. Technol.*, 4(2):185–192, 1996.

[47] D. G. Meyer. Cost translation and a lifting approach to the multirate LQG problem. *IEEE Trans. Automat. Contr.*, 37(9):1411–1415, 1992.

[48] M. Ohshima, I. Hashimoto, M. Takeda, T. Yoneyama, and F. Goto. Multi-rate multivariable model predictive control and its application to a semi-commercial polymerization reactor. *Proc. ACC.*, 12:1576–1581, 1992.

[49] F. Olaleye, B. Huang, and E. Tamayo. Industrial application of a feedback controller performance assessment of time-variant processes. *Ind. Eng. Chem. Res.*, 43(2):597–607, 2004.

[50] P. Van Overschee, W. Favoreel, and B. De Moor. Subspace state space system identification for industrial processes. *J. of Process Contr.*, 10:149–155, 2000.

[51] P. Van Overschee and B. De Moor. N4SID: Subspace algorithms for the identification of combined deterministic-stochastic systems. *Automatica*, 30(1):75–93, 1994.

[52] P. Van Overschee and B. De Moor. A unifying theorem for three subspace system identification algorithms. *Automatica*, 31(12):1853–1864, 1995.

[53] J. Padullés, G. W. Ault, and J. R. McDonald. An integrated SOFC plant dynamic model for power systems simulation. *J. of Power Sources*, 86:495–500, 2000.

[54] J.T. Pukrushpan, A. Stefanopoulou, and H. Peng. Modeling and control for pem fuel cell stack system. In *Proc. of the the 2002 American Control Conf.*, pages 3117–3122, Anchorage, AK, May 2002.

[55] S. J. Qin. Control performance monitoring – a review and assessment. *Comp. and Chem. Eng.*, 23:173–186, 1998.

[56] L. Qiu and T. Chen. $\mathscr{H}_2$-optimal design of multirate sampled-data systems. *IEEE. Trans. Automat. Contr.*, 39(12):2506–2511, 1994.

[57] L. Qiu and K. Tan. Direct state space solution of multi-rate sampled-data $\mathscr{H}_2$ optimal control. *Automatica*, 34(11):1431–1437, 1998.

[58] D. Di Ruscio. Methods for the identification of state space models from input and output measurements. In *Proc. of the 10th IFAC Symp. on Syst. Identification*, pages 675–680, Copenhagen, Denmark, July 1994.

[59] D. Di Ruscio. *A Method for Identification of Combined Deterministic Stochastic Systems.* Lecture Notes in Statistics. Springer, New York, 1997.

[60] D. Di Ruscio. Model based predictive control: an extended state space approach. In *Proc. of the 36th Conf. on Decision and Control*, pages 3210–3217, San Diego, CA, December 1997.

[61] D. Di Ruscio. Model predictive control and identification: a linear state model approach. In *Proc. of the 36th Conf. on Decision and Control*, pages 3202–3209, San Diego, CA, December 1997.

[62] D. Di Ruscio. Subspace system identification of multiple time series and different sampling rates. In *Proc. of the 12th IFAC Symp. on Syst. Identification*, Santa Barbara, CA, June 2000.

[63] T. Sato and K. Z. Liu. LMI solution to general $\mathscr{H}_2$ suboptimal control problems. *Syst. Contr. Lett.*, 36(4):295–305, 1999.

[64] C. Scherer, P. Gahinet, and M. Chilali. Multiobjective output-feedback control via LMI optimization. *IEEE Trans. Automat. Contr.*, 42(7):896–911, 1997.

[65] J. Sheng, T. Chen, and S. L. Shah. Estimation of time delays in multirate sampled-data systems. *Proc. Int. DCDIS Conf. on Eng. Applications and Computational Algorithms*, pages 23–27, 2003.

[66] J. Sheng, T. Chen, and S.L. Shah. Generalized predictive control for non-uniformly sampled systems. *J. of Process Contr.*, 12(8):875–885, 2002.

[67] H. Shu and T. Chen. State space approach to discrete-time $\mathscr{H}_2$-optimal control with a causality constraint. *Syst. Contr. Lett.*, 26(1):69–77, 1995.

[68] N. Stanfelj, T. Marlin, and J. MacGregor. Monitoring and diagnosing process control performance: the single-loop case. *Ind. Eng. Chem. Res.*, 32:301–314, 1993.

[69] Christoph Stiller, BjØrn Thorud, Olav Bolland, Rambabu Kandepu, and Lars Imsland. Control strategy for a solid oxide fuel cell and gas turbine hybrid system. *J. of Power Sources*, 158(1):303–315, 2006.

[70] N. F. Thornhill, B. Huang, and S. L. Shah. Controller performance assessment in set point tracking and regulatory control. *Int. J. of Adaptive Contr. and Signal Processing*, 17:709C727, 2003.

[71] M. L. Tyler and M. Morari. Performance monitoring of control systems using likelihood methods. *Automatica*, 32(8):1144C1154, 1996.

[72] A. Vahidi, A. Stefanopoulou, and H. Peng. Model predictive control for starvation prevention of a hybrid fuel cell system. In *Proc. of the the 2004 American Control Conf.*, pages 834–839, Boston, MA, June 2004.

[73] M. Verhaegen. Identification of the deterministic part of mimo state space models given in innovation form from input-output data. *Automatica*, 30(1):61–74, 1994.

[74] M. Verhaegen and X. Yu. A class of subspace model identification algorithms to identify periodically and arbitrarily time-varying systems. *Automatica*, 32:201–216, 1995.

[75] M. Viberg. Subspace-based methods for the identification of linear time-invariant systems. *Automatica*, 31(12):1835–1851, 1995.

[76] P. G. Voulgaris. $\mathscr{H}_\infty$ and $\mathscr{H}_2$ optimal controllers for periodic and multirate systems. *Automatica*, 30(2):251–263, 1994.

[77] J. Wang, T. Chen, and B. Huang. Closed-loop identification via output fast sampling. *J. of Process Contr.*, 14(5):555–570, 2004.

[78] J. Wang, T. Chen, and B. Huang. Multirate sampled-data systems: computing fast-rate models. *J. of Process Contr.*, 14(1):79–88, 2004.

[79] J. Wang and S. J. Qin. A new subspace identification approach based on principal component analysis. *J. of Process Contr.*, 12(8):841–855, 2002.

[80] X. Wang, B. Huang, and T. Chen. Data-driven predictive control for solid oxide fuel cells. *J. of Process Contr.,* to be published, 2007.

[81] X. Wang, B. Huang, and T. Chen. Multirate minimum variance control design and control performance assessment: A data-driven subspace approach. *IEEE Trans. Contr. Syst. Technol.*, 15(1):65–74, 2007.

[82] X. Wang, L. Zhang, T. Chen, and B. Huang. Minimum variance in fast, slow and dual-rate control loops. *Int. J. of Adaptive Contr. and Signal Processing*, 19(8):575–600, 2005.

[83] R.K. Wood and M. W. Berryr. Terminal composition control of a binary distillation column. *Chemical Engineering Science*, 28:1707–1717, 1973.

[84] B. R. Woodley. *Model free subspace based $\mathscr{H}_\infty$ control.* PhD thesis, Stanford University, Department of Electrical Engineering, January 2001.

[85] Y. Zhu and K. Tomsovic. Developement of models for analyzing the load-following performance of microturbines and fuel cells. *Electric Power Systems Research*, 62:1–11, 2002.